INAUGURAL-DISSERTATION

Zur Erlangung der Doktorwürde

der Naturwissenschaftlich-Mathematischen Gesamtfakultät

der

Ruprecht-Karls-Universität

Heidelberg

vorgelegt von

Carsten H. Baehr, MEM, BSc

aus Bensheim

Tag der mündlichen Prüfung: 04.02.2005

INAUGURAL-DISSERTATION

submitted to the

Combined Faculties for the Natural Sciences and for Mathematics

of the Ruperto-Carola University of Heidelberg, Germany

for the degree of

Doctor of Natural Sciences

presented by

Carsten H. Baehr, MEM, BSc

born in Bensheim

Oral examination: 04.02.2005

Functional and Molecular Aspects of Xenobiotic Transport in Choroid Plexus

Supervisors: Prof. Dr. Gert Fricker
Prof. Dr. Ulrich Hilgenfeldt

To my family

Die vorliegende Arbeit wurde am Institut für Pharmazie und Molekulare Biotechnologie in der Abteilung Pharmazeutische Technologie und Pharmakologie der Ruprecht-Karls-Universität Heidelberg angefertigt.

Mein Dank gilt:

Herrn Prof. Dr. Gert Fricker für die interessante Fragestellung, die Betreuung und den wissenschaftlichen Freiraum, die stete Ansprechbarkeit und die Anregungen bei der Bearbeitung des Themas.

Herrn Prof. Dr. Ulrich Hilgenfeldt für die Anfertigung des Zweitgutachtens.

Herrn Dr. David Miller für die Aufenthalte am Mount Desert Island Biological Laboratory und die gute Zusammenarbeit.

Susanne Angelow für die Einführung in die Choroid-Plexus-Zellkultur.

Ute Hettinger für die Einführung in die Molekularbiologie.

Melanie Ott für die Kapillarendothelzellen.

Dr. Tilo Schönbrodt, Dr. Martin Bultmann und Christoph Vogel für die Lösung zahlreicher Computer- und Netzwerkprobleme.

Der B-Box und deren Vorgängern für die gute Laboratmosphäre.

Allen Kollegen für die tolle Arbeitsatmosphäre und die gute Stimmung am Institut, bei Feierlichkeiten und Betriebsausflügen.

Esther Chucholl für den seelischen Ausgleich.

Uta Hülsermann für die viele Arbeit und Korrektur von Rechtschreibung und Zeichensetzung.

Céline Wilke für die psychologische Unterstützung und liebevolle Zuneigung.

Meinen Eltern, meinem Bruder Daniel-Frank und meiner Omi Josefine für die ständige Unterstützung während des Studiums und der Promotion.

Parts of this thesis were presented in:

Baehr CH, DiPasqual e KD, Fricker G, Miller DS. Regulation and Transport of FL-MTX at the Blood-Liquor Barrier of *Squalus Acanthias*. *American Journal of Physiology: Comparative Physiology*: Submitted.

Breen CM, Sykes DB, Baehr CH, Fricker G, Miller DS. Fluorescein-Methotrexate Transport in Rat Choroid Plexus Analyzed Using Confocal Microscopy. *American Journal of Physiology: Renal Physiology*. 2004; 287(3):F562-9.

Baehr CH, Fricker G. *Naunyn-Schmiedeberg's Archives of Pharmacology*. 2004; 369: Supplement 1.

Reichel V, Baehr CH, Fricker G. *Naunyn-Schmiedeberg's Archives of Pharmacology*. 2004; 369: Supplement 1.

Bauer, B., Hüwel, S., Baehr, C.H., Galla, H.J., Markert, C., Delzer, J. and Fricker, G. "Excretory Transport of Calcium Blocking Pamiles at Blood-Brain-Barrier and Choroid Plexus," *British Journal of Pharmacology*. Submitted.

Baehr CH, Fricker G. *Naunyn-Schmiedeberg's Archives of Pharmacology*. 2003; 367: Supplement 1.

Baehr CH, Bauer B, Hartz A, Miller DS, Fricker G. *MDIBL 17th Annual Report of Progress*. 2002.

Baehr CH, Fricker G. *Archiv der Pharmazie*. 2002; 335: Supplement 1.

Ritter M, Buechler C, Boettcher A, Barlage S, Schmitz-Madry A, Orso E, Bared SM, Schmiedeknecht G, Baehr CH, Fricker G, Schmitz G. Cloning and Characterization of a Novel Apolipoprotein A-I Binding Protein, AI-BP, Secreted by Cells of the Kidney Proximal Tubules in Response to HDL or Apoa-I. *GENOMICS*. 2002; 79(5):693-702.

Posters

Gordon Conference in Tilton, NH, USA, June 2004 (distinguished poster)
45. DGPT Spring Meeting in Mainz, March 2004
BioScience Workshop of Schering AG in Berlin, September 2003
44. DGPT Spring Meeting in Mainz, March 2003
Annual DPhG Meeting in Berlin, October 2002
5th Symposium on Signal Transduction in the Blood-Brain Barriers in Berlin/Potsdam, September 2002

Oral Presentations

Gordon Conference: Barriers to the CNS in Tilton, NH, USA, June 2004
The II International Workshop on Choroid Plexus, King's College, University Of London, England, April 2003

ZUSAMMENFASSUNG

Transport von ZNS-wirksamen Arzneistoffen an der Blut-Liquor-Schranke

Referent: Prof. Dr. Gert Fricker
Koreferent: Prof. Dr. Ulrich Hilgenfeldt

Neben dem cerebralen Kapillarendothel, der so genannten Blut-Hirn-Schranke (BHS), stellen die Plexus chorioidei (CP) die zweite aktive Barriere zwischen Blut und ZNS dar. Während die BHS in erster Linie Barrierefunktion hat, sind die CP unmittelbar an der Bildung der Cerebrospinalflüssigkeit (CSF) beteiligt, synthetisieren und sekretieren Proteine und haben verschiedene andere neurogene und endokrine Funktionen. Im Gegensatz zur BHS sind die CP hinsichtlich Wirkstofftransport und Funktionen bzw. Expression von Carrierproteinen weit weniger gut charakterisiert.

Seit einigen Jahrzehnten ist bekannt, dass die CP aktiv am Export von organischen Anionen aus der extrazellulären Flüssigkeit beteiligt sind (Pappenheimer et al., 1961; Villalobos et al., 2002; Miller et al., 2002; Breen et al., 2004; Baehr et al., in press). Organische Anionen wie auch Kationen in Form von kreislauffremden Xenobiotika, pflanzlichen und tierischen Giften oder auch Arzneistoffen sind von großer physiologischer, pharmakologischer und toxikologischer Bedeutung (Pardridge und Miller, 1993; Wright und Dantzler, 2004). Eingehende Untersuchungen an CP-Gewebe sind jedoch schwierig auf Grund der morphologischen Komplexität, der anatomischen Lage und der Größe des Gewebes. Die molekularen Prozesse, die funktionelle Vielschichtigkeit und die Regulation des organischen Anionentransports an der Blut-Liquor-Schranke sind daher noch weitgehend unerforscht.

Um die Transportprozesse, die für die Elimination von organischen Anionen aus der CSF verantwortlich sind, genauer untersuchen zu können, wurde ein CP-Zellkulturmodell aus Schweineepithel etabliert und auf molekularer, biochemischer und funktioneller Ebene charakterisiert. Alle CP-Kulturen waren frei von kontaminierenden Zellen, bildeten intakte Monolayer und waren vollständig differenziert. Das epitheliale Markerprotein für CP-Gewebe, Prealbumin, wurde durch Genexpressionsanalysen, immunohistochemische Färbungen und Western Blots nachgewiesen. Die Alkalische-Phosphatase- und γ-Glutamyltransferase-Aktivität sowie das CSF-Sekretionsvolumen wurden bestimmt.

Weiter wurden zwei Transportproteine, das MDR1-Genprodukt P-glycoprotein (Pgp) und das Multidrug-Resistance Associated Protein 1 (Mrp1) genauer untersucht. Neben dem Nachweis beider Proteine durch RT-PCR wurde ein semi-quantitativer Vergleich des Expressionsniveaus von Mrp1 zwischen kultivierten und frisch isolierten CP-Epithelzellen durchgeführt. Beide Transportproteine wurden in Immunfärbungen und durch konfokale Fluoreszenzmikroskopie in CP-Epithelzellen (CPEC) lokalisiert. Mrp1 konnte klar der basolateralen CPEC-Plasmamembran zugeordnet werden. Dagegen konnte Pgp nicht eindeutig an einer der CP-Membranen lokalisiert werden, sondern schien subapikal und apikal ausgebildet zu sein. In weiterführenden Western-Blot-Analysen von CP-Membranfraktionen wurde die apikale im Gegensatz zur basolateralen Fraktion gefärbt. In abschließenden *in vitro*-Untersuchungen von Pgp konnte jedoch keine signifikante funktionelle Aktivität des Transportproteins nachgewiesen werden. Der Transport von organischen Anionen wurde in einem Säugetier-CP-Modell (Ratte), einem vergleichenden Elasmobranchii-Modell (Dornhai) und in Zellkultur (Schwein) mit Hilfe des Modellsubstrats Fluorescein-Methotrexat (FL-MTX) untersucht. Die Elimination von FL-MTX aus der CSF erfolgt spezifisch und konzentrativ und ist ein metabolismus- und Na^+-abhängiger Zwei-Stufen-Prozess. Des Weiteren konnte gezeigt werden, dass die Regulation des organischen Anionentransports über die Proteinkinasen (PK) PKC und PKA erfolgt. Die Identifizierung der verantwortlichen Hormone bleibt zu klären.

ABSTRACT

Functional and Molecular Aspects of Xenobiotic Transport in Choroid Plexus

Supervisor: **Prof. Dr. Gert Fricker**
Co-Supervisor: **Prof. Dr. Ulrich Hilgenfeldt**

The choroid plexus (CP) epithelium forms the blood-cerebrospinal fluid (CSF) barrier, which along with the blood-brain barrier (BBB) capillary endothelium maintains the fluid environment of the brain. The CP not only secretes CSF, but also transports potentially toxic xenobiotics and waste products of neural metabolism to the blood for eventual clearance in kidney and liver.

For several decades it has been known that the CP is actively involved in removing organic anions and other organic compounds from the extra-cellular fluid (Pappenheimer et al., 1961; Villalobos et al., 2002; Miller et al., 2002; Breen et al., 2004; Baehr et al., in press). However, studying CP is difficult, due to complex morphology, anatomical location and small size of the tissue and little is known about the molecular mechanisms, functional complexity and hormonal regulation of organic anion secretion.

To further elucidate the underlying mechanisms of organic anion transport across CP epithelium, a primary porcine CP cell culture model was established and characterized on a molecular and functional basis. All cultures were free of contaminating cells, developed intact monolayers and were fully differentiated. Expression of marker protein prealbumin was demonstrated in isolated CP epithelial cells (CPEC) using RT-PCR, immunostaining and Western blot analyses. Alkaline phosphatase and γ-glutamyl transferase were quantified and cerebrospinal fluid secretion was measured. In addition, two active transport proteins, the MDR1 gene product P-glycoprotein (Pgp) and the multidrug-resistance associated protein 1, were assessed by RT-PCR, immunohistological staining and in Western blots of isolated membrane fractions. Integrity of fully differentiated monolayers was ensured by TEER measurements as well as permeability analyses using marker compounds. Further, functional analyses of Pgp were carried out.

Organic anion transport was studied in a mammalian (rat), a comparative elasmobranch and in the *in vitro* porcine CPEC culture model, using the model compound

fluorescein-methotrexate (FL-MTX). FL-MTX transport was shown to be a specific and concentrative, Na^+-dependent and metabolism-dependent two-step process. Finally, for the first time, these studies demonstrate that organic anion transport is regulated by protein kinase C (PKC) and PKA. Responsible hormones remain to be identified.

2,4-D	2,4-Dichlorophenoxyacetic Acid
5-CF	5-Carboxyfluorescein
AB	Apical To Basolateral
ABC	ATP-Binding Cassette
aCSF	Artificial Cerebrospinal Fluid
AP	Alkaline Phosphatase
BA	Basolateral To Apical
BBB	Blood-Brain Barrier
BCEC	Brain Capillary Endothelial Cells
BCSFB	Blood-Cerebrospinal Fluid Barrier
BIM	Bisindolylmaleimide
BSA	Bovine Serum Albumin
CNS	Central Nervous System
Concn	Concentration
CPEC	Choroid Plexus Epithelial Cells
CSF	Cerebrospinalfluid
DANN	Deoxyribonucleic Acid
DMEM	Dulbecco´s Minimal Essential Medium
DMSO	Dimethylsulfoxide
dpm	Decays per Minute
EDTA	Ethylenediaminetetraacetate
FA	Folic Acid
FCS	Fetal Calf Serum
FDA	Food and Drug Administration
FITC	Fluorescein-Isothiocyanat
FL-MTX	Fluorescein-Methotrexate
Forsk	Forskolin
γ-GT	γ-Glutamyl Transferase
GBq	Gigabecquerel
HBSS	Hank's Balanced Salts Solution
HEPES	4-(2-Hydroxyethyl)-1-Piperazinethansulfonic Acid
Ig	Immunoglobuline
kDa	Kilodalton
KRB	Krebs-Ringer Buffer
LTC4	Leukotriene C_4
MDR	Multidrug-Resistance
Mrp	Multidrug-Resistance Associated Protein
MTX	Methotrexate
MW	Molecular Weight
NaCN	Sodium Cyanide
OD	Optical Density
Ouab	Ouabain
PAH	*p*-Aminohippuric Acid
P_{app}	Apparent Permeability Coefficient
PBS	Phosphate Buffered Saline
PCR	Polymerase Chain Reaction
Pgp	Permeability Glycoprotein
PK	Protein Kinase
PMA	Phorbol-12-Myristate-13-Acetate

Prob	Probenecid
RNA	Ribonucleic Acid
RT-PCR	Reverse Transcribed Polymerase Chain Reaction
SEM	Standard Error of the Mean
TA	Taurocholate
TEER	Transepithelial Electrical Resistance

1 INTRODUCTION

1.1 Barriers to the Brain

The brain is most sensitive to changes in its surrounding environment and extracellular homeostasis is crucial to its function. Separated from blood flow it shuts out most water-soluble compounds, maintaining chemical stability and protecting itself from chemical injury. Further, endogenous metabolites and foreign chemicals (xenobiotics) are actively removed from the central nervous system (CNS) (Cserr, 1971; Cserr et al., 1980; Spector and Johanson, 1989; Segal, 2001; Zheng, 2001).

Treatment of certain CNS diseases and cancers is difficult. Besides compartmentalization and consequent poor delivery to the target, metabolism and rapid efflux as well as drug-drug and drug-metabolite interactions reduce the therapeutic potential of drugs in the brain (Saunders et al., 1999; Miller et al., in press).

Anatomically, three structures separate brain and blood flow: the network of brain capillaries, the choroid plexus and the arachnoid membrane (Spector and Johanson, 1989). Both the endothelial cells of blood-brain barrier (BBB) and the blood-cerebrospinal fluid barrier (BCSFB) formed by the choroid plexus (CP) actively regulate type and concentration of molecules transported to and from brain extra-cellular fluid (ECF), cerebrospinal fluid (CSF) and intra-cellular fluid (ICF) (figure 1, Nilsson, 1992). The arachnoid membrane, located between pia and dura mater and composed of 12-15 layers of flat epithelial cells, is largely impermeable for water-soluble compounds and does not actively regulate movement of molecules (Johanson, 1998).

The term “Blut-Hirn-Schranke” or blood-brain barrier was first coined in 1900 by Lewandowsky, who studied penetration of potassium ferrocyanide into the brain. Further experimental evidence of this physical barrier between brain and blood was demonstrated by Paul Ehrlich (1885, 1906). Injecting water-soluble dyes (e.g. the aniline dye coerulean-S) into rats, he noted a conspicuous absence of blue stain in the brain and spinal cord. Experiments by Bouffard (1906) and Goldmann (1909) confirmed these findings. They showed that injecting trypan blue into the spine of animals only stained brain and cerebrospinal fluid (CSF), but not the whole animal. Stern and Gautier (1921, 1922) studied the routes of solutes from blood into CSF across the choroid plexus and coined the term “barrière hématoencéphalique”. How-

ever, it was not until 1941 that the blood-CSF barrier at the choroid plexus was recognized as second barrier between blood and brain (Broman, 1941).

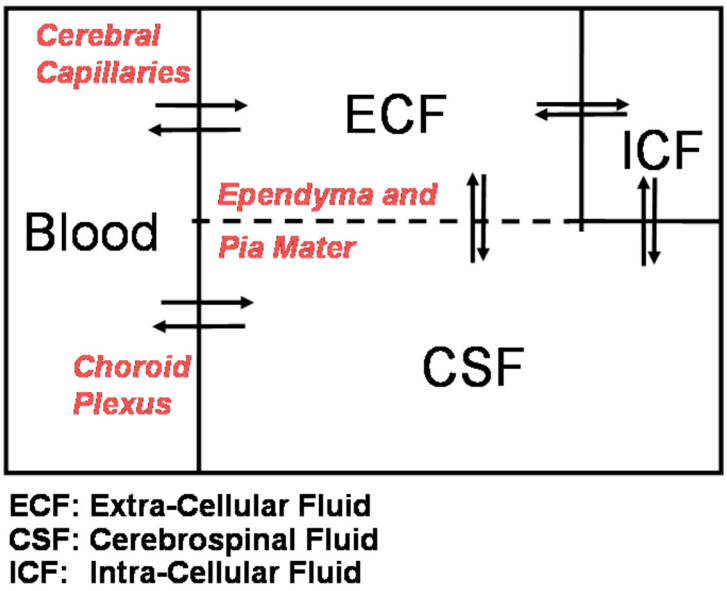

Figure 1: Fluid Compartments of the Brain. The blood-brain barrier separates blood stream from extra-cellular fluid (ECF) and choroid plexus separates blood stream from cerebrospinal fluid (CSF). ECF and CSF are separated by fenestrated ependyma and pia mater, allowing for free diffusion of molecules (Nilsson et al., 1992).

1.2 Choroid Plexus Structure

Choroid plexus are reddish, highly vascularized patches of tissue located within the ventricular system of the brain (Spector and Johanson, 1989). CP tissue is present in all mammalian species, with the exception of *Amphioxus* (Nilsson et al., 1992). Generally, CP makes up 0.2% of total brain in weight or 2-3 g in humans, with 90% of the tissue equally divided between lateral and third ventricles and 10% present in the forth ventricle (Johanson, 1999).

In contrast to the capillary endothelium of the BBB, CP endothelium is fenestrated. The blood vessel lumens form a continuous space with the adjacent extracellular (interstitial) space (figure 2). The surrounding monolayer of polarized epithelial cells is interconnected by tight junctions (figure 2, figure 3), separating apical and basolateral epithelial membranes, with apical membranes facing the ventricular space (CSF) and basolateral membranes facing the blood compartment (Spector and

Johanson, 1989; Suzuki et al., 1997). Thus, the CP epithelium, but not endothelium forms the barrier structure separating blood and CSF.

Tight junctions expressed by CP epithelia form parallel strands resembling those of Sertoli cells of the blood-testis barrier and myelin sheaths of oligodendrocytes (Wolburg et al., 2001). Characteristic of CP epithelial tight junctions are *zonula occludens* protein ZO-1, occludins and claudins. Like the BBB, the BCSFB also expresses ZO-1 and occludins. Claudin 1, 2 and 11 are specific to the BCSFB, 3 and 5 specific to the BBB (Watson et al., 1991; Lippoldt et al., 2000; Wolburg et al., 2001).

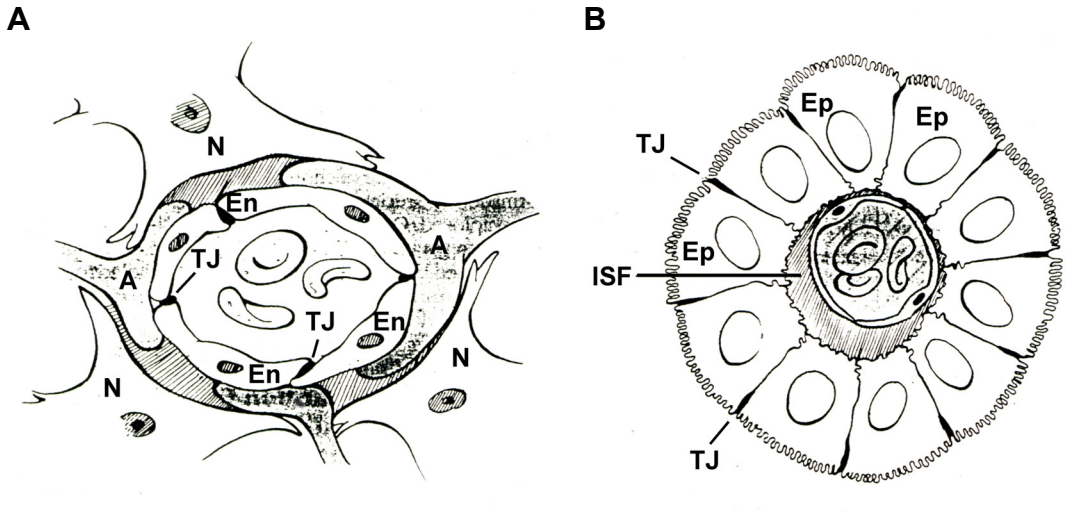

Figure 2: Endothelial Cells of the BBB (A) and Epithelial Cells of the BCSFB (B) with Neurons (N), Astrocytic Foot Processes (A), Endothelial Cells (En), Epithelial Cells (Ep), Tight Junctions (TJ). The anatomical barrier at the BBB is formed by capillary endothelial cells. At the BCSFB, capillaries are fenestrated and epithelial cells express TJ, restricting movement of molecules (Spector, 1999).

The CP bears resemblance to proximal tubules in its epithelial ultrastructure and, like the kidney, transports near isotonic fluid across its epithelium (Spector, 1999). Like the kidney providing a stable chemical composition of blood, the CP is responsible for stability and conduciveness of the CSF. However, instead of only acting as a filter, CSF is produced within the CP and enriched with nutrients derived from blood flow. Fluid and molecules move across a large surface area produced by tightly packed villi at the apical membrane and infoldings at the basolateral membrane. CP epithelium is also equipped with high density mitochondria, a developed golgi-apparatus and endoplasmatic reticulum. Thus, bidirectional transport is available for a variety of brain regulatory factors, in addition to fluid and other molecules (Spector, 1999).

1.3 Choroid Plexus Function

The CP provides a stable chemical environment for brain and CNS, ensuring nourishment and protection. In addition to forming a physical barrier between blood and CNS, it performs vital functions, including production of CSF or liquor, synthesis and secretion of proteins and neurogenic and endocrine regulation (Spector and Johanson, 1989). The CP acts as source, supplying the brain with essential nutrients, vitamins and other solutes, and as sink, removing proteins and catabolites (Spector, 1999). Crossing CP from the blood stream, compounds reach the CSF and can access the brain and CNS. Compounds in the CSF can be taken up by CP or washed out with CSF into venous blood.

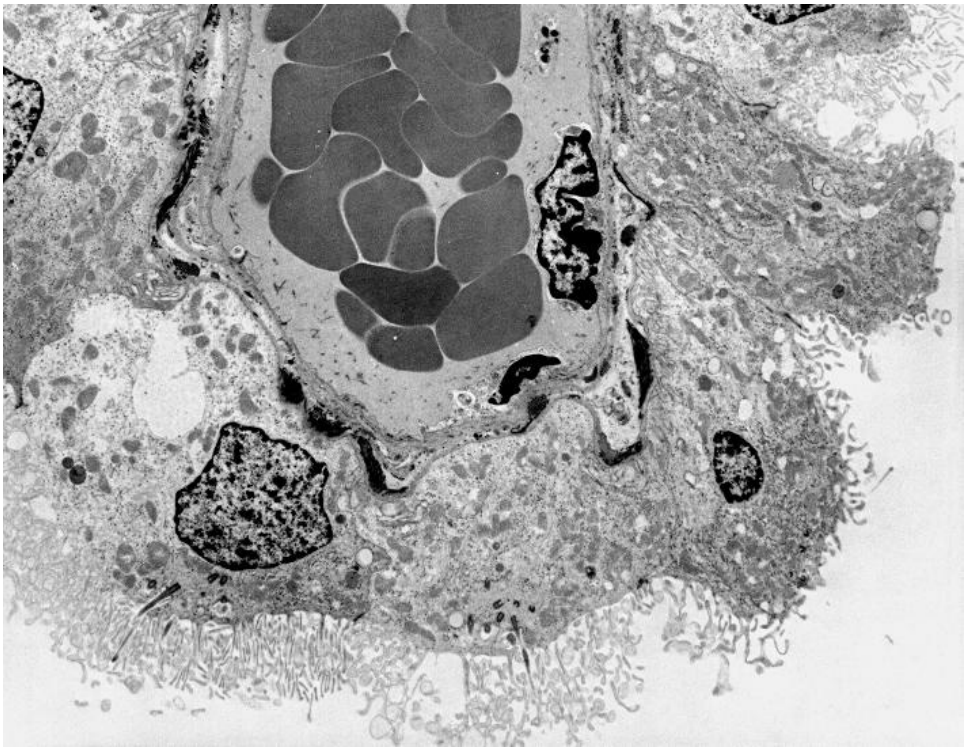

Figure 3: Rat Choroid Plexus TEM Cross Section. The micrograph shows a CP capillary surrounded by a monolayer of epithelial cells, with its polarized ultrastructure, intercellular tight junctions and microvillous ventricular membranes (Villalobos et al., 1997).

One of the most important CP functions is CSF secretion (Spector and Johanson, 1989). CSF baths the brain and circulates between the ventricles through channels or foramina. The total CSF volume in an adult human brain is approximately 140 ml, with fluid filling cortical and cerebellar subarachnoid spaces and basal cisterns (80 ml), ventricles (30 ml) and spinal regions (30 ml) (figure 4; Johanson, 1995). The

total volume is renewed every 4 to 5 hours, with 90% of CSF produced by CP tissue, the remaining 10% by extrachoroidal sources (Cserr, 1971). CSF flows from the telencephalon to rhombencephalon into the subarachnoid space. From there it flows to the fourth ventricle and into the cisterna magna and basal cisterns, before reaching venous blood via arachnoid villi in superior sagittal sinus (figure 4).

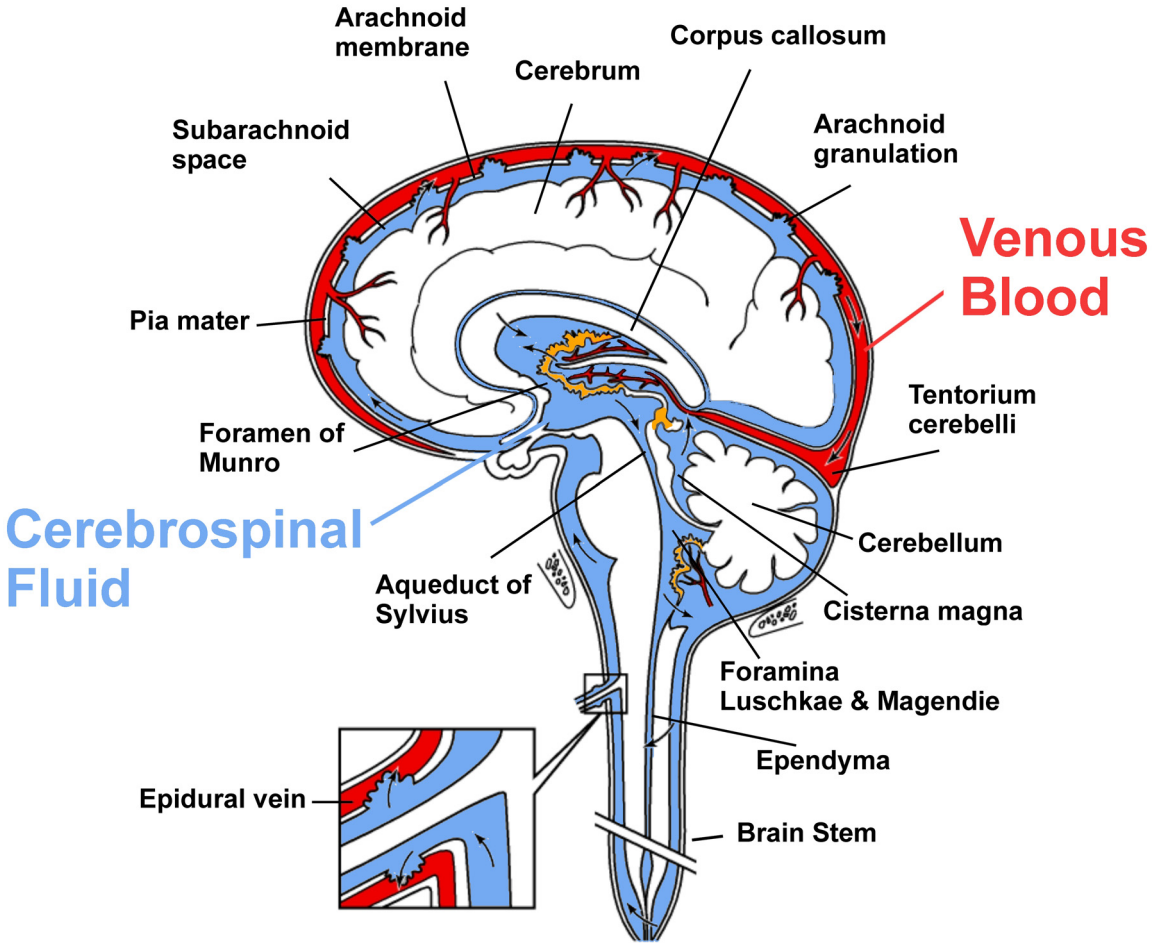

Figure 4: Brain CSF Circulation. CSF is produced by choroid plexus epithelial cells and circulates through ventricular cavities into subarachnoid spaces. Absorption into the venous blood (red) occurs through arachnoid villi in superior sagittal sinuses and along the optic, olfactory and spinal nerve sheaths (inset) (Fishman, 2000).

CSF is a clear colorless solution (pH 7.35), consisting of 99% water and 1% protein and micronutrients (table 1). Major ions are Na^+, Cl^- and HCO_3^-, concentrated by active secretion mechanisms (Davson, 1955). The CSF protein content of 15 to 40 mg/100 ml corresponds to 0.3% of plasma protein (Saunders et al., 1999). Even though total protein content is low, relative concentrations of amino acids are comparable to plasma (Davson and Segal, 1996).

Several proteins, including transthyrethin, ceruloplasmin and transferrin, are specific to the CP and CSF within the brain, synthesized and secreted by either CP or brain parenchyma (Nilsson et al., 1992). Other CP proteins synthesized include neuropeptides, growth factors and cytokines (Chodobski and Szmydynger-Chodobska, 2001).

Many protein receptors are expressed by the CP epithelium and polypeptides can access the CNS via the CP (Chodobski and Szmydynger-Chodobska, 2001; Smith et al., 2004). For example, there is increasing evidence that the CP is involved in receptor-mediated hormone signaling, with several hormone receptors more highly expressed in CP tissue than in other regions of the brain, including bradykinin, insulin, vasopressin and endothelin receptors (Pansky and Hatfield**,** 1978; Baskin et al., 1989; Kohzuki et al., 1991, Chen et al., 2000; Chodobski et al., 2000; Takano et al., 2003). Availability of polypeptides to the brain is regulated via saturable and non-saturable pathways, including receptor-mediated transcytosis (e.g. insulin) and peptide transporters (e.g. PEPT1/2) (Reinhardt and Bondy, 1994; Thomas et al., 2001; Shen et al., 2003; Ocheltree et al., 2004).

Moreover, CP not only supply the brain with proteins, but also clear circulating polypeptides from within the CSF (Chodobski and Szmydynger-Chodobska, 2001). The tissues express a multitude of receptors and metabolizing enzymes at the apical, CSF-facing membranes, acting like sieves within the CSF. For example, leptin and amyloid β-protein were shown to concentrate in CP after intracerebroventricular injection (Maness et al., 1998; Monro et al., 2002).

The CP, with its array of metabolizing enzymes and coupled transepithelial vectorial efflux of conjugated metabolites into the blood stream, is an effective detoxification system within the brain (Ghersi-Egea and Strazielle, 2001). In fact, the CP is one of the main sites of xenobiotic metabolism (el-Bacha and Minn, 1999).

Xenobiotics metabolized at the CP follow the two-phase biotransformation and excretion pathway known from other biological systems (Ghersi-Egea and Strazielle, 2001).

Table 1: Typical Cerebrospinal Fluid (CSF) and Plasma Composition (Fishman, 2000)

	CSF	*Plasma*	*CSF/plasma ratio*
Electrolytes (mEq/l)			
Na^+	138	138	1.0
K^+	2.8	4.5	0.6
Cl^-	119	102	1.2
HCO_3^-	22	24	0.9
Ca^{2+}	2.1	4.8	0.4
Mg^{2+}	2.3	1.7	1.4
PO_4^{3-}	0.5	1.8	0.3
Metabolites (mM)			
Glucose	3.3	5.0	0.7
Lactate	1.6	1.0	1.6
Pyruvate	0.08	0.11	0.7
Urea	4.7	5.4	0.9
Creatinine	0.09	0.14	0.7
Amino acids (µM)			
Alanine	26.0	350	0.1
Arginine	22.4	80.9	0.3
Aspartic acid	0.2	2.0	0.1
Asparagine	13.5	112	0.1
Glutamic acid	26.1	61.3	0.4
Glutamine	552	641	0.9
Glycine	5.9	283	0.02
Histidine	12.3	79.8	0.2
Isoleucine	6.2	76.7	0.1
Leucine	14.8	155	0.1
Lysine	20.8	171	0.1
Methionine	2.5	27.7	0.1
Ornithine	3.8	73.5	0.1
Phenylalanine	9.9	64.0	0.2
Phosphoserine	4.2	8.3	0.6
Serine	29.5	140	0.2
Taurine	7.6	77.2	0.1
Threonine	35.5	166	0.2
Tyrosine	9.5	73.0	0.1
Valine	19.9	309	0.1
Proteins (mg/l)			
Total protein	350	70,000	0.005
Albumin	155	36,600	0.004
Transferrin	14.4	2,040	0.007
IgG	12.3	9,870	0.001
IgA	1.3	1,750	0.001
IgM	0.6	700	0.001

Phase I reactions introduce polar groups into molecules via oxidation, reduction, hydrolysis and also include isomerization reactions. These are followed by phase II reactions, resulting in conjugated products that are more polar, more hydrophilic and

more strongly acidic, thus more easily excreted (Abou-Donia, 1992). The CP possess relatively large amounts of several isoforms of phase I and phase II metabolism enzymes, comparable to ependyma and endothelial cells of brain capillaries (Lowndes et al., 1994). Phase I enzymes include epoxide hydrolase, 7-benzoxyresorufin-O-dealkylase and several cytochromes P450 (CYP; CYP1A1 and CYP1A2), some of which displaying levels of activity comparable to liver (Ghersi-Egea et al., 1994; Morse et al., 1998).

Among phase II metabolizing enzymes, CP tissue expresses UDP-glucuronosyl transferase, γ-glutamyl transpeptidase and glutathione-S-transferase (GST; Shine and Haber, 1981; Johnson et al., 1993; Leininger-Muller et al., 1994; Martinasevic et al., 1998; Ghersi-Egea and Strazielle, 2001). Moreover, several metabolic enzyme systems are exclusively localized to CP within the brain, including glutathione peroxidase and microsomal GST (Tayarani et al., 1989; Otieno et al., 1997; Graff and Pollack, 2004)

1.4 Transport across the Choroid Plexus Epithelium

Transport of xenobiotics and endogenous metabolites is highly regulated in the CNS. The primary interfaces between blood circulation and brain are capillary endothelial cells of the BBB and choroid plexus epithelial cells (CPEC) of the BCSFB (Lee et al., 2001).

In the past, CP size and surface area estimations led to the assumption that the BCSFB is much less involved in controlling the brain's surrounding environment compared to the BBB and its exchange capacity was assumed to be 5000-times lower (Pardridge et al., 1981). However, detailed morphometrical analyses revealed a relatively comparable surface area for brain capillary endothelium and choroid plexus. In rat, calculated apical CP membrane surface area (75 cm^2) is three times the basolateral membrane surface area (25 cm^2) and only just half the brain's endothelial surface (155 cm^2, Keep and Jones, 1990).

Several *in vivo*, *ex vivo* and *in vitro* techniques and models have been used to study transport across the CP epithelium, each with its advantages and drawbacks (Johanson, 1999; Lee et al., 2001). *In vivo* techniques are difficult, as the experimental procedure is involved and requires surgical skill. Common methods include the serial sampling of CSF following drug administration and deconvolution of data to

determine transport profiles. Isolated tissue is used in extracorporal perfusion studies or in *in situ* chamber isolations of CP. In *ex vivo* experiments CP tissue is mounted as a sheet between Ussing chambers or incubated in artificial CSF (aCSF). *In vitro* methods include primary culture of isolated CPEC from a variety of different species or culture of immortalized epithelial cells. Both primary and cell line CPEC cultures develop an impermeable monolayer and display characteristics of CPEC in vivo.

Factors influencing movement of compounds across the CP epithelium into the CSF and eventual brain penetration include barrier characteristics, physiological, physicochemical and pharmacokinetic parameters (Pardridge, 1993; Saunders et al., 1999; Lee et al., 2001; Begley, 2004). High plasma concentrations, low volumes of distribution, slow metabolism and slow excretion favor uptake into the brain. Important physicochemical parameters are size, lipophilicity and electrical charge. Generally, compounds larger 5000 kDa are restricted from entering the brain and the more hydrophilic and charged molecules are less likely to passage across the BCSFB. There are several routes for compounds to traverse the BCSFB (Suzuki et al., 1997; Saunders et al., 1999; Huber et al., 2001; Lee et al, 2001; Begley, 2004; Graff and Pollack, 2004). Some cross via paracellular diffusion, with intercellular movement limited by tight junctions, or transcellular diffusion, restricted by amphiphilic lipid bilayers and cytoplasm composition. Inorganic ions are transported through ion channels, e.g. K^+-gated, or ion-symport channels, e.g. the Na^+-K^+-Cl^--cotransporter. Some compounds are actively moved by facilitated diffusion, such as glucose by GLUT-1, by active antiport transport as Na^+,K^+-ATPase and A-system amino acid transport or receptor-mediated endocytosis, e.g. transferrin and insulin. Finally, some drugs and compounds are actively excreted by energy consuming efflux pumps, e.g. multidrug-resistance and multidrug-resistance associated proteins.

1.5 Transporters of the Choroid Plexus

Most compounds cross cellular membranes via the transcellular route, with tight junctions limiting entry via paracellular pathways. Levin (1980) demonstrated a positive correlation between lipophilicity (octanol/water partition coefficient and square route of molecular weight) and brain permeation across the BBB for 27 different compounds. Notably, some compounds did not fit the correlation, including doxorubicin, epipodophyllotoxin, vincristine and bleomycin. The static wall concept alone was not

able to explain the poor distribution of these compounds into the brain and the idea of active efflux proteins at the BBB and BCSFB was proposed (Kusuhara and Sugiyama, 2001).

In general, transporters can be separated into solute carrier proteins and others and are classified into active and passive transporters (figure 5, Hedinger et al., 2004). In passive transport, solutes follow their electrochemical gradient. In contrast, active transport creates ion/solute gradients across membranes, utilizing energy. Depending on the directness of coupling to energy utilization, such as adenosine-triphosphate (ATP) hydrolysis, these transporters are classified into primary or secondary active transporters.

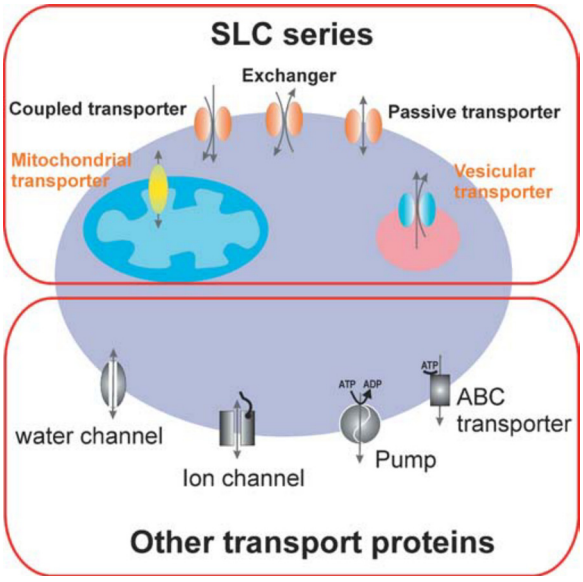

Figure 5: Solute Carrier (SLC) - and Non-SLC-Transporters Expressed in Plasma Membranes and in Intracellular Compartment Membranes (Hedinger et al., 2004).

Distribution of xenobiotic compounds across cellular polarized membranes is dependent on presence, density and distribution of transporters in the tissue (Miller et al., in press). For example in kidney, excretory transporters are located at the basolateral membrane, where they move compounds to the apical side for eventual excretion into bile or urine (figure 6, Wright and Dantzler, 2004). Consistent with this functional polarization, transporters of the organic anion transporter (OAT) family, e.g. OAT1 and OAT2, and organic cation transporter (OCT) family, e.g. OCT2, are present at the basolateral membrane, mediating anion and cation transport, respectively

(Sweet et al., 1997; Sweet et al., 1999; Motohashi et al., 2002; Sweet et al., 2003; Denk et al., 2004; Ljubojevic et al., 2004; Wright and Dantzler, 2004; Miller et al., in press). Drug efflux transporters, such as the multidrug-resistance gene product P-glycoprotein (Pgp) or the multidrug-resistance associated protein 2 (Mrp2), are located at the apical membrane and actively excrete compounds (Harris et al., 2001; Mahmood et al., 2001; Nies et al., 2002; Wright and Dantzler, 2004). A similar polarized distribution is seen in capillary endothelial cells of the BBB, where compounds are excreted from brain back into the blood stream for eventual elimination in urine and bile (Golden and Pollack; 2003; Schinkel et al., 2003, Sun et al., 2003; Begely, 2004; Ohtsuki, 2004; Miller et al., in press)

The choroid plexus is atypical in its distribution of transporters (Rao et al, 1999; Gao and Maier, 2001; Lee et al., 2001; Sweet et al., 2001; Miller et al., in press). Many transporters do not follow the functional pattern observed in kidney or brain endothelium; rather protein localization is reversed (figure 6). Excretory transporters present at the basolateral membranes in kidney, liver or brain are localized to the CSF-facing side in CP epithelia and efflux transporters are found at basolateral membranes. Thus, not only presence and density, but also the polarized distribution of relevant transport proteins has to be considered when examining transport at the BCSFB (Miller et al., in press).

To date, a total of eleven transporter families with almost 30 individual transport proteins, of which 13 are expressed at moderate to high levels, are known to be expressed at the CP (Choudhuri et al., 2003). However, many are expressed at low levels and only 8 are localized to specific membrane (figure 6; Miller et al., in press). Table 2 summarizes important properties of transporters expressed in and localized to CP membranes. The transporters are members of the Solute Carrier family (SLC) and members of the active and energy consuming ATP-binding cassette (ABC) transporter family. Gene locus, Entrez database accession number, tissue distribution and reference summaries are listed.

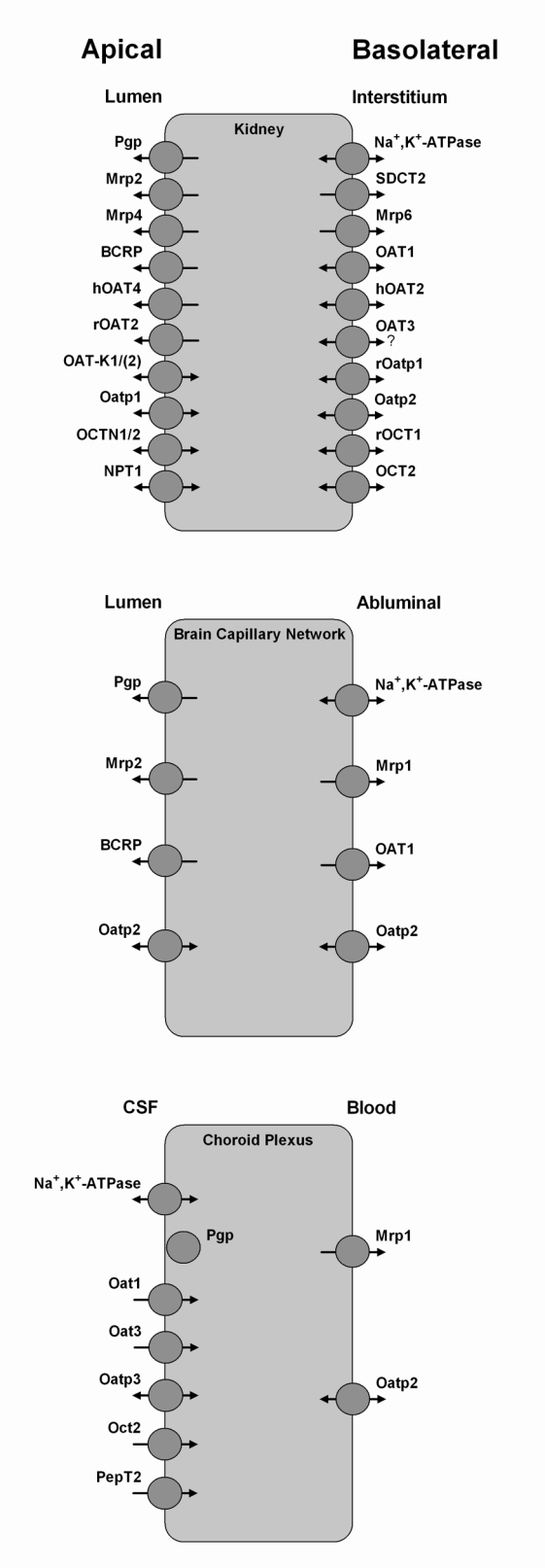

Figure 6: Localization of Transporters in Kidney Epithelium, Brain Endothelium and Choroid Plexus. (r: rat and h: human, only). Notably, the expression of a number of transporters is reversed at the CP, when compared to expression in other barrier structures such as kidney or blood-brain barrier.

Table 2: Properties of Solute Carrier and ABC-Type Transporters at the Choroid Plexus

Isoform	*Gene Locus Accession ID*	*Tissue distribution*	*Transport mode*
SLC15A2 PEPT2	3q13.3-q21 NM_021082	kidney, lung, brain, mammary gland, bronchial epithelium	H^+-dependent cotransport
SLC21A5 OATP2	4 (r) 6G2 (m) NM_131906 NM_030687	Liver, blood-brain barrier, ciliary body, retina	Na^+-independent bidirectional transport
SLC21A7 OATP3	4q44 (r) 6G2 (m) NM_030838 NM_020495	jejunum, neural cells, hypothalamus, thalamus, olfactory bulb, brain endothelium	Na^+-independent bidirectional transporter
SLC22A2 OCT2	6q21.1-2 AF210455 AF097518 AY050498	human: kidney (basolateral membrane of proximal tubules), placenta, brain (neurons), rat: thymus, choroid plexus	membrane potential dependent, Na^+-independent, facilitative diffusion
SLC22A6 OAT1	11q12.3 AF057039 AB009697	kidney, basolateral membranes of proximal tubules, placenta, brain,	Na^+-dependent organic anion exchange
SLC22A8 OAT3	11.12.3 AF097491	kidney, basolateral membranes of proximal tubules, liver, brain, eye, skeletal muscle, developing bone	Na^+-dependent organic anion exchange
ABCB1 MDR1	7q21.1 AF016535	intestine, heart, kidney, brain (endothelium, astrocytes, microglia)	ATP-hydrolysis coupled efflux
ABCC1 Mrp1	16p13.1 L05628	ubiquitous	ATP-hydrolysis coupled efflux

1.5.1 The Solute Carrier Families of Transport Proteins

The Solute Carrier (SLC) families of transporters include passive transporters, ion coupled transporters or exchangers and are classified according to the Human Genome Organization (HUGO) Nomenclature Committee Database (Hedinger et al.,

2004). There are more than 300 SLC transporter genes identified and constantly additional transporters are being identified. Members of several families are identified at the CP in humans and other mammals.

1.5.1.1 The SLC15 Family

The SLC15 family contains four members according HUGO (Hedinger et al., 2004). All members of this proton-oligopeptide cotransporter family are predicted to contain 12 transmembrane domains (TMD) and transport short-chain peptides and peptide mimetics against concentration gradients, using proton-motive force. Two members, PEPT1 and PEPT2, are expressed in polarized epithelia, taking up substrates into cells. For example in the kidney, peptides are reabsorbed by SLC15 proteins. In the CP, PEPT1 and PEPT2 are expressed, but only PEPT2 was localized to the apical membrane by immunohistochemistry (Shu et al., 2002; Choudhuri et al., 2003). Here, PEPT2 is thought to mediate uptake of peptides and peptide-like compounds from CSF (Ocheltree et al., 2004). ,

PEPT2, in contrast to PEPT1, is a high affinity, low-capacitance transporter (Daniel, 2004; Daniel and Kottra, 2004). Both PEPT, exhibiting different proton to substrate stoichiometry, have the ability to transport any of the 400 different dipeptides and 8000 different tripeptides, derived from the 20 proteinogenic L-α-amino acids, regardless of charge, in addition to any peptide-like compounds (Daniel and Rubio-Aliaga, 2003; Daniel and Kottra, 2004). Well-known substrates include alafosfalin, 5-aminolevulinic acid, β-lactam antibiotics, bestatin, carnosine, cefadroxil, glycylsarcosine, L-Val-ACV, nateglinide and inhibitors are, besides low temperature ($4^{o}C$), amoxicillin, ampicillin, bestatin, cefadroxil, cefdinir, ceftibuten, cefixime, cephalexin, cephradine, cyclacillin, glibenclamide, L-Val-ACV, *p*-aminohippurate and quinapril (Ganapathy et al.,1995; Ganapathy et al.,1997; Ganapathy et al.,1998; Doring et al., 1998; Sawada et al., 1999; Fujita et al., 2004; Neumann et al., 2004; Ocheltree et al., 2004; Teuscher et al., 2004)

1.5.1.2 The SLC21 (OATP) Family

Two organic anion transport proteins (OATPs, SLC21 family) of the “liver”-like organic anion transport system are expressed in CP tissue, mediating bidirectional, sodium-independent transport of a wide range of amphipathic endogenous and ex-

ogenous organic compounds (Gao and Meier, 2001; Hagenbuch and Meier, 2004; Miller et al., in press). According to HUGO, the SLC21 family series contains 11 members (Hedinger et al., 2004). OATPs contain 12 TMDs with an extracellular loop between TMD 9 and TMD 10. The OATPs are organic anion exchangers, Na^+- independent bidirectional transporters, coupling uptake of anions to the export of counter ions such as bicarbonate, glutathione and/or glutathione-*S*-conjugates (Hagenbuch and Meier, 2004). Even though a large number of OATPs (>50) have been cloned from various species, only few have been identified in CP tissue (Miller et al., in press). Choudhuri et al. (2003) revealed high expression levels of OAPT3 and moderate expression levels for OATP2, OATP8 and OATP12 in CP tissue of rat. Immunohistochemical analyses revealed OAPT2 and OATP3 localization to basolateral and apical CP membranes, respectively (Gao et al., 1999; Ohtsuki et al., 2003; Ohtsuki et al., 2004).

Substrates and inhibitors of OATP2 and OATP3 include a number of bile salts, hormones, amino acids and peptides (Asaba et al., 2000; Konig et al., 2000; Gao et al., 2000; Gao and Meier, 2001; Kusuhara and Sugiyama, 2001; Montfoort et al., 2003; Breen et al., 2004; Hagenbuch and Meier, 2004). Interestingly, OATP2 transports the cardiac glycoside digoxin. Further, compounds include *N*-(4,4-azo-n-pentyl)-21-deoxyajmalinium, biotin, bile acids, bromosulfophthalein, cholyltaurine, dehydroepiandrosterone, dehydroepiandrosterone sulfate, 17β-glucuronide-estradiol, estrone sulfate, fluorescein-methotrexate, leukotriene C_4 (LTC_4), monoglucuronosyl bilirubin, ouabain, [D-penicillamine^{2,5}]enkephalin, pravastatin, rocuronium bromide and bromosulfophthalein.

OATP3 substrates include dehydroepiandrosterone, 17β-glucuronide-estradiol, estrone sulfate, glycochenodeoxycholate, glycocholate, glycodeoxycholate, glycoursodeoxycholate, sulfotaurolithocholate, taurochenodeoxycholate, taurocholate, taurodeoxycholate, tauroursodeoxycholate, thyroxine and triiodo-L-thyronine. Inhibitors include cholate, dehydroepiandrosterone sulfate, digoxin, probenecid, bromosulfophthalein, taurocholate, thyroxine and triiodo-L-thyronine.

1.5.1.3 The SLC22 (OCT/OAT, OCTN) Family

One of the most prominent families of transporters is the SLC22 family, with a total of 18 members identified by HUGO (Hedinger et al., 2004). The family includes OCTs (SLC22A1-3), zwitterion/cation transporters (OCTNs, SLC22A4-5), OATs (SLCA6-11), URAT1 (SLC22A12) as well as hCT2 not named by HUGO and several orphan transporters (Koepsell and Endou, 2004). The SLC22 transporter family is characterized by 12 predicted α-helical TMD, with a large extracellular loop between TMD1 and TMD2. OCTs are uniporters, mediating facilitated diffusion in one direction, OAT1, OAT3 and URAT1 are anion exchangers and OCTN2 is a Na^+/carnitine co-transporter.

Interestingly, in the kidney, OCT2 expression levels were gender dependent, with higher levels in males, but levels in females only comparable after administration of testosterone (Koepsell et al., 2003). In the CP, expression levels of Oct2 were low when compared to Oct1 and Oct3 and it is likely that other organic cation transport systems exist (Sweet et al., 2001; Choudhuri et al., 2003; Miller et al., in press).

In CP tissue, OCT2 is localized to the apical membrane. In the kidney, where OCT2 is localized facing the interstitium, the transporter mediates the first step in polyspecific organic cation reabsorption via membrane-potential dependent, Na^+-independent, facilitative diffusion. Thus in the CP, OCT2 might be involved in clearing the CSF from organic cations (Gorboulev et al., 1997; Sweet and Pritchard, 1999; Sweet et al., 2001). OCT2 carries a range of compounds, including neurotransmitters, drugs and other cations (Montfoort et al., 2003). Well known substrates of OCT2 include tetraethylammonium (TEA), 1-methyl-4-phenylpyridinium (MPP), choline, *N*-methylnicotinamide, norepinephrine, histamine, dopamine, serotonin, and the anti-parkinsonian drugs memantine and amantadine (Busch et al., 1998; Miller et al., 1999; Koepsell et al., 2003; Koepsell and Endou, 2004). Inhibitors include corticosterone, cyanine 863, desipramine, decynium, KCN, quinine, procainamide, 3-*O*-methylisoprenaline, tetramethylammonium.

Of the OAT family, the “kidney”-type organic anion transporters OAT1 and OAT3 are localized to apical CP membranes in human tissue and rOat3 was localized to apical membranes, with low levels of Oat1 and moderate levels of Oat3 expressed (Nagata et al., 2002; Choudhuri et al., 2003; Alebouyeh et al., 2003; Miller et al., in press). In the kidney, the first step of polyspecific organic anion excretion is

anion uptake by a polyspecific α-ketoglutarate/organic anion transport system, driven by a large α-ketoglutarate gradient, in turn maintained by a separate Na^+/dicarboxylate co-transport system, deriving its energy from the Na^+-gradient produced by basolateral Na^+,K^+-ATPase (Pritchard et al., 1999; Gao and Meier, 2001). In the CP, this organic anion transport system is reversed, with Na^+,K^+-ATPase and α-ketoglutarate/organic anion transport systems located to the apical membrane and OATs removing organic anions from the CSF.

However, functional studies with rat CP tissue using *p*-aminohippurate and benzylpenicillin as substrates demonstrated that nearly all transport is mediated by Oat3 (Nagata et al., 2002). Conversely though, studies on an Oat3-null mouse indicate that organic anion transport across the CP has not been solved in its entirety (Sykes et al., 2004). In the Oat3 knock-out mouse, transport of small organic anions was nearly completely inhibited, however, transport of estrone sulfate, a substrate specific for Oat3, was only reduced by 33% and transport of taurocholate was unchanged. Evidence for partial transport on additional Na^+-dependent and Na^+-independent systems were identified.

Nevertheless, OAT1 and OAT3 carry a wide range of substrates, including a range of organic anions, hormones, toxins and drugs and are affected by numerous inhibitors (Pulaski et al., 1996; Sekine et al., 1997; Stride et al., 1997; Apiwattanakul et al., 1999; Hosoyamada et al., 1999; Jariyawat et al., 1999; Lu et al., 1999; Pritchard et al., 1999; Tsuda et al., 1999; Burckhardt and Wolff, 2000; Inui et al. 2000; Sekine et al. 2000; Wada et al., 2000; Koh et al, 2000; Kusuhara and Sugiyama, 2001; Montefoort et al., 2003; Koepsell and Endou, 2004; Wright and Dentzler, 2004). Substrates of OAT1 include N-acetylcysteine, acetylsalicylate, α-ketoglutarate, benzylpenicillin, cAMP, cephalothin, cGMP, cidofovir, dideoxynucleotides, dimercaptopropanesulfonate, 17β-glucuronide-estradiol, folate, glutarate, indometacin, methotrexate, ochratoxin A, *p*-aminohippurate, probenecid, prostaglandin E_2, salicylates, urate and zidovudine. Several substrates can compete for transport and additional inhibitors are acetylsalicylate, furosemide, carbenicillin, cefazolin, cephaloridine, cephalothin, cephalexin, ibuprofen, paracetamol, benzylpenicillin, phenacetin, piroxicam, salicylurate and salicylate. Substrates of OAT3 include allopurinol, benzylpenicillin, cimetidine, 2,4-D, dehydroepiandrosterone sulfate, estrone sulfate, 5-

fluorouracil, *L*-carnitine, 6-mercaptopurine, ochratoxin A, *p*-aminohippurate, prostaglandin E_2 and prostaglandin $F_2\alpha$.

1.5.2 ABC Transport Proteins

Members of the ATP-binding cassette (ABC) family of transporters, including families B and C, are expressed at the BCSFB (Choudhuri et al., 2003; Begley, 2004). These efflux transporters couple hydrolyses of ATP to export of compounds out of cells or into cellular organelles (Dahl et al., 2004).

1.5.2.1 The ABCB Family (P-Glycoproteins)

The best characterized ABC transporter is the MDR gene product P-glycoprotein (Pgp). In rodents, there are three mdr genes, mdr1a, mdr1b and mdr2, in humans there are two, MDR1 and MDR2 (Sun et al., 2003; Begley, 2004). Of these, only mdr1a, mdr1b and MDR1 transport drugs and confer multidrug resistance (Ng et al., 1989). The mdr2/MDR2 gene products transport phosphatidylcholine from liver to bile (Smit et al., 1993; Smit et al., 1998).

The MDR1 gene product is a 170 kDa plasma membrane protein consisting of 12 TMDs with two drug-binding domains and two intracellular ATP-binding domains (Walker domains) (Lee et al., 2001). Modeling revealed that the substrate binding domain is formed at two TMD/TMD interfaces, between TMD segments 3 and 11 and 5 and 8, respectively (Pleban et al., 2004). Inserted into the membrane, both drug-binding sites are most likely located close to each other (Begley, 2004). There are a number of MDR gene polymorphisms, frequently single nucleotide polymorphisms (SNPs), but most are silent and do not affect Pgp function (Marzolini, 2004). In some cases however, Pgp polymorphisms can alter drug pharmacokinetics and also susceptibility to diseases, e.g. Parkinson's disease, inflammatory bowel disease and refractory seizures (Marzolini 2004; Mealey, 2004).

In general, Pgp is localized at barrier and excretory sites (de Lange, 2004; Miller et al., in press). At the BBB, the efflux transporter Pgp is inserted into the luminal membrane of the capillary network and responsible for removing compounds from endothelial cells and restricting entry of compounds from the blood stream. (figure 6; Sun et al., 2003; Begley et al., 2004).

In CP epithelia, Pgp expression was demonstrated by immunostaining and Western blot analyses (Rao et al., 1999). Pgp was stained in preparations from rat, human and wild type mice, but not in preparations from mdr1a/1b knock-out mice. Further staining experiments and functional analyses suggested sub-apical and/or apical localization. The localization has since been controversial (Lee et al., 2001; Sun et al., 2003; Begley, 2004). The opposing efflux function of Pgp and multidrug-resistance associated protein 1 (Mrp1) are conflicting. Thus, it remains to be determined whether Pgp is actually functionally inserted into the apical membrane and or whether Pgp is vesicularized and removes compounds from the cytoplasm by eventual exocytosis across the basolateral membrane (Begley, 2004).

The transporter is responsible for efflux of a wide range of structurally dissimilar compounds ranging from approximately 300 to 2000 Da in mass, generally lipophilic, planar, cationic or neutral, including cytotoxic drugs, pesticides, steroid hormones, peptide antibiotics, immunosuppressive agents, cardiac glycosides and others (Begley et al., 2004; de Lange, 2004; Kimura et al., 2004). Compounds also include anthracyclines, β-adrenoceptor blockers, calcium-channel blockers, glucocorticoids, glucuronide conjugates, HIV protease inhibitors and vinca alkaloids such as aldosterone, CSA, digoxin, diltiazem, etoposide, ivermectin, loperamide, methotrexate, morphine, phenytoin, ranitidine, rapamycin and rhodamine-123 (Oude Elferink et al., 1995; Kusuhara et al., 1998; Schinkel, 1999).

The first Pgp modulators included compounds such as quinidine, verapamil and cyclosporine A (CSA) (Johnson, 2002; Begley, 2004). The inhibitory effect of CSA spurned the pharmaceutical industry's interest and led to the search for further Pgp inhibitors. Second generation and third generation compounds include SDZ-PSC833 (valspodar), LY335979 and GF120918, which are generally more specific and exhibit less toxic side effects.

1.5.2.2 The ABCC Family (Multidrug-Resistance Associated Proteins)

The multidrug-resistance associated proteins (Mrp) comprise a closely related family of gene products, with currently nine members identified. (Kruh and Belinsky., 2003; Begley et al, 2004; de Lange, 2004). As the MDR1 gene product Pgp, Mrps confer multidrug resistance and contribute to the intrinsic or acquired resistance of cells against drugs (Wijnholds, 2002). Mrp1 through Mrp6 were localized in human brain

(Nies et al., 2004). In the CP, expression of Mrp1 through Mrp6 was demonstrated in RT-PCR analyses, but expression levels can vary (Choudhuri et al, 2003). In rat, Mrp1 expression was highest, followed by Mrp4, Mrp5 and Mrp6, in contrast to levels of Mrp2 and Mrp3, which were low to none existent.

Only Mrp1 was localized in CP tissue by immunohistochemistry (Rao et al, 1999). Its membrane distribution was confirmed in numerous functional studies, including Mrp1 (-/-) knock-out studies in mice (Nishino et al., 1999; Wijnholds et al., 2000). The subcellular localization and functional role of the other Mrp proteins remains to be identified (Miller et al., in press).

Mrp1 is a 190 kDa plasma membrane protein, with 17 transmembrane domains and two nucleotide binding domains and is the best characterized protein within the ABCC family (Lee et al., 2001; Begley et al., 2004). Mrp1 utilizes energy derived from ATP hydrolysis for transport. But, in contrast to Pgp, Mrp1 predominantly mediates efflux of anionic compounds including a number of anticancer agents, including anthracyclines, epipodophyllotoxins and vinca alkaloides, especially when conjugated to glutathione and glutathione-S-transferase (van Aubel et al., 1999; Lee et al., 2001; Miller et al., in press). Compounds transported include 3-α-sulfatolitho-cholyltaurine, daunorubicin, etoposide, fluorescein, fluo-3®, fluorescein-methotrexate, glucuronosyl etoposide, leukotrienes C_4, D_4 and E_4, methotrexate and vincristine (van Aubel, 2000; Sun et al., 2003; Begley, 2004). Mrp inhibitors are less well defined and less specific than Pgp inhibitors, with even some overlap in specificity. For example, probenecid, sulfinpyrazone and benzobromarone inhibit Mrp1, but also Mrp2 activity and are likely to effect other ABCC family members (Begley, 2004). Other inhibitors include leukotriene C_4, the leukotriene antagonist MK571, LY329146, a structural analog of raloxifene, *S*-(decyl)-glutathione and probenecid (van Aubel et al., 1999; Lee et al., 2001; Sun et al., 2003; Begley, 2004).

2 MATERIALS AND METHODS

2.1 Materials

All chemicals were purchased at reagent grade or better, from Sigma-Aldrich Chemie GmbH, Steinheim, or from similar sources. Fluorescent compounds, fluorescein-methotrexate and BODIPY-verapamil, were obtained from Molecular Probes, Eugene, USA. Cyclosporine A (CSA) and PSC833 were from Novartis, Basel, Switzerland, diazepam from Roche, Basel, Switzerland, MK571 from Biomol, Hamburg.

All radioactive compounds were purchased from Amersham Pharmacia Biotech, Freiburg, including [2-^{14}C]-diazepam (2.04 GBq/mmol), [6,6´(n)-^{3}H]-sucrose (348 GBq/mmol) and [U-^{14}C]-sucrose (20.9 GBq/mmol). Radioactive samples were analyzed in Ultima Gold MV Liquid Scintillation Cocktail and measurements carried out in a Tricarb 2000 CA Scintillation Counter, both from Canberra Packard, Frankfurt.

For cell culture, Dulbecco's Modified Eagle Medium/Ham's F12 medium, L-Glutamine (200 mM), antibiotics Penicillin/Streptomycin (10,000 E/10,000 µg/ml) and Amphotericin B (50 mg/ml) were obtained from Biochrom AG, Berlin. Fetal Calf Serum (FCS, Gold) was purchased from PAA Laboratories, Pasching, Austria. Laminin was from TEBU-Bio, Offenbach. Table 3 lists cell culture materials used. Monolayer electrical resistance was measured with the Millicell-ERS Electrode System STX-2 from Millipore, Eschborn.

For molecular biology, the RNeasy Kit® was obtained from Qiagen GmbH, Mannheim, the Promega Reverse Transcription System® and Ethidium Bromide were purchased from Promega GmbH, Mannheim and Supert*aq*® PCR Polymerase from MoBiTec GmbH, Freiburg. Primers were obtained either from GIBCO Life Technologies GmbH, Karlsruhe or Sigma-Ark GmbH, Darmstadt. Reverse transcription (RT) and polymerase chain reactions (PCR) were carried out in a PCRSprint® PCR cycler from Thermo Hybaid, Heidelberg.

For protein isolation, CellLytic® for mammalian tissue was obtained from Sigma-Aldrich Chemie GmbH, Steinheim and Complete® protease inhibitors from Roche Diagnostics, Mannheim. Aqua Poly Mount® was obtained from Polysciences Inc., Warrington, USA. Tris-HCl pH 8.3 and pH 6.8 as well as polyacrylamide solution were obtained from Bio-Rad GmbH, Munich.

Fluorescent analyses were carried out in the Ascent Fluoroscan, obtained from Labsystems, Helsinki, Finland. Confocal laser scanning microscopes used included the Leica DM IRBE from Leica, Bensheim, the Olympus Fluoroview from Melville, NY, USA and the Zeiss Pascal from Zeiss, Jena.

Table 3: Cell Culture Materials

Equipment	*Company*
Transwell® Clear, 12-Well Polyester, Area 1.13 cm^2, Pore Size 0.4 µm	Corning Costar, Wiesbaden
Transwell® Clear, 12-Well Polycarbonat, Area 1.13 cm^2, Pore Size 0.4 µm	Corning Costar, Wiesbaden
Transwell® Clear, 6-Well Polyester, Area 2.4 cm^2, Pore Size 0.4 µm	Corning Costar, Wiesbaden
96-Well Plate	Corning Costar, Wiesbaden
Cell Culture Flask, 75cm^2	Corning Costar, Wiesbaden
LabTek Chamber Slide, 8-well Permanox Slide	Nalge Nunc Corp., Naperville, USA

2.2 Choroid Plexus Epithelial Cell Culture and *Ex Vivo* Models

Three types of models were used to characterize and assess choroid plexus epithelial cell (CPEC) function, biochemical and molecular features. The first is a primary *in vitro* cell culture model of porcine CPEC. The second and third are *ex vivo* models of a mammalian and an elasmobranch species, using excised CP tissue of Wistar rat (*Rattus norvegicus*) and of dogfish shark (*Squalus acanthias*). Preparation of CPEC cell cultures and CP tissues is described below.

2.2.1 Porcine Choroid Plexus Epithelial Cell Isolation and Cell Culture

Porcine choroid plexus epithelial cells were isolated and cultured according to Crook et al. (1981) and Gath et al. (1997), with minor modifications. Porcine brains were obtained from the local slaughterhouse in Mannheim (Germany) and placed in ice cold artificial cerebrospinal fluid (aCSF, in mM: 118 NaCl, 3 KCl, 0.7 Na_3PO_4, 0,7mM, 18 $NaHCO_3$, 2 Urea, 0.8 $MgCl_2$, 1.4 $CaCl_2$, 12 Glucose, pH 7.4) (Villalobos et al., 1997) with 100 µl/ml penicillin/streptomycin (10,000 E/10,000 µg/ml) added. Both lateral CP were removed and the number of tissues recorded. Following mechanical fractionation in ice cold HBSS, magnesium and calcium free, CP were weighed and wet weight (ww) was recorded. Then, the tissue was degraded by cold trypsination in 10 ml/g ww 0.25% trypsin at 4°C for 2.5 h, followed by two 20 min in-

cubation cycles at 37°C. Addition of an equal volume of fetal calf serum (FCS) terminated the enzymatic reaction. Isolated cells were removed, both batches combined and centrifuged at 300 rpm for 10 min at 4°C. Cells were resuspended in incubation medium containing DMEM/Ham's F12 (1:1), 100 µl/ml penicillin/streptomycin (10,000 E/10,000 µg/ml), fetal calf serum (10%), L-glutamine (4 mM), insulin (5 µg/ml), cytosine arabinoside (20 µM), epidermal growth factor (EGF, 10 ng/ml) and HEPES (10 mM). The number of live and dead CPEC was determined by trypan blue exclusion using a Neubauer cell count chamber, and viability was calculated.

After CPEC isolation, cells were seeded in 96-well plates, on 6- or 12-well Transwell® filter plates, on 8 well chamber slides or in 75 cm^2 culture flasks. All culture material was coated with 5 µg/cm^2 laminin, with exception of culture flasks. Seeding density was at minimum 1 g ww/60 cm^2. Uniform adherence was ensured by slow agitation of the culture vessels one hour after seeding. For the first nine days of culture, cells were incubated in incubation medium and medium was changed every three days. On the ninth day of incubation, cells were switched to serum free medium containing DMEM/Ham's F12 (1:1), 100 µl/ml penicillin/streptomycin (10,000 E/10,000 µg/ml), L-glutamine (4 mM), insulin (5 µg/ml), hydrocortisone (200 ng/ml) and HEPES (10 mM). Cells were washed three times and, for the next five days, culture medium was changed every two days. Throughout the culture period the incubation chamber was set at 37°C, 5% CO_2 and 95% relative humidity.

2.2.2 Rat Choroid Plexus *Ex Vivo*

Fresh lateral CP were isolated from male Wistar rats (250 to 400 g). All rats were obtained from the University of Heidelberg animal facility. Animals were anaesthetized by gassing with isofluran (Abbott, Wiesbaden, FRG) and sacrificed by cervical dislocation. Following removal of the head, first the brain, then both lateral CP were excised and placed in ice cold, gassed (95% oxygen/ 5% CO_2) artificial cerebrospinal fluid (aCSF) (in mM: 118 NaCl, 3 KCl, 0.7 Na_2PO_4, 18 $NaHCO_3$, 2 urea, 0.8 $MgCl_2$, 1.4 $CaCl_2$, and 12 glucose, pH 7.4) (Villalobos et al., 1997) when used in transport experiments or directly in 95% EtOH when used in immunohistochemical analysis.

2.2.3 Dogfish Shark Choroid Plexus *Ex Vivo*

Lateral CP were isolated from adult spiny dogfish shark (*Squalus acanthias*). Sharks (~2 kg) were collected from waters around Mount Desert Island, ME, USA and kept in salt water tanks for 1-7 days. Animals were decapitated and pithed and the cranial compartment removed. The brain was excised and placed in ice cold, gassed (1% CO_2) elasmobranch Ringer (ER) solution (in mM: 280 NaCl, 6 KCl, 4 $CaCl_2$, 3 $MgCl_2$, 1 NaH_2PO_4, 0.5 Na_2SO_4, 350 urea, 72 trimethylamine oxide, 2.5 glucose, and 8 $NaHCO_3$, pH 7.8) (Villalobos et al., 2002). Both lateral CP were isolated and cleared of all extraneous neuronal and connective tissue before being used in functional analyses.

2.3 Gene Expression Analyses

To assess gene expression, messenger ribonucleic acid (mRNA) was analyzed by reverse transcription - polymerase chain reaction (RT-PCR). All molecular analyses were carried out using either porcine tissue or cultured CPEC. Following isolation of total RNA, mRNA was transcribed and specific complementary deoxyribonucleic acids (cDNA) segments amplified. Qualitative and semi-quantitative analysis was carried out. For semi-quantitative analyses, β-actin was used as internal standard and mRNA expression was compared on a relative basis. All results presented are from single experiments representative of at least three experiments.

2.3.1 Total RNA Isolation

Porcine tissue samples were collected from the slaughterhouse in Mannheim (Germany), stored in ice cold RNALater® for transport and frozen at -70°C upon arrival. Cultured CPEC were washed in KRB, pH 7.4, 37°C three times to remove all remaining medium, before starting RNA isolation procedures. Total RNA was isolated from all samples according to the Qiagen RNeasy® protocol. Tissues or cells cultured in flasks were lysed in β-mercaptoethanol containing RLT buffer according to the Qiagen tissue and cell lyses protocols. An equal volume of 70% EtOH was added and samples were transferred to supplied spin columns. Following the Qiagen wash and spin regimen, total RNA was finally eluted in a small volume of nuclease free water. The amount of isolated RNA was quantified by spectrophotometric determination, measuring OD at 260 nm, with OD of 1 corresponding to 40 µg of single

stranded RNA (Sambrook et al., 1987). Purity was further established by taking the OD ratio of 260 nm over 280 nm. Only samples with a ratio of 1.7 to 2.0 were used, as low ratios are characteristic of protein and high ratios of residual β-mercaptoethanol contamination.

2.3.2 Reverse Transcription

Reverse Transcription (RT) was carried out according to the Promega Reverse Transcription System®. In brief, 1 µg of total RNA was incubated at 70°C for 10 min and after adding the reaction mixture (in 20 µl: 4 µl 25 mM $MgCl_2$, 4 µl 5X transcription buffer, 2 µl 10 mM dNTP mixture, 0.5 µl RNasin® ribonuclease inhibitor, 0.5 µg oligo$(dT)_{15}$ primer and nuclease free water) containing 5 units of avian myeloblastosis virus reverse transcriptase (AMV-RT), further incubated at 42°C for 60 min. The reaction was terminated by raising the temperature to 95°C for 5 min, deactivating all enzymes in the reaction, and the cDNA product cooled to 4°C. Resulting cDNA was either used directly in further reactions or frozen at -20 °C.

2.3.3 Polymerase Chain Reaction

The polymerase chain reaction (PCR*) method, first described in 1985 (Saiki et al., 1985), allows selective amplification of DNA fragments *in vitro*, thereby emulating *in vivo* cellular DNA replication. Here, the PCR reaction was used to amplify selective regions of generated cDNA obtained from transcribed mRNA. For each PCR reaction, 10 to 100% of the cDNA generated from 1 µg total RNA was used. All reactions were carried out using a hot-start protocol (D'Aquila et al., 1991) in order to maximize sensitivity and specificity. Following an initial 8 min cDNA incubation in reaction mixture (in 50 µl: 5 µl 10 X reaction buffer with $MgCl_2$, 0.5 µl 1 mM primer, 2 µl dNTP and water) at 94°C, 0.5 units of Super*taq*® were added to each reaction tube. Denaturation, annealing and extension were optimized (Innis and Gelfand, 1990; Eckert and Kunkel, 1991; Rolfs et al., 1992; Douglas and Atchinson, 1993) and set at 94°C, 50°C and 72°C for 30 sec, respectively. The samples were run for a total of 15 to 50 cycles. Each reaction was terminated after a final extension period of 72°C for 10 min and products were stored at 4°C for maximal 24 hours. Finally, PCR products were separated in a 1.5% ethidium bromide stained agarose gel at 100 V for 1 hour and visualized under UV-light.

*PCR is licensed under U.S. patent numbers 4,683,202, 4,683,195, 4,965,188 and 5,075,216 or their foreign counterparts, owned by Hoffmann-La Roche Inc. and F. Hoffmann-La Roche Ltd.

2.3.4 Semi-Quantitative RT-PCR

Semi-quantitative mRNA analysis allowed RNA expression levels to be estimated on a relative basis. β-actin expression was used as internal standard. First, total RNA was isolated and transcribed, and selective regions amplified as described above. Then, density readings of ethidium bromide stained PCR products were obtained, using the Scion Image software (NIH, USA), and normalized in relation to β-actin expression. To determine the phase of linear amplification, a series of amplifications in five-cycle intervals was run. A range of concentrations was amplified to ensure that results were not affected by initial amounts of mRNA and cDNA in any particular sample.

2.3.5 Primer Design

The selection of suitable primers is a prerequisite for amplification of specific cDNA products. One of the difficulties in using porcine samples in PCR, however, is that for most targets of interest no RNA or DNA sequences are published as yet. In cases in which porcine sequences were not available, human sequences were used. These were entered in a BLAST (Altschul et al., 1990) search and conserved sequences within the nucleotide target were defined. Table 4 lists the individual sequences used in the process. After identifying conserved structures within a target, primers were chosen to (1) efficiently hybridize to the chosen sequence only, (2) exhibit minimal primer-primer interaction, (3) have the desired physical and chemical properties and (4) be of desired length (Persing, 1993; Hayashi, 1994; Innis, and Gelfand, 1990). All primers were optimized using either Primer3 (Massachusetts Institute of Technology) or WebPrimer (University of Stanford). A BLAST cross-search was carried out to ensure primers did not hybridize to any other known sequence.

2.4 Enzyme and Protein Analyses

The expression of a number of proteins expressed by CPEC was assessed. Activity of enzymes of interest was quantitatively determined in colorimetric assays. Expres-

sion of TTR and ABC transport proteins Mrp1 and Pgp was examined in cultured CPEC and in *ex vivo* tissue, as well as in apical and basolateral membrane preparations by immunohistochemical staining and western blots, respectively.

T able 4: Primer Nucleotide Sequences:

Target	*Accession Number*	*Forward Primer Reverse Primer*	*Product (bp)*
Transthyretrin (TTR, Prealbumin)	X87846	TGGTCAAAGTCCTGGATGCT TTACATGCAAGCCTGTCCCT	371
β-Actin	U07786	TTTGAGACCTTCAACACGCC TGATCCACATCTGCTGGAAG	703
Mrp1	L05628	TTCGTTCTCAGGCACATCAATG AACACAAGGATCTTCGTCTTCCTC	436
Pgp	AF016535	GAGAGGGGCCCAGTTGAGTG CACAAGCCCAAGACAGAAAGC	468

2.4.1 Protein Isolation

Tissue samples collected for total protein isolation from the slaughterhouse in Mannheim were stored in ice cold RNALater® for transport and frozen at -70°C upon arrival. Cultured cells were washed in KRB, pH 7.4, 37°C three times to remove all remaining medium. Tissue and cultured CPEC were lysed in CellLytic® and Complete® according to protocol. The lysate was homogenized and placed on ice. After 1 hour, samples were centrifuged at 10,000 rpm for 30 min at 4°C. Pellets were discarded and the remaining protein isolates stored at -70°C until further use.

2.4.2 Protein Concentration

Protein concentration was determined according to Bradford (1976). In principal the assay is based on the equilibrium between the three forms of Coomassie Blue G dye and its proportional binding to proteins. Under acidic conditions and bound to protein, the dye is most stable in its unprotonated blue form detected at an OD of 595 nm. The more dye binds to protein, the more intensely the solution colors. One drawback to the assay is that the dye binds favourably to arginyl and lysyl residues, which may cause some variation in response to different proteins.

For each sample 0.2 ml Bradford protein reagent was added to 0.8 ml water without (control) and with protein lysate added. OD was determined at 595 nm. Absolute quantification was carried out with an appropriate standard curve of bovine serum albumin (BSA).

2.4.3 Alkaline Phosphatase Activity

The alkaline phosphatase (AP) assay used is based on hydrolysis of p-nitrophenyl phosphate by the enzyme, yielding p-nitrophenol and inorganic phosphate. Alkaline p-nitrophenol is converted to a yellow complex upon its synthesis in solution, with developing color intensity proportional to phosphatase activity. All AP analyses were carried out using the Sigma AP kit according to the manufacturer's instructions. In brief, 0.5 ml of 221 alkaline buffer solution was mixed with 0.5 ml stock substrate solution (1 mg p-nitrophenyl phosphate/ml) and added to either 0.1 ml water (control) or 0.1 ml cell suspension or protein lysate. The reaction mixture was incubated at 37^{o}C for 15 min, after which the reaction was terminated by adding 10 ml 0.05 N NaOH. The OD was determined at 410 nm and AP activity quantified using an appropriate standard curve. Sigma units were converted to enzyme activity (EA) in µmol of p-nitrophenol/hour, according to Bessey et al. (1946). All measurements were carried out in triplicate. Results presented are from a single experiment representative of at least three experiments.

2.4.4 γ-Glutamyl Transferase Activity

This assay is based on conversion of γ-glutamyl-p-nitroanilid to p-nitroanilin by γ-glutamyl transferase (γ-GT). The formation of p-nitroanilin is proportional to the amount of enzyme present. For each reaction 0.5 ml reaction mixture (100ml containing in g: 0.405 $MgCl_2$ x 6 H_2O, 0.53 glycylglycin, 0.15 L-γ-glu-nitroanalid and 7.3 TRIS) was added to 0.5 ml protein lysate or cell suspension. Whole cells were homogenized by passing the cell suspension through a 20 gauge needle. After 40 min incubation at 37^{o}C the reaction was terminated adding 0.5 ml 3 N acetic acid. Resulting p-nitroanilin concentrations (C) were determined by dividing adsorption (A) at 410 nm by its molar absorption coefficient (8800 M^{-1} cm^{-1}) according to (1):

$$(1) \quad C = A/8800 \qquad [mol/L]$$

Amount of substrate (N) was determined according to (2):

$$(2) \quad N = C \times 0.0015\ L \qquad [mol]$$

Finally, enzyme activity (EA) (1 nmol p-nitroanilin/ min) at 37°C was calculated (3):

$$(3) \quad EA = N \times 10^9/min \quad [U]$$

All measurements were carried out in triplicate. Results presented are from single experiments representative of at least three experiments.

2.5 Immunohistological Staining

Series of immunohistological stains were carried out to characterize CPEC at the protein level. Several targets were visualized, including the marker proteins prealbumin and f-actin as well as a number of active transport proteins. Target proteins were stained in freshly isolated tissue or cultured CPEC. Further, western blot analysis was performed, using whole cell protein samples as well as isolated apical and basolateral membrane fractions. Table 5 lists the different proteins labelled, including source of primary antibodies. Secondary antibodies are listed in table 6. F-actin was visualized in cultured CPEC only, using fluorescent-labelled phalloidin (phalloidin-FITC). Results presented are from single experiments, representative of at least three experiments.

2.5.1 Immunocytological Staining

Fresh rat lateral CP and porcine CPEC 13 to 15 DIC were fixed in 95% EtOH for 15 min at RT. Cells were permeated in 0.1% Triton X-100 for 15 min. Specimens were then blocked in blocking buffer (1% BSA and 1% milk powder) for 1 hour. Following blocking, samples were incubated with target antibody at a dilution of 1:10 in blocking buffer at RT overnight. After washing in 0.05% Triton X-100 three times for 5 min, samples were incubated with a FITC-labeled secondary IgG (DakoCytomation) for 2 hours at 1:100 in blocking buffer, with 10 µM propidium iodide (PI) added. For controls, primary antibody was omitted. F-actin stained cultured CPEC were incubated with 10 µM phalloidin-FITC and 10 µM PI or with PI only for treatment and control, respectively. Samples were embedded in Aqua Polymount® and viewed through an inverted Leica DM-IRB confocal microscope, using a x 40 oil immersion objective (NA 1.2), a 488-nm argon ion laser excitation and a 500-nm long-pass emission fil-

ter. Data are results from single experiments, representative of at least three experiments.

Table 5: Primary Antibodies

Primary Antibodies	
Anti-TTR (monoclonal, human), goat IgG	Sigma-Aldrich Chemie GmbH, Steinheim
Anti-Pgp (monoclonal C219), mouse IgG	Alexis, Grünberg
Anti-Mrp1 (monoclonal Mrpr1), rat IgG	Alexis, Grünberg

Table 6: Secondary Antibodies

Secondary Antibodies	
Anti-Goat IgG, FITC-labeled	Sigma-Aldrich Chemie GmbH, Steinheim
Anti-Mouse IgG, FITC-labeled	Sigma-Aldrich Chemie GmbH, Steinheim
Anti-Rat IgG, FITC-labeled	Sigma-Aldrich Chemie GmbH, Steinheim
Anti-Goat IgG, HRP-labeled	DAKO, Glostrup, Denmark
Anti-Mouse IgG, HRP-labeled	DAKO, Glostrup, Denmark
Anti-Rat IgG, HRP-labeled	DAKO, Glostrup, Denmark

2.5.2 Isolation of Apical and Basolateral Membrane Fractions

Methods for apical and basolateral CPEC membrane fraction isolation were adapted from a spinning and cation precipitation protocol for kidney membranes (Hilden et al., 1989). Freshly isolated lateral CP was homogenized in homogenizing solution (HS, in mM: 300 mannitol, 0.1 PMSF, 1 EDTA and 18 Tris HCL, pH 7.5) using 6 g CP per 50 ml HS. The homogenate was centrifuged (in a Beckmann centrifuge) at 5,000 rpm for 10 min 1 % of volume 1 M $MgCl_2$ was added to the resulting supernatant (S1) and stirred for 20 min on ice. The solution was then centrifuged at 4,000 rpm for 10 min. The resulting supernatant (S2) was used for isolation of basolateral membrane fractions and resulting pellet (P2) for the isolation of apical membrane fractions.

For the isolation of apical membrane fractions, S2 was centrifuged at 16,500 rpm for 20 min. The resulting pellet was resuspended in half the original volume of HS, and 1 M $MgCl_2$ was added to arrive at a concentration of 10 mM $MgCl_2$. After 20 min on ice, the solution was centrifuged at 6,000 rpm for 12 min and the pellet discarded. This procedure was repeated twice. Finally, the solution was centrifuged at 7,250 rpm for 12 min, the pellet discarded and the supernatant further centrifuged at 16,500 rpm for 20 min. The resulting pellet was the apical membrane fraction.

Basolateral membrane fractions were obtained by resuspending P2 in HS and further centrifuging at 20,000 rpm for 20 min. This procedure was repeated twice. Then the pellet was resuspended in a small volume of HS and mixed with 2 ml percoll per 10 ml. The mixture was centrifuged at 20,000 rpm for 30 min, after which two layers became evident. The upper layer was removed and remaining percoll washed out by adding an excess amount of PBS (without magnesium and calcium) and centrifuging at 20,000 rpm for 30 min. The final pellet was taken up in a small volume of HS. Both membrane fractions were characterized, the apical by analysis of alkaline phosphatase and γ-glutamyl transferase activity, the basolateral by determination of Mrp1 expression in western blot analyses.

2.5.3 Western Blots

CPEC whole cell protein samples or enriched membrane fractions were studied in western blot analyses according to Sambrook et al. (1989). Proteins were denatured and reduced in a SDS-containing sample buffer (100 mM tris-Cl (pH 6.8), 4% SDS, 2% bromophenol blue, 20% glycerol) and reduced using either β-mercaptoethanol or D,L-dithiothreitol. Protein samples were heated to 95°C or 60°C for 10 min or 5 min analyzing marker proteins and ABC-transporters, respectively. Following SDS-PAGE (15 to 6% polyacrylamide gels) at 80 V for 2 h in running buffer (25 mM tris (pH 8.3), 250 mM glycine, 0.1% SDS), samples were blotted on nitrocellulose at 250 mA for 2.5 h in blotting buffer (39 mM glycine, 48 mM tris-base (pH 8.3), 0.037% SDS, 20% methanol). After one hour blocking in blocking buffer, samples were incubated with target antibody at a dilution of 1:100 in blocking buffer at 4°C overnight, followed by incubation in horse radish peroxidase (HRP)-labeled secondary IgG (DakoCytomation) at a dilution of 1:1,000 in blocking buffer for two hours. Blocking and antibody incubation were both done in blocking buffer. The resulting bands were visualized with diaminobenzidine in combination with $NiCl_2$. Porcine brain capillary endothelial cells, liver and kidney samples were used as positive controls.

2.6 Choroid Plexus Functional Analyses

Secretion of CNS active compounds across CP epithelium was assessed *in vitro* and correlated to *ex vivo* findings. A number of different functional experiments were carried using cultured CPEC, with cells either cultured on Transwell® filter systems or

cells grown in 96-well plates. All experiments using cultured CPEC were carried out with cells grown for 13 DIC to 15 DIC ensuring the development of a confluent monolayer and full cellular differentiation.

Besides molecular and biochemical characterization, CSF production was measured in cultured CPEC, as an indicator for complex cellular differentiation. Further, for experiments using cells grown on Transwell® filter systems, monolayer integrity was assessed measuring transepithelial electrical resistance (TEER) and running samples of the permeability marker 5-carboxyfluorescein (5-CF) simultaneously. Monolayers were regarded intact with TEER values greater 100 Ωcm^2 and 5-CF apparent permeability coefficient (P_{app}) values < 3 x 10^{-5} cm/s. To ensure monolayer confluence for cells grown on 96-well plates, all wells were checked by inverted light microscopy.

In vitro results were correlated to *in vivo* data, obtained from fresh excised, live tissue in real time analyses, using a mammalian and an elasmobranch lateral CP model. Transport of substrates across CP tissue was visualized by quantitative fluorescent confocal microscopy, allowing detailed analyses at the cellular and subcellular level.

All compounds used, including substrates and inhibitors, were dissolved in KRB, aCSF, ER or dimethylsulfoxide (DMSO). DMSO concentrations were kept below 0.5%, shown to be non-detrimental to CP tissue (Breen et al., 2002).

2.6.1 CPEC Cerebrospinal-Fluid Secretion

To assess CSF secretion by cultured CPEC, cells were cultured on permeable, polyester 6-well Transwell® filter plates for 13 to 15 DIC. Cells were washed three times in CSF secretion buffer (CSFB, in mM: 122 NaCl, 4 KCL, 1 $CaCl_2$, 1 $MgCl_2$, 15 $NaHCO_3$, 15 HEPES, 0.5 Na_2HPO_4, 0.5 $NaHPO_4$ and 17.5 Glucose, pH 7.3, 37°C, with 5 µg/ml insulin added, Hakvoort et al., 1998). Following a 1 hour preincubation with CSFB, 1.0 ml 1.0 µM 67 kDa fluorescent-dextran (FITC-dextran) in CSB was added to both apical and basolateral chambers. Filters were incubated at 37°C, 5% CO_2 and 95% relative humidity for up to eight hours. 200 µl samples were taken on the hour from either the apical or basolateral chamber and replaced with fresh dextran solution. Samples were analyzed in a fluorescent plate reader and sample concen-

tration corrected for the sample regimen as described below (section 2.6.3). CSF volumes secreted were then calculated according to equation (1):

$$(1) \quad V_{CSF} = (C_{n\ corr\ Dex\ (initial)} - C_{n\ corr\ FD\ (final)})/C_{n\ corr\ FD\ (initial)} \times V_0$$

Where,

V_{CSF}	=	CSF volume	[µl]
$C_{Dex\ (initial)}$	=	initial FITC-dextran concentration	[µM]
$C_{Dex\ (final)}$	=	final FITC-dextran concentration	[µM]
V_0	=	initial volume applied	[µl]

Wells containing CSFB-dextran only served as control, ensuring that resulting dextran concentrations were not affected by any outside factors (e.g. vaporization). A 67 kDa fluorescent dextran standard curve was run to warrant that values obtained were linear over the resulting concentration range.

2.6.2 Transepithelial Electrical Resistance (TEER)

TEER values were determined for CPEC grown on permeable polyester Costar Transwell® membranes, using the Millicell®-ERS and STX-2 electrode system. The electrode system is made up of two electrode holders, containing a silver-/ silver chloride electrode to measure voltage and a silver electrode to measure current. With one of the electrode holders being 2.5 mm longer than the other, direct measurements within the filter system were possible. Electrical resistance was determined from voltage and current values are in Ohm (Ω). Control values obtained from coated filters without cells (blank) were subtracted and the resulting values multiplied by the filter surface area, resulting in TEER values of Ωcm^2.

2.6.3 The Apparent Permeation Coefficient (P_{app})

Apparent permeation coefficient (P_{app}) values for secretion of compounds across CPEC grown on permeable Costar Transwell® membranes were determined according to Thöle (2000). Samples were taken at defined times and quantified using an appropriate standard curve. Then, substrate concentrations were adjusted according to the sample regimen and corrected substrate concentrations ($C_{n\ corr}$) were calculated as follows (1):

$$(1) \quad C_{n\,corr} = C_n \times V_{total} + \sum_{i=1}^{n-1} (C_i \times V_{sample}) / V_{total}$$

Where,

$C_{n\,corr}$	=	corrected concentration of sample n; n>1	[µg/ml] or [µmol/ml]
C_n	=	concentration of sample n	[µg/ml] or [µmol/ml]
V_{total}	=	total volume in acceptor compartment (acceptor = compartment into which compounds diffuse)	[ml]
V_{sample}	=	sample volume	[ml]

The relative amount diffused into the acceptor chamber at time (t) was then calculated according to (2):

$$(2) \quad S_t = (C_{n\,corr} / C_0) \times 100$$

Where,

S_t	=	compound transported at time (t)	[%]
C_0	=	concentration in donor chamber at time zero	[µg/ml] or [µmol/ml]

Finally, the apparent permeation coefficient (P_{app}) was calculated as shown in (3):

$$(3) \quad P_{app} = (C_{n\,corr} \times V_{total}) / t \times 1 / A \times 1 / C_0$$

Where,

P_{app}	=	apparent permeation coefficient	[cm/s]
t	=	time	[s]
A	=	filter surface area	[cm^2]

2.6.4 Choroid Plexus Permeability Assays

In general, permeability assays were carried out on permeable polyester Transwell® membranes. Before starting experiments, cells were washed in KRB, pH 7.4, 37°C three times and pre-incubated for 60 min, without (control) and with inhibitor added in an atmosphere of 5% CO_2 and 95% relative humidity. Volumes were set at 0.5 ml in

the apical and 1.5 ml in the basolateral compartment. After substrate addition, 200 µl samples were drawn at 5, 10, 15, 30, 45, 60, 90 and 120 min and for each sample taken sample volumes were replaced with KRB, pH 7.4, 37°C.

Radioactive samples were analyzed in a Tricarb 2000 CA scintillation counter adding 5 ml Ultima Gold MV liquid scintillation cocktail, allowing for a 24 h equilibration. Fluorescent samples were analyzed using a fluorescent plate reader (Ascent Fluoroscan).

2.6.5 Choroid Plexus Uptake Assays

Uptake assays were carried out with CPEC cultured in 96-well plates. For all experiments CPEC were cultured at least 13 DIC, but not more than 15 DIC. Before carrying out experiments, cells were washed three times and then pre-incubated in KRB, pH 7.4, 37°C, for 30 min, without (control) and with inhibitor added in an atmosphere of 5% CO_2 and 95% relative humidity. After 90 min incubation with substrate or substrate and inhibitor for control and treatment samples, respectively, cells were washed five times with KRB, pH 7.4, 37°C, lysed in 1% Triton X-100 and wells analyzed in a fluorescent plate reader (Ascent Fluoroscan). Wells containing CPEC incubated with KRB only served as blank. Apparent uptake was calculated by subtracting blanks from fluorescent values. Fluorescent values were quantified using an appropriate standard curve.

2.6.6 Transport across Live Choroid Plexus Epithelia in Real-Time

Mammalian and elasmobranch CP tissue was analyzed using rat and dogfish shark tissue, respectively. Lateral CP were used either whole or cut in halves. Rat and shark CP pieces were incubated in aCSF or ER, respective of the species, with substrate and without (control) or with inhibitors added. All samples were gassed with 99% O_2/1% CO_2 (rat) or 95% oxygen/5% CO_2 (shark) and kept in zip-lock bags at all times. When inhibitors were used, CP pieces were pre-incubated in experimental solution for 30 min in ER or aCSF without substrate. Experiments with rat CP were carried out at 37°C and elasmobranch experiments at 10°C.

To acquire images, CP segments and incubation solution were transferred to covered Teflon chambers with a glass cover slip bottom, and placed on an inverted confocal microscope (Olympus Fluoview, Zeiss Pascal or Leica DMIRB). The speci-

mens were viewed in transmitted light, using a X 40 water or oil immersion objective (NA 1.2), a 488-nm argon ion laser excitation, a 505-nm dichroic filter and a 510-nm long-pass emission filter. Photomultiplier gain was set to yield an average fluorescence intensity of 20 – 200 (full scale, 255) and 200-2,000 (full scale, 2,500) for Zeiss or Leica and Olympus, respectively, with tissue autofluorescence being undetectable. A factor of X 16 was applied to convert between both types of imaging systems. For each piece of choroid plexus, 5 to 15 undamaged areas were selected and a fluorescence image (512 X 512 X 8 bit frames averaged) recorded. Fluorescence intensities were measured from stored images using the NIH Scion Image software as described previously (Breen et al., 2002). Data presented are results from single experiments, representative of at least three experiments and reported as average pixel intensity.

2.7 Statistics

All values presented are means +/- SEM. Control and treatment groups were compared by either student's *t*-test or one-way analysis of variance, followed by either a Bonferroni or Dunnett's post hoc test. Differences were considered moderately significant at *P<0.05 and significant at **P<0.01. Regression analysis was carried out to analyze appropriateness of standard curves used and only linear relationships with an R^2-value greater than 0.95 were used for transformations.

3 RESULTS AND DISCUSSION

3.1 Choroid Plexus Cell Culture and Animal Models

Choroid plexus epithelial cells (CPEC) were characterized using several different models. *In vitro* studies were carried out using porcine CP. *Ex vivo* studies on excised live tissue were performed using rat and dogfish shark. Porcine experiments were carried out at the Heidelberg laboratory, dogfish shark experiments at the Mount Desert Island Biological Laboratory, Maine, USA.

Porcine brain is advantageous for use in cell culture, due to its free availability, large size and number of epithelial cells per tissue. However, due to slaughter procedure and distance from laboratory to slaughterhouse the tissue was less suitable for *ex vivo* or real time analysis in live cells. In spite of the close evolutionary linkage between pig and man, the porcine genome has not been sequenced and relatively little molecular and biochemical information is available. Rat CP tissue on the other hand could be easily excised in the laboratory and live cell experiments commenced immediately after sacrificing the animal. Further, the rat genome has been fully sequenced and comparative molecular and biochemical data is readily available (NIH, 2004). The dogfish shark is probably least characterized, however, there are several advantages to using this evolutionary ancient species. Dogfish CP tissue is easily accessible, as the brain is enclosed by cartilage not bone, large in size and can be maintained intact for longer periods of time when compared to mammalian CP tissue. Further, with the shark being a poikilothermic animal, experiments could be carried out at lower temperatures.

3.2 Porcine Choroid Plexus Epithelial Cell Isolation and Culture

Several different approaches have been developed trying to establish a CPEC *in vitro* model. Crook et al. (1981) were first to publish a protocol on epithelial cell isolation and cultivation using CP isolated from bovine brains. Other species used thereafter include rabbit (Mayer and Sanders-Bush, 1993; Ramanathan et al., 1997), rat (Southwell et al., 1993; Strazielle and Ghersi-Egea, 1999; Tsutsumi, et al., 1989; Villalobos et al., 1997) and pig (Gath et al., 1997). Typically, CP tissue was removed from lateral ventricles and mechanically fractionated. Individual CP were digested using proteolytic enzymes, such as trypsin, pronase, collagenase and also DNAse,

yielding an isolate of epithelial cells. The goal is to obtain a maximum of live CPEC, whilst reducing the number of undesired cells, such as fibroblasts and macrophages.

Two strategies can be used to cull unwanted cells. Fibroblasts, macrophages and endothelial cells attach faster to culture surfaces compared to CPEC, allowing cell selection based on settling speed. Second, addition of inhibitors to the medium, such as cis-hydroxyproline or cytosine arabinoside, favors growth of CPEC and suppresses fast proliferating fibroblasts.

Isolation and culture protocols used for isolation and culture of porcine CPEC in the studies presented were adapted from Crook et al. (1981), with modification according to Gath et al. (1997). Following mechanical fractionation, lateral porcine CP were digested by cold trypsination. Table 7 lists amount of CP tissue obtained and the corresponding number of live and dead cells isolated over a two year time period (n=25). Viability was calculated from counted live and dead cells.

Table 7: Isolation of Choroid Plexus Epithelial Cells (n = 25)

	CP Tissue (g)	*Live Cells ($x10^7$)*	*Dead Cells ($x10^7$)*	*Viability (%)*
Mean	4.22	2,75	1,44	65.86
SEM	0.25	0.22	0.15	2.42
Max	6.25	4.70	2.88	85.29
Min	1.90	0.49	0.25	41.27

Following isolation, cells were seeded on either Transwell® filter systems, 96-well plates or in culture flasks at a seeding density of at least 1g per 50 cm^2 or 1.2 x 10^5 cells per cm^2. With the exception of culture flasks, all culture material was coated with 5 µg laminin per cm^2. Haselbach et al. (2001) showed that CPEC grown on laminin not only adhere to a higher percentage, but also proliferate at a higher rate, compared to cells grown on BSA, fibronectin, collagen type IV or thrombospondin-1 coated surfaces. For the first nine days of culture, cells were cultured in serum-containing medium, with cytosine arabinoside added. After nine days in culture, cells were washed and incubated in serum-free medium.

3.3 Characterization of Cultured Choroid Plexus Epithelial Cells

In general, CPEC growth was slow and proliferation rates were low. Addition of cytosine arabinoside suppressed growth of contaminating cells and epithelial cell cultures

developed into an integer monolayer within 9 days of culture (DIC), displaying the typical cobblestone appearance. After 9 DIC, serum was removed from the medium and CPEC monolayers allowed to fully differentiate. Detailed characterization of cultured CPEC was carried out to ensure cellular viability, integrity and differentiation.

Functional, biochemical and molecular function was assessed and *in vitro* and *in vivo* activity compared. Cultured CPEC characterization included epithelial cytoskeleton analyses, CP specific transthyrethin expression, cerebrospinal-fluid (CSF) secretion, transepithelial resistance measurements and transcellular secretion profiles for compounds of low and high permeability.

Two active transport proteins, the multidrug-resistance MDR1 gene product P-glycoprotein (pgp) and multidrug-resistance associated protein 1 (Mrp1) were assessed on a molecular, biochemical and functional level. Following RNA expression analysis, proteins were localized by immunohistological staining and visualization carried out using confocal laser scanning microscopy analysis. To further provide evidence for preferential membrane distribution, Western blots were done on isolated membrane fractions.

Last, CPEC were functionally characterized *in vitro* and *ex vivo*, using two different approaches. First, activity of one active transport protein was assessed measuring transport of a substrate with high affinity for the protein of interest. Specifically, functional activity of Pgp was quantified measuring transport of Rhodamin123 into cells cultured in 96-well plates. Accumulation of Rho123, a specific Pgp substrate, provided a measure for protein expression and activity in presence and absence of additional transport inhibitors.

Second, the movement of a compound with affinity for a number of transporters was investigated. Transporters involved in transepithelial secretion were identified using a classical pharmacological approach. Movement of the organic anion fluorescein-methotrexate (FL-MTX) was followed in freshly excised tissue from medium, through the epithelium and into CP blood vessels. Changing ionic composition and addition of various inhibitors to the surrounding medium allowed revealing molecular mechanisms governing organic anion secretion across CP tissue. Comparisons to transport of another organic anion, fluorescein, were made. Finally, for the first time it was shown that different protein kinases are involved in regulating organic anion transport across the CP.

3.3.1 Choroid Plexus Epithelial Cell F-Actin

Actin is the most abundant protein in eukaryotic cells and highly conserved (Goodson and Hawse, 2002). Involved in many basic phenomena, the protein is crucial to many structural and regulatory cell functions (Rodriguez et al., 2003).

The filamentous or fibrous form of actin (f-actin) is formed by polymerisation of globular actin (g-actin) with bound adenosine-triphosphate (ATP). Together with intermediate filaments and microtubules, actin filaments make up the cytoskeleton. In general, the cytoskeleton plays a major role in cellular differentiation, cell shape development and intracellular trafficking. With respect to epithelial cells, its role includes development of polarity, formation of the apical-basolateral axis and facilitation of topographic contacts between cells and extracellular matrix (Bacallao, 1995; Louvard, 1996). Further, actin filaments are associated with tight junctions and perijunctional actin is directly involved in controlling paracellular permeability (Anderson and Van Itallie, 1995).

Isolated CPEC were grown in serum-containing medium for nine days and then kept in serum-free medium for an additional five days, allowing full differentiation. After 14 DIC cells were washed and following fixation in 95% EtOH, cells were permeated with Triton-X 100. To visualize actin distribution throughout the epithelium, the protein was stained with fluorescent-labeled phalloidin (FITC-phalloidin). Phalloidin is a toxin, isolated from the toadstool "Death Cap" (*Amanita phalloides*), that binds specifically to f-actin by association with individual subunit junctions (Loew and Wieland, 1974; Faulstich et al., 1993). Propidium iodide (PI) was also added to permeated cells, staining cell nuclei.

Figure 7 shows images of CPEC 14 DIC after incubation with FITC-phalloidin and PI (figure 7A) and PI only (figure 7B, control), visualized by confocal laser scanning microscopy. Samples were viewed through an inverse microscope equipped with a X 40 water immersion objective (NA 1.2). The FITC label was excited at 485 nm with an argon-ion laser and the resulting emissions recorded through a 505-nm dichroic filter and a 510-nm long-pass emission filter.

F-actin is shown in green and cell nuclei are shown in red. Overall, cultured epithelial cells appeared as a confluent monolayer with individual cells of polygonal, cobblestone-like shape. No undesired and contaminating cells (e.g. fibroblasts or macrophages) were present. All CPEC abundantly expressed f-actin and, as ex-

pected from fully differentiated cells, the stain revealed actin filaments in networks and bundles, some of which spanned the whole cell.

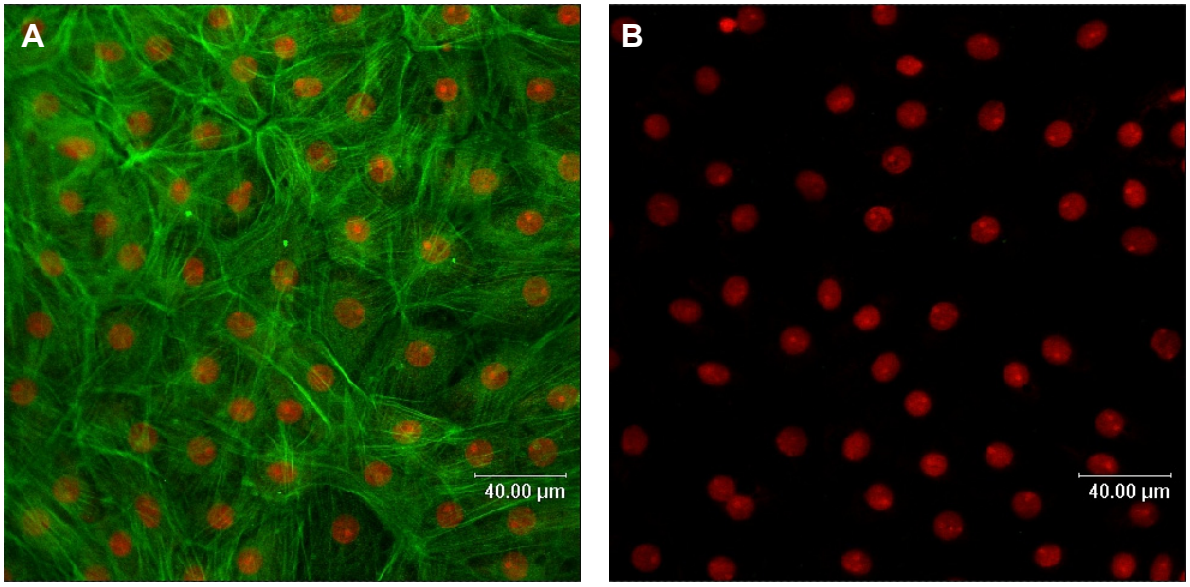

Figure 7: Phalloidin Stained F-Actin (Green) in Cultured CPEC 14 DIC with PI (A) and PI Only (Control, B).

3.3.2 The Marker Protein Prealbumin (Transthyrethin, TTR)

Upon discovery in the 1950s, thyroxin-binding prealbumin was first known for plasma transport of thyroid hormones (Schonenberger et al., 1956). Later its role in vitamin A transport, through interaction with retinol-binding protein, was revealed (Robbins, 2002). It was then renamed transthyrethin (TTR).

In the mammalian brain, TTR is specifically localized to the CP, demonstrated by Northern analysis, in situ hybridization with specific cDNA probes and immunocytochemical analysis (Dickson et al., 1985; Herbert et al., 1986; Stauder et al., 1986, Jacobsson, 1989). Otherwise, TTR is found in liver, pancreatic islets, in endocrine tumors and the eye (Inada, 1988; Jacobsson, 1989).

Due to its specific localization within the brain, TTR is a convenient marker for CPEC (Gath et al., 1997; Zheng and Zhao, 1998; Zheng et al., 2002; Zheng and Zhao, 2002). So far TTR was used to characterize primary cultured CPEC from rat and pig and also an immortalized CPEC cell line. Approximately 20% of total protein synthesized by CPEC is TTR and 50% of protein secreted into the CSF by CPEC is TTR (Schreiber et al., 1990). Thus protein within cells as well as protein secreted into the surrounding medium can be used in CPEC characterization.

TTR mRNA expression was analyzed in fresh CP tissue and cultured CPEC 14 DIC. Further, the protein was immunolocalized in cultured CPEC and visualized by confocal laser scanning microscopy. Finally, TTR was stained in Western blots, following whole cell lysate SDS-PAGE.

3.3.3 TTR Analysis in Choroid Plexus Epithelial Cells

TTR is a cytoplasmic 55 kDa, 130 amino acid tetramer comprised of identical subunits of approximately 15 kDa (Docherty et al., 1989). The unpublished mRNA sequence for porcine specific TTR, accession number X87846, was submitted to the Nucleotide Entrez database by Archibald et al. (1995).

For TTR mRNA expression analysis, cells were grown for 9 DIC in serum-containing medium and allowed to fully differentiate in serum-free medium for additional five days. Fresh porcine CP, cleared from all surrounding brain tissue, and porcine liver were isolated in the slaughterhouse and transferred to RNALater® storage solution and stored at 4°C according to the manufacturer's directions. mRNA was isolated from all samples using the Qiagen RNeasy® isolation kit and carried out according to the manufacturer's protocol. Only RNA samples with an OD ratio of 260 nm over 280 nm of 1.7 to 2.0 were used in mRNA transcription.

Following reverse transcription of 1.0 µg of total RNA with the Promega Reverse Transcription System®, samples were amplified from 10% of the produced cDNA using TTR and β-actin specific primers (table 4). Amplification was run for 15 to 35 cycles with annealing temperature set at 55°C at 30 sec time intervals. Resulting PCR products were separated on a 1.5% agarose gel and stained with ethidium bromide.

Figure 8 shows amplified cDNA of liver (control), fresh CP, CP 9 DIC and CP 14 DIC in an ethidium bromide gel visualized under UV-light. TTR amplified at 371 bp specific for TTR mRNA expression and is shown in the top lanes. β-Actin, used as internal standard, amplified at 703 bp and is shown in bottom lanes. For each sample, lanes one through five show amplification results for 15 to 35 cycles, with lanes corresponding to PCR products with five cycles of additional amplification (cycles number: lane 1, 15; lane 2, 20; lane 3, 25; lane 4, 30; lane 5, 35).

Fresh CP (CP 0 DIC) TTR amplification produced gel bands after 15 amplification cycles. The signal for cultured CPEC was less intense, with signals visible after

25 amplification cycles. β-actin amplified with similar intensity in all CPEC samples. Thus, TTR mRNA expression was higher in fresh CP tissue when compared to TTR expressed in cultured CPEC.

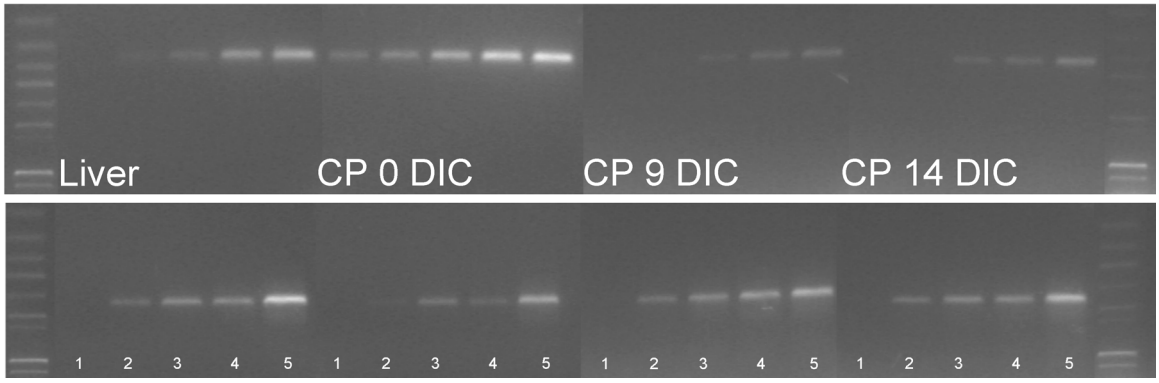

Figure 8: Liver, Freshly Isolated, CPEC 9 DIC and CPEC 14 DIC RT-PCR of TTR (371 bp) and β-Actin (703 bp).

TTR protein expression was investigated in immunological staining of cultured CPEC 14 DIC and in Western blot analysis, using fresh and cultured CPEC 14 DIC. For immunohistological analysis, CPEC were grown on chamber slides for nine days in serum-containing medium followed by additional five days in serum-free medium. After fixing cells in 95% EtOH and permeation with Triton-X 100, samples were blocked and then incubated with TTR specific antibody (table 5). After primary incubation, samples were stained with FITC-labeled secondary antibody. Following addition of fluorescence enhancer, samples were visualized by confocal laser scanning microscopy, using an inverted Leica DM-IRB confocal microscope, equipped with a X40 oil immersion objective (NA 1.2), a 488-nm argon-ion laser excitation and a 500-nm long-pass emission filter.

Figure 9A shows confocal images of a cultured CPEC monolayer stained with anti-TTR and PI in *xy*, *xz* and *yz* sections. Cells formed an intact monolayer and appeared cobblestone-shaped. TTR is shown in green and cell nuclei in red. In cultured CPEC, TTR localized throughout the cytoplasm, with most intense staining around the cell nuclei. Fewer signals were observed towards the cell membrane. No TTR staining was seen in control (figure 9B) images.

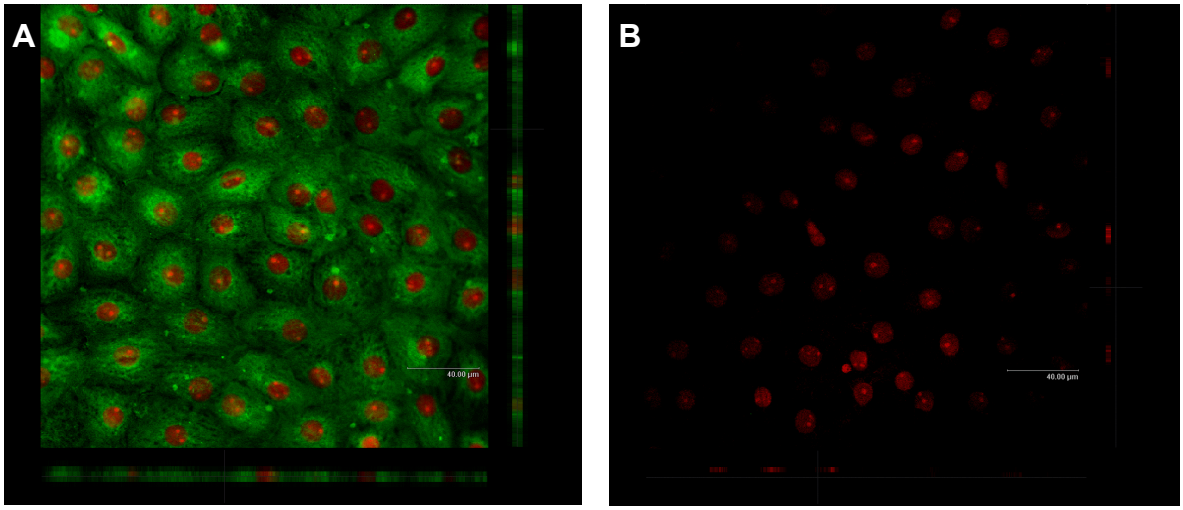

Figure 9: TTR (Green) and PI (Red) Stained CPEC (A) and Control (B)

For Western blot analysis, whole cell protein was isolated from porcine liver tissue (control), fresh CP tissue and cultured CPEC 14 DIC. For protein isolation, fresh CP tissue and liver were collected and immediately placed in RNALater®, according to the manufacturer's directions, before use. Cultured CPEC were lysed directly in culture flasks. All samples were homogenized in CellLytic®, with protease inhibitors added, denatured in SDS-buffer and reduced with β-mercaptoethanol. A total of 10 µg whole cell protein was applied to each lane and samples were separated by SDS-PAGE in a 15% polyacrylamide gel. Then, proteins were transferred to a nitrocellulose membrane, incubated with anti-TTR antibody and labelled with HRP-secondary antibody. Finally, stains were visualized with diaminobenzidine in presence of $NiCl_2$.

Figure 10 shows the Western blot of TTR denatured to 15 kDa TTR fragments in fresh CPEC and cultured cells 14 DIC. Porcine liver was used as positive control. Samples without primary antibody incubation are included as negative control. Lanes 1 and 2 are liver TTR without and with primary TTR antibody added. Lanes 3 and 4 show freshly isolated CP TTR without and with primary antibody. Lanes 5 and 6 are 14 DIC CPEC TTR bands without and with primary antibody added. All samples with primary antibody added show TTR staining. All samples with primary antibody omitted remained blank.

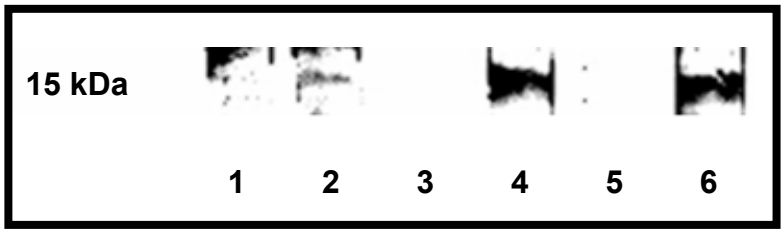

Figure 10: TTR Western Blot of Liver (Lane 1 and 2), Freshly Isolated CP (Lane 3 and 4) and CPEC 14 DIC (Lane 5 and 6)

3.3.4 Enzyme Analysis

Two enzymes, alkaline phosphatase (AP) (EC 3.1.3.1) and γ-glutamyl transferase (γ-GT) (EC 2.3.2.1), were used to characterize cultured CPEC. Both membrane-bound enzymes are well known markers for the BBB *in vivo* and *in vitro* (Schlosshauer, 1993; Beuckmann et al., 1995; Moller and Kummer, 2003). Both AP and γ-GT are present at the BCSFB in different species, including pig, and have been previously used to characterize CP membrane preparations (Sessa et al., 1976; Yoshioka et al., 1988; Bourne et al., 1989; Whittico et al., 1991; De Bault and Mitro, 1994; Narisawa et al., 1994; Ogawa et al., 1998).

AP catalyzes hydrolysis of phosphorylated metabolites, such as hexose and mono-nucleotides and controls their passage into the brain (Pino et al., 1995). And AP contributes to the enzymatic BCSFB, activating or deactivating enzymes by dephosphorylation (Meyer et al., 1990). γ-GT is critical to the γ-glutamylcycle and glutathione homeostasis. It catalyzes transpeptidation in glutathione metabolism by transferring the γ-glutamyl moiety of a donor peptide to amino acids and peptides. γ-GT also plays an important role in phase II detoxification processes (Caspers und Diglio, 1984).

AP activity was determined hydrolyzing p-nitrophenyl phosphate in presence of an amino alcohol, 2-amino-2-methyl-1-propanol. In this reaction, AP transferred the phosphate moiety onto the amino alcohol, yielding p-nitrophenol and inorganic phosphate. The resulting yellow phenolate was measured (OD 410 nm) and quantified using an appropriate standard curve.

γ-GT activity was determined following a protocol by Caspers and Diglio (1984). γ-Glutamyl-p-nitroanilid was converted to p-nitroanilin with glycylglycine acting as acceptor in the reaction. p-Nitroanilin was then measured at an OD of 410 nm and concentrations were determined via its molar absorption coefficient.

Figure 11 shows enzyme activity (EA) measured in units of nmol of substrate converted per min per mg of protein. Activity was determined for cultured CPEC at 9 DIC, before serum was removed from culture medium, and at 14 DIC, after cells were fully differentiated. Measured enzyme activity was compared to freshly isolated CPEC (0 DIC).

AP activity (figure 11A) decreased from 11.9 nmol/min/mg down to 1.5 nmol/min/mg and 1.4 U/mg from 0 DIC to 9 DIC and 14 DIC, resembling an 88.6% and 87.1% decrease compared to activity measured after cell isolation. The reduction in γ-GT (figure 11B) was more gradual, with values decreasing from 11.4 nmol/min/mg to 9.5 nmol/min/mg and 5.0 U/mg from 0 DIC to 9 and 14 DIC, resembling a 25.0% and 45.4% decrease after 14 DIC.

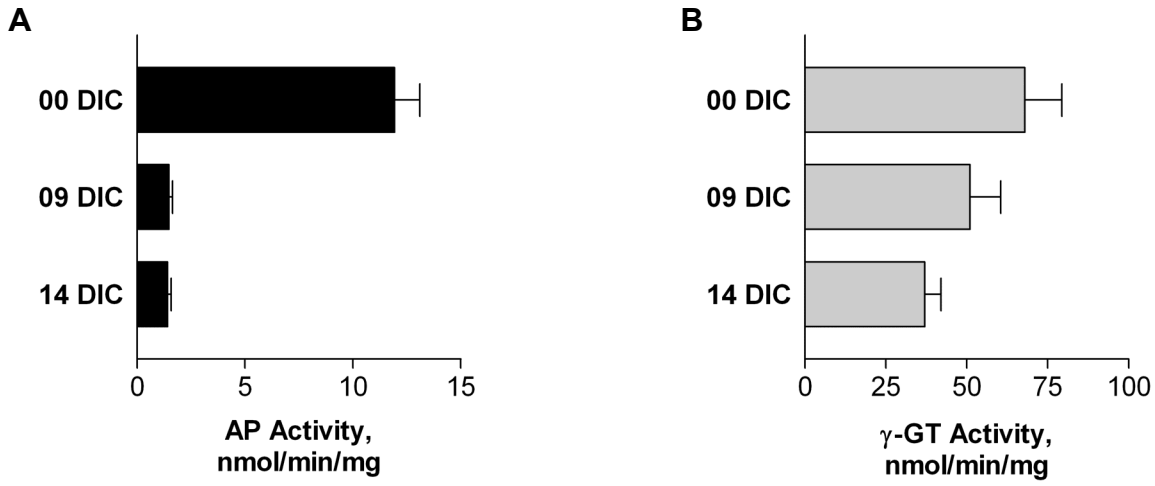

Figure 11: Alkaline Phosphatase (AP, A) and γ-Glutamyl-Transferase (γ-GT, B) Activity in Freshly Isolated and CPEC 9 DIC and 14 DIC.

Enzymatic activity is often reduced in *in vitro* preparations when compared to live tissue *in vivo*, as culture conditions, medium and surrounding environment differ. For example, reduced AP and γ-GT activity was observed in primary BCEC cultures, with activity decreased during cell proliferation and continuingly low even after cells had grown into a confluent monolayer and fully differentiated (Fukushima et al., 1990; Meyer et al., 1990). Enzyme activity could only be regained after adding angiogenic and astroglial factors to the medium (Meyer et al., 1991; Roux et al., 1994) or by treating with 8-(p-chlorophenylthio)-cyclic 3',5'-adenosine monophosphate (C1PhS-cAMP) (Beuckmann et al., 1995).

3.3.5 Cultured Choroid Plexus Epithelial Cell Cerebrospinal-Fluid Section

The high rate of CSF secretion is fueled by rapid blood flow through the vascularity of the plexus (5 ml/g/min), which is about tenfold faster than average cerebral blood flow (Johanson, 1995). Figure 12 depicts the major elements involved in CSF production and their direction of vectorial transport. Two pathways determine transepithelial flow of water, one ion-dependent and the other ion-independent (Speak et al., 2001).

The driving force behind the ion-dependent pathway is transport of sodium and potassium ions by Na^+/K^+-ATPase, located at the apical membrane of CPEC, producing a transmembrane Na^+-gradient. Intracellular Na^+-concentrations are in the range of 20-30 mmol/l compared to 140 mmol/l in the extracellular space. This gradient is a strong secondary driving force for Na^+ into the cell, facilitated by Na^+-H^+-exchanger and Na^+-Cl^--cotransporter, both located at basolateral membranes. Thus, the transepithelial osmotic gradient, following movement of Na^+, is coordinated by basolateral Na^+-influx and apical Na^+-efflux.

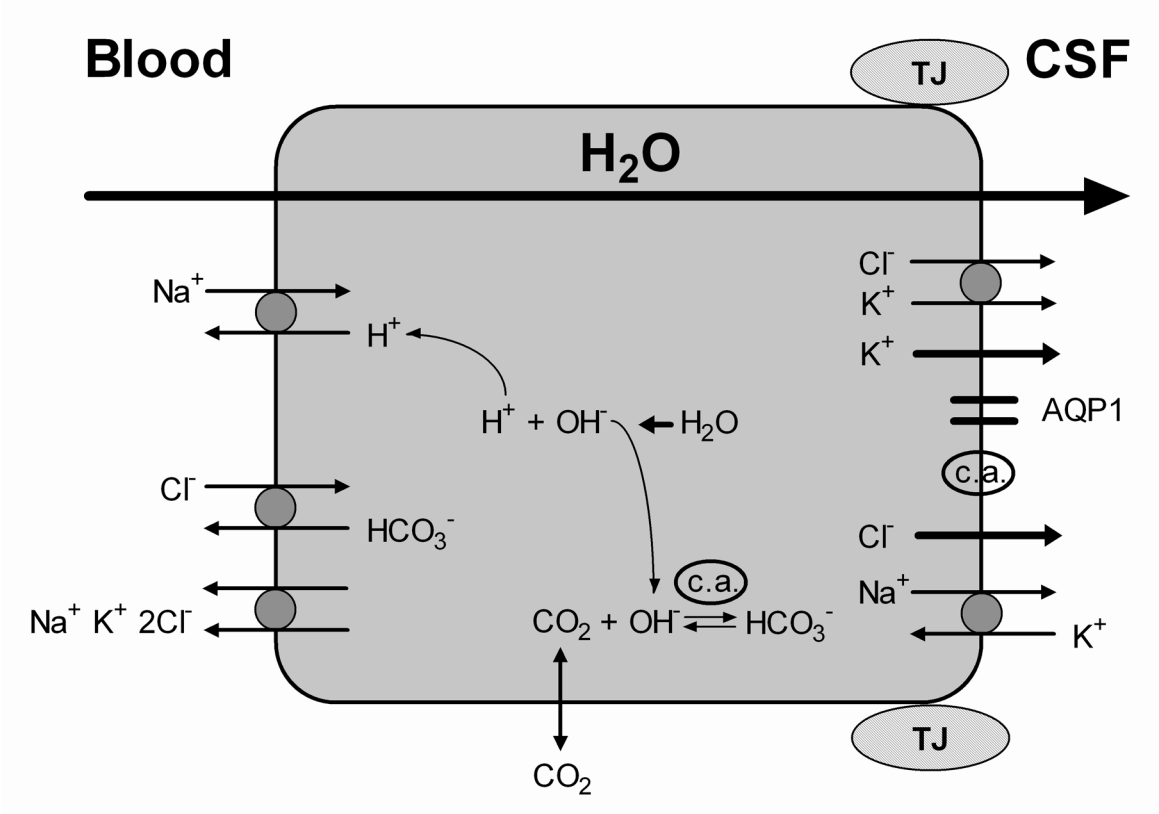

Figure 12: CSF Secretion across Choroid Plexus Epithelial Cells

The ion-independent pathway is dependent mainly on aquaporin 1 (AQP1), previously shown to be expressed in CPEC (Nielsen et al., 1993; Nielsen et al., 1996; Lee et al., 1997; Venero et al., 2001). In the brain, AQP1 is specific to the BCSFB.

Peripheral capillary endothelial cells express AQP1, but the endothelium of the BBB does not (Kobayashi et al., 2001). Further, human CP AQP1 mRNA expression levels are very high and comparable to those of renal cortex and pancreatic ducts (Mobasheri and Marples, 2004). In immunostaining studies, AQP1 was found in lateral and forth CP of rat, predominantly localized to apical CPEC membranes, with only low signal at the basolateral membrane (Nielsen et al., 1993; Masseguin et al., 2000; Speake et al., 2001, Speak et al., 2003). In addition to AQP1, AQP4 may also be involved in the transepithelial movement of water in CP tissue. However, the protein could not be assigned to either membrane, but was found to distribute throughout the cytoplasm (Speak et al., 2003).

CPEC CSF secretion was analyzed with cells grown on 6-well Transwell® filters systems coated with 5 µg/ml laminin. Cells were incubated for 9 DIC with serum-containing medium followed by another 5 DIC in serum-free medium. After washing cells with CSFB, 1 µM 67 kDa FITC-dextran was added to the CSFB (2.5 ml in both apical and basolateral compartments). Samples were taken at 1 hour time intervals and volumes removed were replaced with fresh CSFB. Sample FITC-dextran concentrations were determined using a fluorescent plate reader equipped with 485 nm excitation and 520 nm emission filters. Final concentrations were adjusted according to the sample regimen and secreted CSF volumes (in µl/cm^2) calculated as a function of FITC-dextran concentration change.

Figure 13 shows CSF volumes secreted by cultured CPEC for up to eight hours. Volumes of CSF secreted by the cell monolayer increased in linear fashion, reaching a plateau after five hours, with approximately 150 µl/cm^2 produced. No further increase in CSF volume secreted was measured thereafter. Using measurements made during the first four hours of linear CSF secretion, CSF production rates were measured to be 46.70 ± 4.47µl/cm^2/h.

The volume of CSF produced in the model system presented compares to results obtained by Hakvoort et al. (1998). Using similar *in vitro* conditions, a secretion rate of approximately 45 µl/cm^2/h was calculated over four hours of incubation. In another study, saturation of CSF production was reached after six hours with 12% of the basolateral chamber volume secreted into the apical compartment (Hakvoort et al., 1998). In our studies, saturation was reached after five hours with an increase of approximately 15% in apical volume.

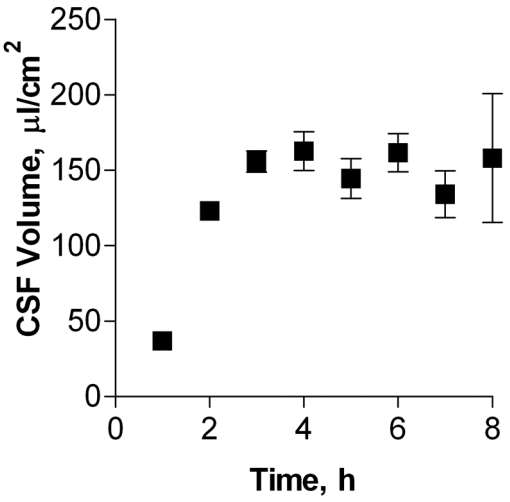

Figure 13: CSF Secretion in CPEC 14 DIC

Comparing *in vitro* data to *in vivo* CSF secretion measurements is difficult however, assuming a total apical surface area of 75 cm^2 (rat, Keep and Jones, 1990) and a secretion rate of 2.2 µl/min (rat, Cserr, 1971) CSF production is at the rate of approximately 1.76 µl/cm^2/hour in rat. Assuming that human CSF secretion is about 150-fold higher when compared to rat, a production rate of approximately 280 µl/cm^2/hour is calculated for humans.

3.3.6 Cultured Choroid Plexus Monolayer Transepithelial Resistance Values

The BCSFB, as all other cellular barriers, relies on membrane polarization for barrier function and on tight intercellular contacts. In development, epithelial cell polarization is a multistage process, requiring extracellular cues and reorganization of proteins in cytoplasm and plasma membranes (Vega-Salas et al., 1987; Rodriguez-Boulan and Nelson, 1989). The polarized phenotype is maintained by protein sorting and differential trafficking of proteins and lipids to apical and basolateral membrane domains along actin filaments (Low et al., 2000; Mostov et al., 2003). Grown on permeable surfaces, a number of different epithelial cell types, including CPEC, show polarized distribution (Mauchamp et al., 1987; Haselbach et al., 2001).

The structural basis of cellular barrier function is expression of tight junctions (TJ). These protein complexes, formed between adjacent cells, allow for cell-cell contact and separate apical and basolateral membranes (Kniesel et al., 1994; Van Itallie, 2004). TJs were first described in 1965 for a number of cell linings of glands and cavi-

tary organs and regulate paracellular diffusion of solutes and water as well as electrical resistance and ionic charge selectivity (Fagqmiag and Palade, 1965; Mitic et al., 2000). In the BBB, BCEC express TJ and form the cellular barrier. In the BCSFB the cellular barrier is formed by CPEC and TJ between neighboring epithelial cells (Spector and Johanson, 1989).

Cellular polarization and TJ formation cause a vectorial distribution of charged inorganic ions and consequently cellular barriers *in vivo* and *in vitro* produce differential electrical resistances (Segal and Burgess, 1974; Mollgard and Rostgaard, 1978; Zeuthen and Wright, 1981; Smith and Rapoport, 1986; Wegener et al., 1996). Epithelial cells display transepithelial resistances and endothelial barriers specific transendothelial resistances. TEER values have been used extensively as a permeability measure determining leakiness of cellular barriers, including CPEC *in vivo* and *in vitro* as well as other epithelial barriers, such as the intestine, or the other barrier to the brain, the BBB (Crook et al., 1981; Gath et al., 1997; Hakvoort et al., 1998; Strazielle and Ghersi-Egea, 1999; Haselbach et al., 2001; Zheng and Zhao, 2001).

Cerebral capillaries are characterized by high endothelial resistance values. *In vivo* TEER values for BBB are in the range of 1500 to 2000 Ωcm^2, with some measurements as high as 8000 Ωcm^2, compared to peripheral endothelial cells displaying resistance values of 3 to 33 Ωcm^2 (Garberg, 1998). *In vitro* measurements for TEER values are in the range of 1000 to 2000 Ωcm^2 for primary derived BCEC cultures, including porcine preparations, and around 100 to 300 Ωcm^2 for immortalized BCEC cell lines from such species as pig or mouse (Nitz et al., 2003; Omidi et al., 2003; Lauer et al., 2004). Primary preparations of human BCEC yield TEER values of 100 to 250 Ωcm^2 (Muruganandam et al., 1997; Zenker et al., 2003).

Transmucosal intestinal resistance determined in pigs was measured at values of 10 Ωcm^2 to 50 Ωcm^2, increasing with time after weaning of piglets (Boudry et al., 2004). Transepithelial resistance across the intestinal barrier of humans is in the range of 300 Ωcm^2 to 700 Ωcm^2, as determined from Caco-2 cells derived from human colonic adenocarcinoma cells and is able to express differentiation features resembling mature intestinal cells, grown in the 3-day or the 21-day model (Violante et al., 2004).

Due to morphological complexity, small size and anatomical location of the CP, there is no data on *in vivo* TEER available for mammals and no TEER information on

lateral CP TEER for any species. IV-ventricle CP TEER measurements were carried out in bullfrog IV-ventricle with values at approximately 170 Ωcm^2 (Saito and Wright, 1983). Elasmobranches resistance values were measured with values of 70 to 107 Ωcm^2 (Villalobos et al., 2002).

In primary cultures of rat CPEC, TEER values were in the range of 100-500 Ωcm^2 (Southwell et al., 1993 and Zheng et al., 1997; Rao et al., 1999; Strazielle and Ghersi-Egea, 1999). Porcine CPEC models displayed resistance values in the range of 100 to 170 Ωcm^2 (Gath et al., 1997; Hakvoort et al., 1998). One research group reported TEER values exceeding 1500 Ωcm^2, for cells grown in serum-free medium (Hakvoort et al., 1998; Angelow et al., 2004). However, these resistance measurements were taken using a unique device.

CPEC for use in transport studies were grown on permeable membranes until fully differentiated (figure 14). Permeable filter systems are routinely used for permeability measurements across CP monolayers and also across various other barrier models (Haselbach et al, 2001; Youdim et al., 2003). CPEC TEER values were measured using the Millicell®-ERS and STX-2 electrode system, before starting permeability analyses. In the primary porcine CPEC model presented, monolayers displayed TEER values in the range of 100 to 150 Ωcm^2 and were judged confluent at values > 100 Ωcm^2.

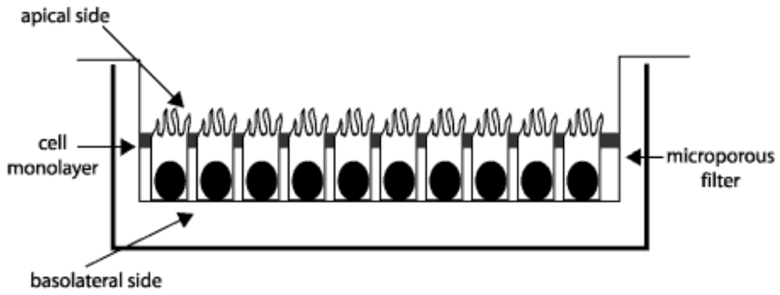

Figure 14: Schematic Diagram of CPEC Grown on Transwell® Filter Systems

The drawback to using TEER to determine tightness of a cellular monolayer and subsequent permeability analyses is that resistance measurements are influenced by temperature, pH, age of tissue or culture and type of culture medium or buffer used and that TEER values do not take toxicity considerations into account (Zheng et al., 1997; Mukherjee et al., 2004). Therefore, all monolayers grown for

permeability analyses were assessed not only by measuring TEER values, but also control by light microscopy and use of permeability markers. Combination of these methods for judging epithelial cell monolayer tightness has been used extensively in the past (Gath et al., 1997; Zheng and Zhao, 2002; Ancillotti et al., 2003; Yoo et al., 2003).

3.3.7 Permeability Marker Analyses

For cells of the BBB or BCSFB and other barrier forming cells, such as epithelial cells of the small intestine or Sertoli cells of the blood-testis barrier, *in vitro* cell culture and experimental conditions influence cell differentiation, including TJ expression and complexity and thus barrier morphology (Jegou, 1992; Wolburg et al., 1994; Gath et al., 1997; Hakvoort et al, 1998; Behrens and Kissel, 2003; Berezowski et al., 2004). Comparative studies on BBB endothelial cells for example revealed that cell monolayers were more permeable in culture (Tao-Cheng and Brightman, 1988; Wolburg et al., 1994; Kniesel et al., 1994; Risau et al., 1998). Thus, even though *in vitro* endothelial models can be a good tool for assessing BBB secretion, predictions tend to overestimate *in vivo* drug movement and correlation between both types of data is necessary (Pardridge et al., 1990; Dehouck et al., 1992; Pardridge et al., 1999; Terasaki et al., 2003; Zenker et al., 2003).

Through use of marker compounds in brain permeability studies, limitations inherent to cell culture systems are overcome. Comparative studies provide a measure of cell monolayer differentiation and thus allow for comparison between different culture systems and *in vivo* drug permeability data (Takakura et al., 1991; Gumbleton and Audus, 2001; Lohmann et al., 2002; Lundquist et al., 2002; Deguchi et al., 2004; Lauer et al., 2004). A wide range of compounds has been used to characterize BBB and BCSFB membranes, including the zero permeability marker PEG-4000 (FDA, Biopharmaceutical Classification System: Guidance for Industry, 2000), compounds secreted via paracellular routes such as carboxyfluorescein (5-CF), fluorescein-labeled dextrans, mannitol and sucrose (Gath et al., 1997; Thomas and Segal, 1998; Fletcher et al., 2000; Masungi et al., 2004), lipophilic transcellular markers such as propranolol, morphine and diazepam (Lin and Lin, 1990; Omidi et al., 2003), as well as markers for transport-mediated secretion, including glucose, alanine and leucin (Dehouck et al., 1992; Omidi et al., 2003; Deguchi et al., 2004).

For paracellular marker analyses, CPEC were grown on Transwell® filter systems for 9 DIC in serum-containing medium followed by another 5 DIC in serum-free medium. Only polyester membrane filters (pore size 0.3 µm) were used and coated with 5µg/cm^2 laminin prior to seeding of CPEC. Marker compounds were applied from either the apical or basolateral chamber and accumulation was measured in the corresponding compartment. All markers were used at a concentration of 10 µM.

Figure 15 shows permeability of 5-CF (0.4 kDa) and fluorescent-labeled dextrans ranging from 4.4 kDa to 500 kDa in size across CPEC 14 DIC monolayers, grown on either polyester or polycarbonate membranes of equal thickness (10 µm) and with equal pore size (0.4 µm), but 4 x 10^6 and 1 x 10^8 pores per cm growth area, respectively. Permeation was measured from apical into basolateral compartments. Values are presented as amount of compound transported (in percent, %). Measurements were carried out over a two hour time period.

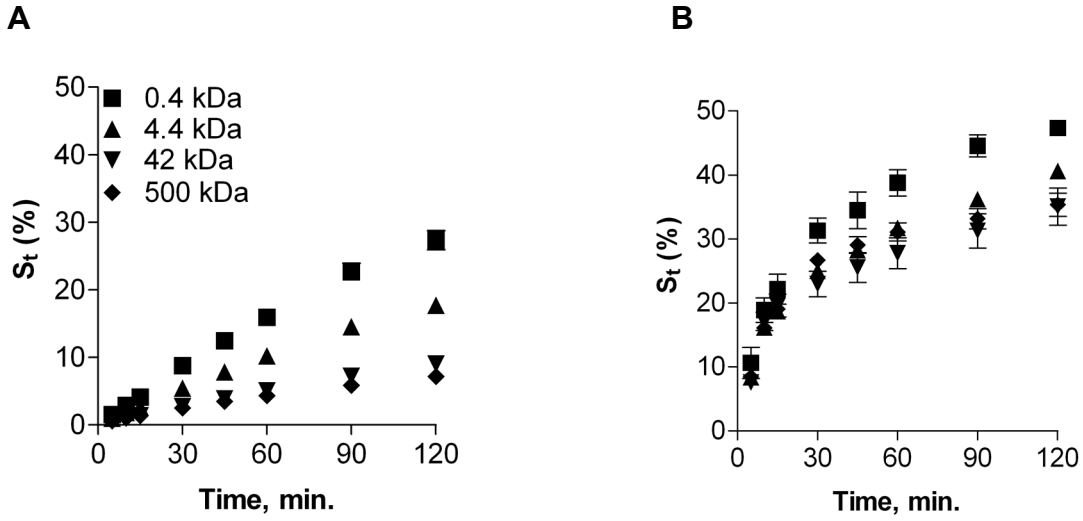

Figure 15: 5-CF and Dextran Permeation across CPEC 14 DIC with Transport across Polyester (A) and Polycarbonate (B) Membranes

Molecules larger in size permeated slower across cell monolayers. Whereas permeation was linear for all compounds across polyester membranes, permeation across polycarbonate membranes followed saturation-like curves. For polyester membranes, total amount of compound permeated for smallest and largest molecules was 16.00% and 4.35% after one hour and 27.36% and 7.20% after two hours, respectively. In contrast, for polycarbonate membranes smallest markers (0.4 kDa) reached approximately equal concentrations in apical and basolateral chambers after

two hours. Differences in amount of compound permeated were almost not detectable. Thus, only polyester membranes allowed isolated CPEC to differentiate into an integer CPEC monolayer suitable for permeation and secretion experiments.

Figure 16 shows apparent permeability coefficients (P_{app}) of 5-CF and dextrans, ranging from 0.4 kDa to 500 kDa in size. Transport was quantified across CPEC 14 DIC grown on polyester membranes, measuring secretion from apical to basolateral chambers. P_{app} values ranged from 4.56 +/- 0.26 x 10^{-5} cm/s for smallest down to 1.42+/- 0.13 x 10^{-5} cm/s for largest molecules. Notably, permeation reached a plateau at approximately 40 kDa, with P_{app} values for 42 kDa dextrans not significantly different from P_{app} for 500 kDa dextrans.

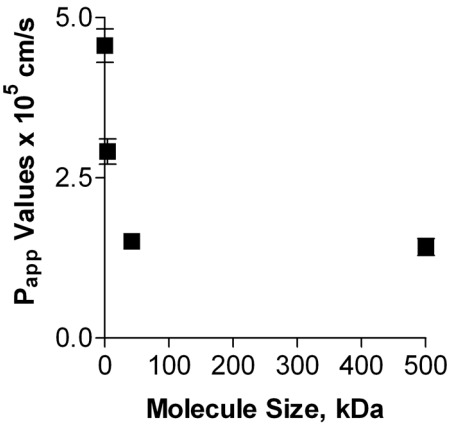

Figure 16: P_{app} Values of 5-CF and Dextrans 0.4 kDa to 500 kDa

Further evidence for CPEC monolayer differentiation and TJs expression was gained from comparing permeation across monolayers with intact or opened TJs. One method of opening TJs is to remove free calcium from surrounding medium. Previous studies on epithelia showed that following addition of EDTA and complexion of Ca^{2+}, cells retracted and TJ protein ZO1 as well as actin redistributed from the junctional zone back into the cytoplasm (Grebenkamper and Galla, 1994; Chang et al., 1997). Figure 17 shows transport of 5-CF (10 µM) in CPEC 14 DIC, grown on polyester membranes, without and with 0.25% EDTA added to the medium. Permeability of the paracellular marker is significantly higher through monolayers with opened TJs, with P_{app} values nearly doubling.

Barrier structure development for CPEC *in vitro* was investigated measuring permeation at different time intervals during cell culture (figure 18). Transport of 5-CF

and dextrans, with molecules ranging from 0.4 kDa to 500 kDa in size, was quantified at 9 DIC, before changing growing CPEC to serum-free medium, at 14 DIC and after serum-free culture for up to 21 DIC. Values for 5-CF (0.4 kDa) ranged from 4.20 +/- 0.22 x 10^{-5} cm/s, 3.51 +/- 0.13 x 10^{-5} cm/s to 4.41 +/- 0.16 x 10^{-5} cm/s for 9 DIC, 14 DIC and 21 DIC, respectively. A similar pattern was observed for dextrans larger in size. Thus, removal of serum from the medium increased CPEC barrier tightness for an initial culture period before barrier function was lost with time. Results with effects of serum removal similar to those demonstrated were obtained previously (Chang et al., 1997; Hakvoort et al., 1998).

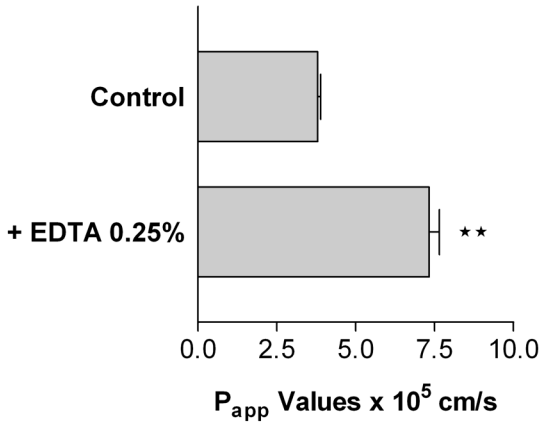

Figure 17: Permeation of 5-CF without and with Open Tight Junctions

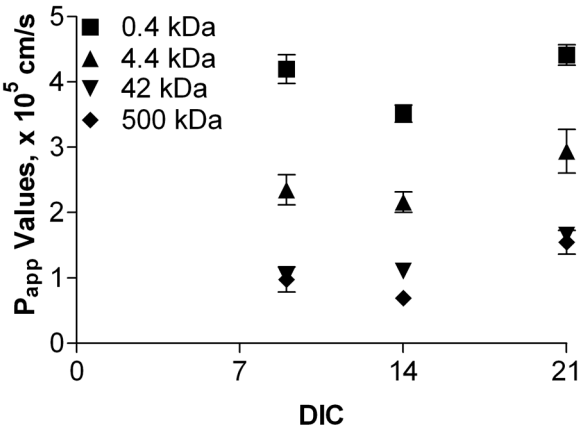

Figure 18: Permeation of 5-CF and Dextrans in Cultured CPEC over Time

Transport of the zero permeability marker PEG-4000, the small paracellular marker sucrose and the highly lipophilic transcellular marker diazepam was meas-

ured in CPEC 14 DIC. P_{app} values were determined for permeation from apical to basolateral compartments and vice versa. Figure 19 shows 5-CF corrected P_{app} values obtained for all three compounds. P_{app} values for all compounds were not significantly different applied to either apical or basolateral chambers. P_{app} values between compounds were significantly different (P≤0.01), with PEG-4000 ranking lowest, followed by sucrose and diazepam.

Compared to other pharmacologically relevant cellular barriers, the BCSFB cell culture model presented was relatively leaky, i.e. compounds permeated more freely. Permeation coefficients for low permeation compounds (PEG-4000) were at approximately 5 x 10^{-6} cm/s, compounds of medium permeability (sucrose) at approximately 3 x 10^{-5} cm/s and high permeability compounds (diazepam) in the range of 5 x 10^{-5} cm/s.

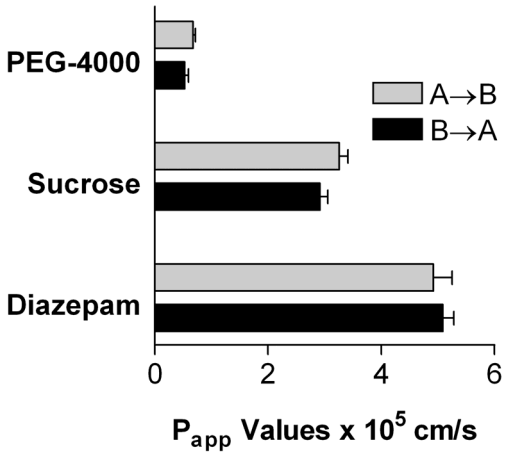

Figure 19: Transport of Permeability Markers from Apical to Basolateral (A→B) and Basolateral to Apical (B→A) Chambers

The intestinal barrier, for example, is another important epithelial barrier of the body. It regulates resorption of many pharmacological relevant compounds following oral ingestion. Caco-2 cells are commonly used as an *in vitro* intestinal permeation model to estimate drug uptake across the small intestine. A study comparing permeation of 20 different drugs and peptides across Caco-2 cell monolayers cultured on permeable surfaces revealed permeability coefficients ranging from 5 x 10^{-8} cm/s to 5 x 10^{-5} cm/s for compounds of low and high permeability, respectively (Artursson and Karlsson, 1991). Permeation values of greater 1 x 10^{-6} cm/s corresponded to 100% drug absorbed, 1 x 10^{-6} cm/s - 0.1 x 10^{-6} cm/s for more than 1% but less than 100%

absorption and equal to or lower than 1 x 10^{-7} cm/s for drugs absorbed 1% or less. Another study employing Caco-2 cells reported good correlations for monolayer permeability coefficients to drug absorbed for P_{app} values ranging from 1 x 10^{-7} cm/s to 4 x 10^{-5} cm/s, with fraction of drug absorbed for high permeability drug in the range of 90% and higher (Pade and Stavchansky, 1998). Another study using Caco-2 cells, distinguishing compounds into poorly, moderately and well absorbed classes of drugs, determined P_{app} values of < 1 x 10^{-6}, 1 -10 x 10^{-5} cm/s and > 10 x 10^{-6} cm/s for these classes, respectively (Yee, 1997).

Generally, when comparing *in vitro* BBB and BCSFB model permeation, BBB models *in vitro*, as *in vivo*, tend to be less diffuse. In an *in vitro* BBB model using cultured BCEC grown on semi-permeable membranes, permeation of fluorescein (0.3 kDa) and FITC-dextran (4.4 kDa) were measured with P_{app} values of 2.2 +/- 0.10 x 10^{-6} cm/s and 0.48 +/- 0.03 x 10^{-6} cm/s, respectively (Gaillard and de Boer, 2000). P_{app} values obtained in the BBB model were thus approximately an order of magnitude lower, comparing to values of 4.56 +/- 0.26 x 10^{-5} and 2.9 +/- 0.20 x 10^{-5} for 5-CF (0.4 kDa) and FITC-dextran (4.4 kDa). Permeability of sucrose was measured in different model systems using cultured Caco-2 cells (Johnson and Anderson, 1999). P_{app} values ranged from 2.8 x 10^{-5} cm/s measured in the Biocoat® system to 2.3 x 10^{-5} cm/s across polyester and 1.8 x 10^{-5} cm/s across polycarbonate membranes. In astrocyte-BCEC co-cultures of immortalized porcine brain endothelium, sucrose P_{app} values were in the range of 5.4 x 10^{-6} cm/s (Lauer et al., 2004). In comparison, the sucrose P_{app} values measured across cultured CPEC were in the range of 3 x 10^{-5} cm/s.

One study comparing permeability of 15 drugs across cultured monolayers of BCEC, including L-dopa, glucose and albumin, measured drug permeability coefficients ranging from 6.5 x 10^{-5} to 4.2 x 10^{-3} cm/s for low and high permeability compounds, respectively (Pardridge et al., 1990). Comparing *in vitro* measurements to *in vivo* permeability, using sucrose solution as blood volume reference, values ranged from 1.7 x 10^{-7} cm/s to 3.5 x 10^{-4} cm/s. Another *in vitro* BBB study, using compounds with a broad range of physicochemical characteristics, measured permeability coefficients from 0.9 x 10^{-5} cm/s to 7.5 x 10^{-5} cm/s for low and high permeability compounds, respectively (Hansen et al., 2002).

Notably, culture and experimental conditions affecting tightness of a monolayer and thus permeation of compounds across cultured cells have to be taken into account when comparing P_{app} values from different studies originating from different laboratories.

3.4 Choroid Plexus ABC Transport Protein Gene Expression

The BBB separates blood from brain and the BCSFB separates blood from cerebrospinal fluid, limiting access to the CNS. Effective treatment of CNS diseases and cancers depends on delivery of therapeutic agents across these barriers and penetration into the brain. In general, the more lipophilic a molecule, the more likely it partitions into brain (Levin, 1980). But, for a number of compounds there is a discrepancy between lipophilicity and CNS permeation, with permeation several orders of magnitude lower than expected (Golden and Pollack, 2003; Sun et al., 2003).

Active excretion by ABC efflux transporters limits brain uptake and penetration of many therapeutic compounds (Begley, 2004). Expression of ABC transporters has been extensively studied at the BBB. With delivery across the CP gaining importance and information regarding ABC transporters at the BCSFB is limited, further investigation into the role of these transporters in CPEC is crucial (de Lange, 2004). Two proteins contributing to multidrug resistance are of particular importance due to the large number and diversity of compounds transported: the MDR phenotype Pgp, part of the ABCB subfamily, and Mrp1, part of the ABCC subfamily (Ecker and Noe, 2004; Graff and Pollack, 2004; Zhang et al., 2004).

Transport proteins, including those of the ABC families, show equal affinities for specific substrates, regardless in which types of cells they are expressed in. Main differences in function arise from differences in expression intensity and localization within polarized cells. Pgp and Mrp1 gene expression at the BCSFB was analyzed on a qualitative and quantitative basis and distribution and localization of both proteins to polarized CPEC membranes determined. Studies focused on gene expression of both proteins *in vivo*, before comparing Mrp1 gene expression *in vivo* to levels *in vitro*. Then, protein partitioning to membranes was determined by immunohistological staining as well as by Western blot analyses using fractionated membrane preparations.

3.4.1 Choroid Plexus Pgp and Mrp1 Gene Expression

As for all proteins, there are two steps in gene expression, transcription and translation that eventually lead to protein expression and appearance of the particular phenotype. First, the gene is transcribed into messenger ribonucleic acid (mRNA), with molecules encoded by the nucleotide sequence of the gene. In translation the mRNA in turn transfers the encoded information to a series of amino acids arranged in a polypeptide chain. This polypeptide chain then may go on to develop into a mature protein producing a cellular response based on the original genetic information.

Studies on yeast showed that there is a correlation between mRNA and protein abundance and that in some cases mRNA abundance allows prediction of protein levels (Gygi et al., 1999). ABC-transporter expression can be regulated at the DNA, RNA and protein level and there is evidence that Pgp and Mrp1 mRNA expression correlates to protein abundance and even functional activity of mature protein inserted into cell membranes (Zhang and Ling, 2000; Young et al, 2001, Bauer et al., 2004). Compared to the BBB, relatively little is known about gene expression of ABC-transport proteins Pgp and Mrp1 in CP epithelium and data on CPEC Pgp and Mrp1 mRNA is only available for rat (Nishino et al., 1999; Choudhuri, 2004).

There is no data comparing CPEC ABC-transporter expression *in vivo* and *in vitro*. With regard to the BBB, there is one comparative study that investigated expression levels in fresh brain and cultured BCEC (Torok et al., 2003). Analyses of Pgp and Mrp1 in whole-brain tissue, isolated brain capillaries and cultured cells showed that gene expression levels varied up to 7-fold after capillary isolation and that expression in cultured cells can be reduced up to 5-fold. The study presented is first to provide data on Pgp and Mrp1 mRNA expression in porcine CPEC, and first to present comparative results for Mrp1 mRNA expression in freshly isolated and cultured CPEC on a semi-quantitative basis.

For Pgp and Mrp1 gene expression analyses, porcine RNA was isolated from fresh CP, cultured CPEC 14 DIC and liver tissue (positive control). Total RNA was extracted using the Qiagen RNeasy® isolation kit, according to the manufacturer's protocol. Only RNA with 260 nm/280 nm-OD ratios between 1.7 and 2.0 were used, ensuring that samples were free of protein or reducing agent contamination. Further, RNA quality was confirmed in negative DNA gels (data not shown).

RT-PCR was performed in a two-tube system. First, cDNA was synthesized by reverse transcription, and then an aliquot of that cDNA was used in PCR amplification. Following target amplification, using target specific primers (table 4), amplicons were separated in an ethidium bromide gel and corresponding bands were visualized under UV light.

To account for sample-to-sample variation, β-Actin amplification was run simultaneously. β-Actin, one of the first genes used as internal standard, is recognized as reliable reference and commonly used in quantitative RT-PCR (Kreuzer et al., 1999). Nevertheless, the method of using housekeeping genes such as β-actin to standardize sample variation is prone to limitations (Bustin, 2000).

Figure 20 shows the amplified 468 bp Pgp DNA product and β-Actin product at 703 bp visualized under UV-light. Pgp was amplified for 50 cycles and β-actin for 35 cycles. Fresh and cultured CPEC expressed Pgp mRNA at low levels, comparable to the signal obtained from liver samples (positive control). Similar results, in terms of expression level, were obtained in previous studies by Choudhuri et al. (2003).

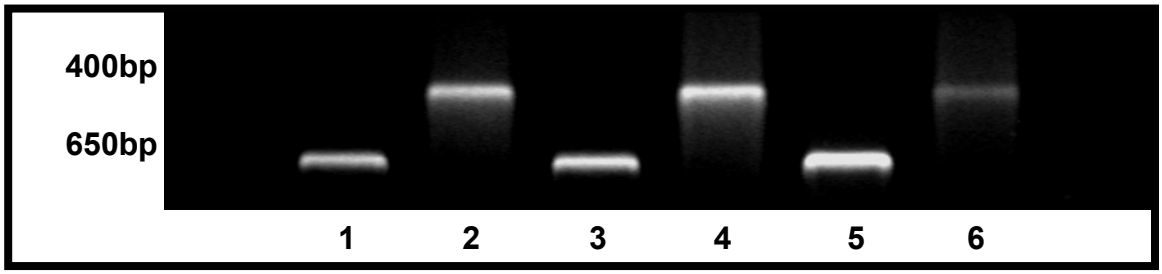

Figure 20: RT-PCR of Pgp (468 bp) and β-Actin (703 bp); From Left to Right: Liver (Lane 1 and 2), Fresh CP Tissue (Lane 3 and 4) and CPEC 14 DIC (Lane 5 and 6)

Figure 21 shows the amplified 436 bp Mrp1 DNA product and β-actin product at 703 bp. Mrp1 was amplified for 50 and β-Actin (internal standard) for 35 cycles. Analyses revealed Mrp1 mRNA expression in fresh and cultured CPEC. Liver mRNA was used as positive control.

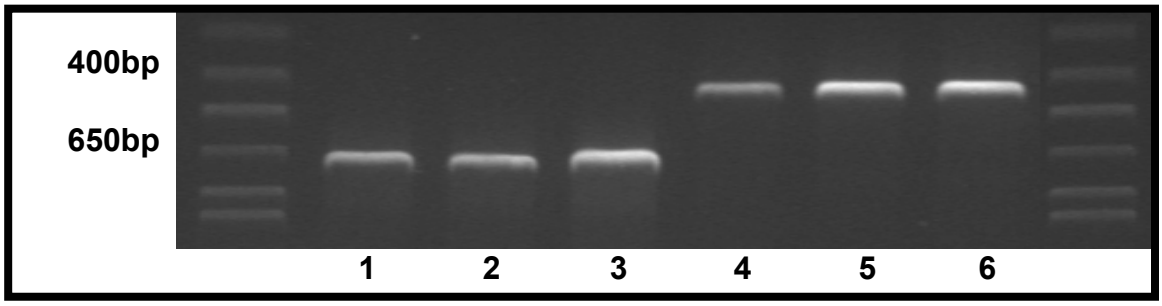

Figure 21: RT-PCR of Mrp1 (436 bp) and β-actin (703 bp) in CPEC 14 DIC (Lane 1 and 4), Fresh CP Tissue (Lane 2 and 5) and Liver (Lane 3 and 6)

3.4.2 Semi-Quantitative Analyses of Mrp1 in Choroid Plexus

To further assess Mrp1 expression in CPEC, semi-quantitative RT-PCR analyses were carried out and mRNA transcription *in vivo* compared to transcription *in vitro*. Generally, RT-PCR is the method of choice for mRNA quantification, as it is more sensitive compared to other methods, including Northern blot, ribonuclease protection, RNA blot, or solution hybridization assays (Chen et al., 1999). In contrast to absolute quantification, amounts of mRNA were normalized against β-actin expression and relative differences between freshly isolated and cultured CPEC determined. Absolute quantification relies on construction of an absolute standard curve, requiring a clone of the desired gene (Bustin, 2000). Clones for the targets of interest are not available for porcine samples yet.

RT-PCR was carried out as described, with 1 µg total RNA used in each reverse transcription reaction. In a second tube, 10% of the resulting cDNA product was used for each PCR amplification reaction. Following target amplification, amplicons were separated in an ethidium bromide gel and corresponding bands visualized under UV light. Band density was determined digitally, using the Scion Image Software (NIH, USA).

Relative differences in target transcription were judged by threshold cycle (C_t), the only concept allowing for accurate and reproducible quantification of mRNA in RT-PCR analyses (Higuchi et al., 1993). The C_t is defined as the point in amplification at which density values are first significantly different from background levels. The starting amount of target mRNA is directly proportional to amplification kinetics of the PCR product, with more target mRNA in a sample leading to earlier detection. Therefore, by definition, the C_t is always in the exponential amplification phase and quantification is not limited by individual reaction components.

To further provide evidence for PCR reaction accuracy, a series of known concentrations of total RNA was reverse transcribed, amplified for a set number of PCR amplification cycles and separated on an ethidium bromide gel, before determining absolute band densities. Starting out with 1 µg of CPEC 14 DIC total mRNA, 5%, 10% and 15% of the cDNA synthesized was used to amplify Mrp1 and β-actin for 30 and 20 cycles, respectively.

Figure 22 shows density values plotted versus the initial amount of RNA (ng) for both targets. Resulting band densities are inversely proportional to initial amounts

of mRNA in a sample and increase in log-linear fashion with increasing amounts of mRNA. The regression coefficients obtained for Mrp1 (figure 22, A; R^2 = 0.9973) and β-actin (figure 22, B; R^2 = 0.9920) are a measure of PCR reaction accuracy and thus experimental consistency.

Figure 23 shows density values plotted against the number of cycles run for β-actin (figure 23, A) and Mrp1 (figure 23, B) amplicons from freshly isolated CPEC. Data for cultured CPEC 14 DIC is comparable (not shown). All mRNA targets amplified exponentially until reaching a plateau, as reaction components became limited. Sample variation was accounted for by normalizing Mrp1 against β-actin.

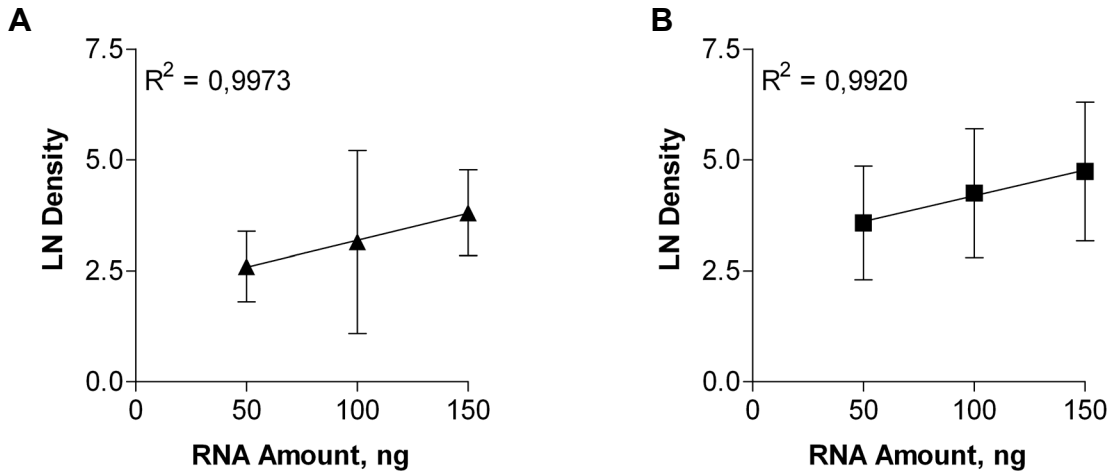

Figure 22: Amplicon Density of Mrp1 (A, 30 Cycles) and β-Actin (B, 20 Cycles) in CPEC 14 DIC

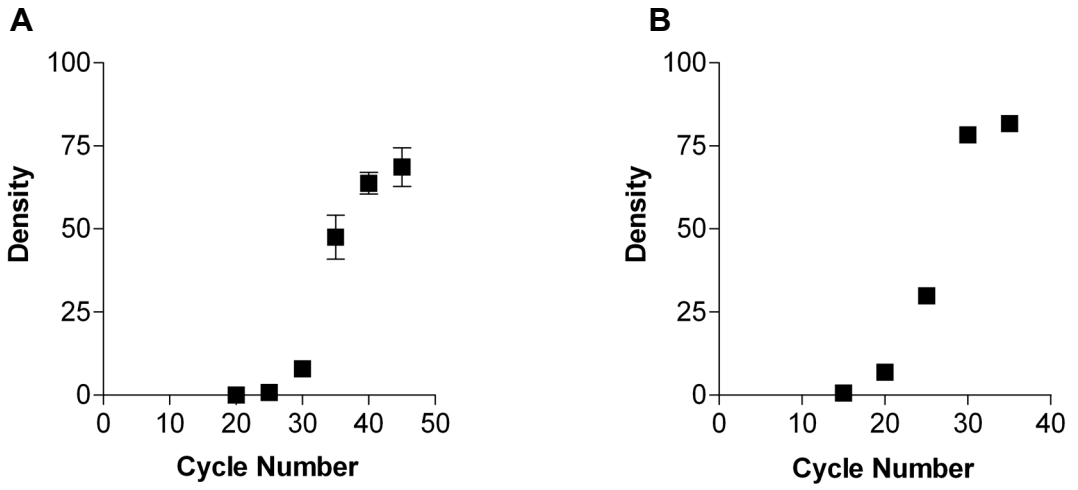

Figure 23: C_t Analysis of Mrp1 (A) and β-Actin (B) in Freshly Isolated CP Tissue

To compare expression levels in CPEC samples, the C_t for Mrp1 was set at 30 cycles and mRNA of cultured CPEC 14 DIC was compared to freshly isolated CPEC. Data presented in table 8 and figure 24 show that there was no significant difference between Mrp1 gene expression in cultured CPEC 14 DIC and freshly isolated CPEC.

Table 8: Mrp1 mRNA Expression in Cultured CPEC 14 DIC and Fresh CP Tissue

Sample	*RNA (µg)*	*Ratio (Mrp1/ß-Actin)*	*SEM*	*Relative (%)*	*SEM (%)*
Mrp1 00DIC	1.0	1.10	0.0636	100,00	5,81
Mrp1 14DIC	1.0	1.05	0.0601	95,78	6,01

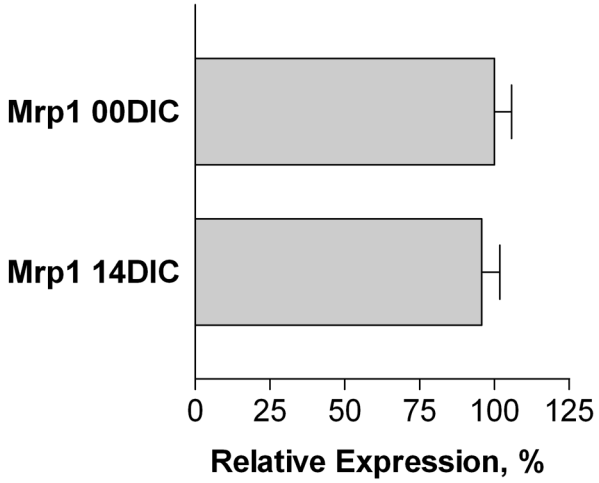

Figure 24: Relative Mrp1 Gene Expression in CPEC 14 DIC and Fresh Isolated CP Tissue

3.4.3 Immunostaining and Localization of ABC-Transport Proteins

Following gene expression, translocation of mRNA into the cytoplasm, transcription and modifications of the resulting polypeptides eventually lead to formation of intact and functional proteins. Further cellular localization within the cytoplasm or in polarized membranes is critical for proteins to gain full functional activity.

For ABC-transporters Pgp and Mrp1 immunostaining and localization at the BCSFB, rat CP tissues and cultured porcine CPEC were fixed, permeated and stained with specific antibodies as described in the materials and methods section. Briefly, excised rat CP tissue and cultured porcine CPEC were fixed in 95% EtOH. Following permeation in Triton-X 100, tissues and cells were blocked and then incubated with antibody at RT over night. After washing, tissues and cells were incubated with FITC-labeled secondary antibody. Immerged in fluorescence enhancer, tissues

placed in glass bottom Teflon chambers and cells enclosed with a glass cover slip, fluorescent stains were visualized by inverted confocal laser scanning microscopy.

The technique of confocal scanning microscopy allows visualizing selective *xy*-sections within tissues (limited to approximately 1µm resolution) and digital reassembling of series of sections along the *z*-axis, resulting in a 3D-view of objects. Figure 25 depicts a graphic representation of a single *xy*-section (dark green) and a digitally assembled stack of multiple *xy*-sections (light green).

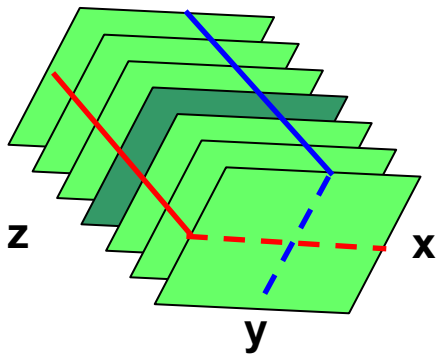

Figure 25: Representation of Confocal Scanning Microscopy *XYZ*-Sections

Antibody stained ABC-transporters were localized within CP tissue in relation to epithelial cell nuclei. CPEC nuclei were stained with propidium iodide (PI). PI binds to nucleic acids by intercalating between bases with little or no sequence preference, with a stoichiometry of one molecule of dye per 4.5 base pairs of DNA (Waring, 1965). Upon binding, PI fluorescence (max. absorption at 535 nm and emission at 617 nm) increases 20- to 30-fold (Arndt-Jovin and Jovin, 1989). However, the dye does not differentiate between RNA and DNA.

Figure 26 shows confocal microscopy *xy*-sections of isolated rat CP tissue in a transmitted light image and fluorescence, with PI staining in blue. Panels A, B and C show sections of single, PI stained CP capillaries, with focus moving from the top through an intermediate section of the lumen down to a bottom section of blood vessels.

3.4.3.1 Mrp1 Immunostaining and Localization in Choroid Plexus

The 190 kDa membrane protein Mrp1 protein was visualized in freshly isolated rat CP and cultured porcine CPEC. Epithelial cells were stained with MRPr1 (Alexis, Grün-

berg), previously shown to bind specifically to its antigen (Scheffer et al., 2000). Figure 27A is a transmitted light *xy*-section of rat CP tissue and fluorescent labeled Mrp1 stained green and cell nuclei stained red, shown in fluorescence. Figure 27B is a negative control image and shows a transmitted light image with nuclei stain only.

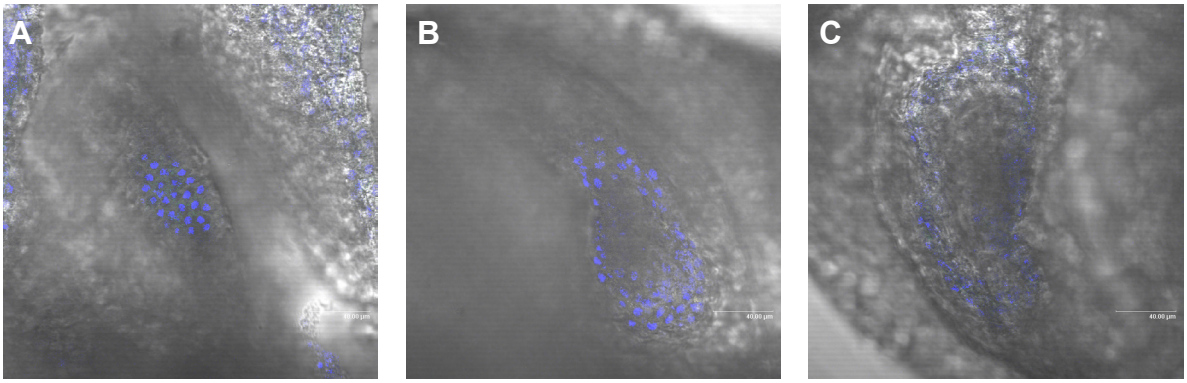

Figure 26: Rat CPEC Nuclei Stained with PI and Shown in Blue

As can be seen, the image depicts a large single CP blood vessel, surrounded by a single layer of epithelial cells. All epithelial cell nuclei within the focus plane are shown in red. The inside of CP blood vessels appears black. Mrp1 was clearly present in CP epithelium. Staining was most intense towards the basolateral, blood side of the epithelium, facing CP capillary vessels. Thus, Mrp1 is expressed and localized to the basolateral membrane in rat.

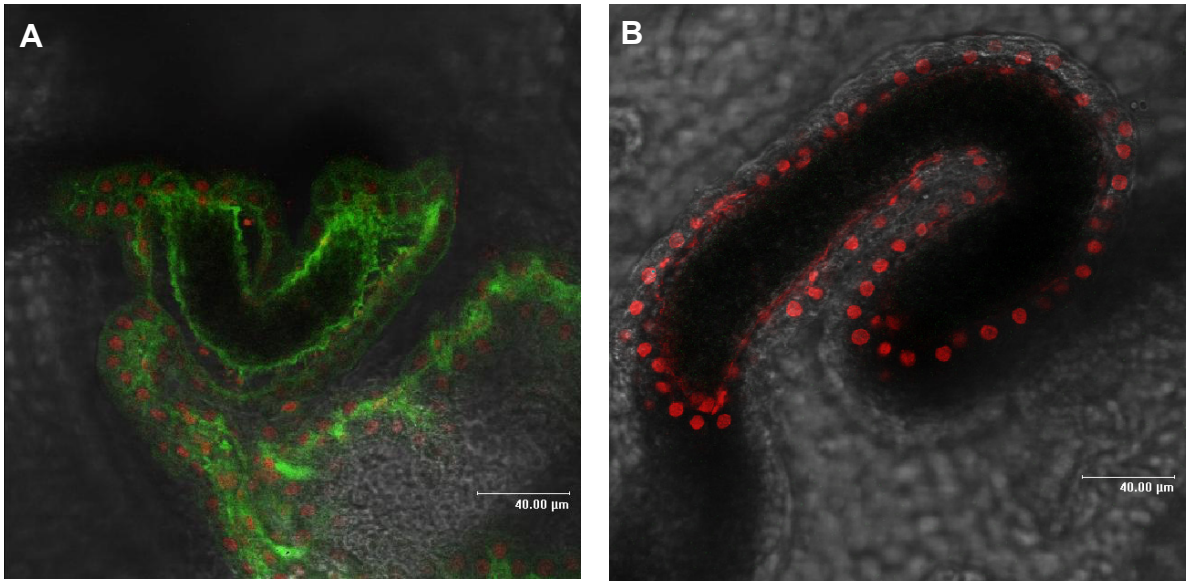

Figure 27: Mrp1 (Green) and PI (Red) Stained Rat CP Tissue (A) and Control (B)

Mrp1 expression was also analyzed in porcine CPEC 14 DIC. Cells were stained with Mrp1 specific antibody (MRPr1, Alexis, Grünberg) and PI, with Mrp1 shown in green and PI in red. Figure 28 shows one *xy*-section and a digitally reassembled construct of 20 *xy*-sections taken at 1 µm intervals, showing *xz*- and *yz*-sections.

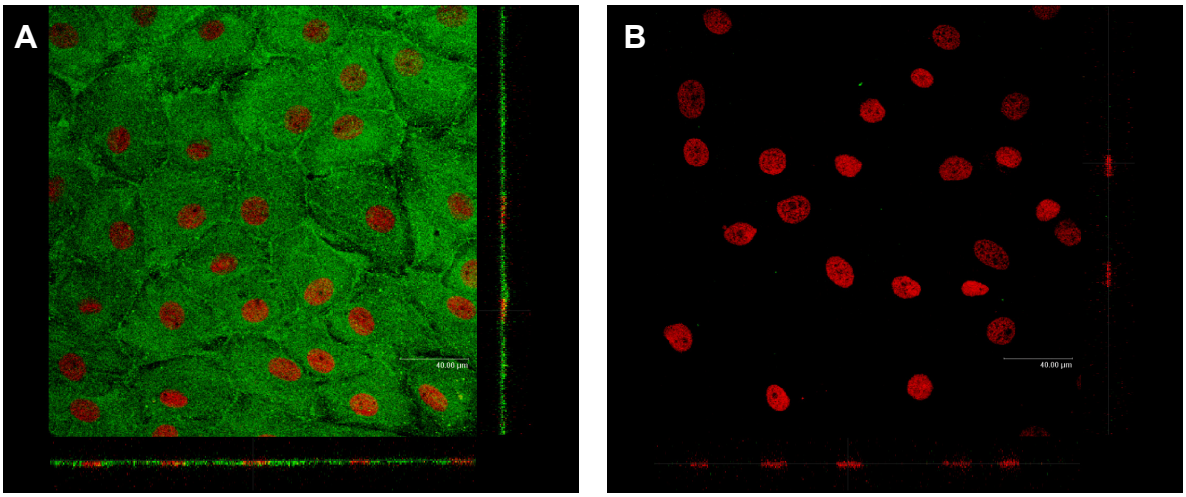

Figure 28: Mrp1 (Green) and PI (Red) Stained Porcine CPEC (A) and Control (B)

As in fresh CP tissue, Mrp1 is highly expressed in cultured CPEC, and is concentrated at the basolateral membrane (figure 28A). Figure 28B is a negative control image.

Other studies localized Mrp1 to the basolateral side of CPEC *in vivo* and *in vitro* (Rao et al., 1999; Wijnholds, et al., 2000; Saito et al., 2001). In rat BBB, even though Mrp1 concentrated to the apical plasma membrane of BCEC, expression of Mrp1 was stronger in brain parenchymal cells and astrocytes (Regina et al., 1998; Decleves et al., 2000; Zhang et al., 2004). Thus, in both CPEC and BBB, clustering of Mrp1 is comparable, but expression levels are considerably lower in BCEC than in CPEC (Begley et al., 2004).

3.4.3.2 Pgp Immunostaining and Localization in Choroid Plexus

The ABC-transporter Pgp was stained with C219 (Alexis, Grünberg). C219 was previously shown to stain Pgp, but does not differentiate between MDR1 and MDR3 (corresponding to mdr1b and mdr1a in rodents) and in fact cross-reacts between both isoforms (Schinkel et al., 1991; Scheffer et al., 2000). However, even though mRNA expression of MDR3 and MDR1 isoforms is comparable in CP tissue, the function of

MDR3 in transport has not yet been assigned and its expression may be limited to the level of RNA (Schinkel et al., 2000; Choudhuri et al., 1993; Duan et al., 2004).

Figure 29A and 29B show a transmitted light image and fluorescence *xy* sections of C219-stained CP epithelial cells and blood vessels and control, respectively. Epithelial cell nuclei, stained with PI, are depicted in red and C219 stained Pgp in green. The Pgp stain, located between CPEC nuclei, suggests that the protein is expressed in CP epithelium.

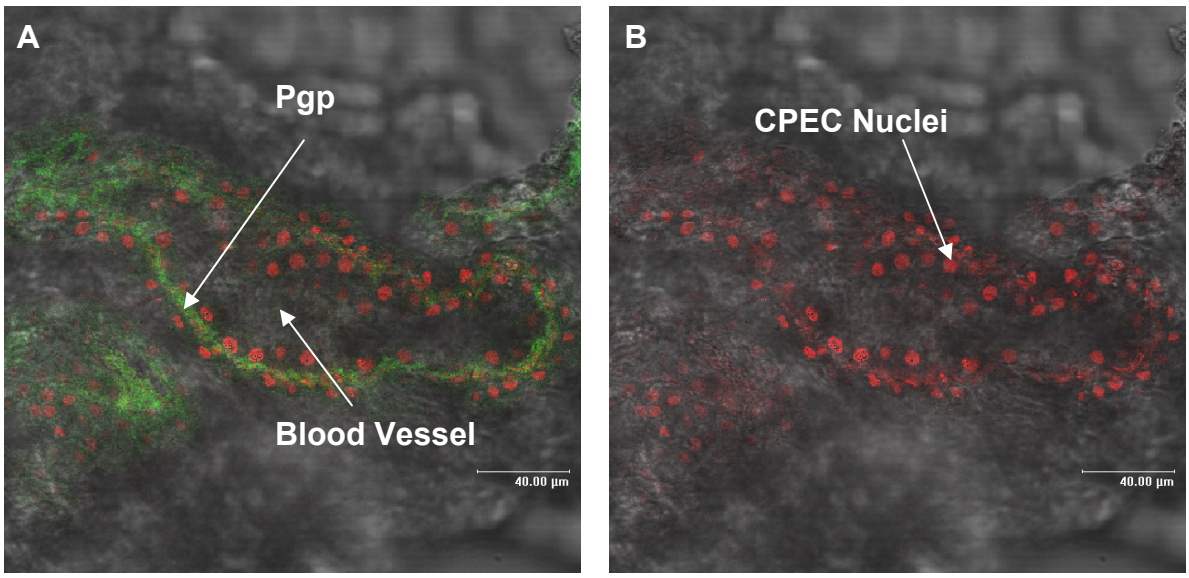

Figure 29: Rat CP Stained with PI and with Alexis C219 (A) and without (Control, B) in Transmission and Fluorescence

To further assess Pgp localization in CPEC, a three-dimensional fluorescence image was recorded (figure 30). A stack of 40 *xy* sections was taken at 1 µm intervals and digitally assembled to create a three-dimensional image, to allow viewing of MDR expression from all perspectives. Again, CPEC nuclei were stained red and antibody-bound Pgp green. These images show Pgp to be primarily localized at the apical membrane of CPEC, with some of the protein associated with the brush-border membrane.

At the BBB, Pgp is one of the most studied and best characterized ABC-transport proteins. Much less is known about Pgp at the blood-CSF barrier. In addition, Pgp expression was analyzed in fully differentiated porcine CPEC 14 DIC grown on chamber slides. Figure 31A shows a three-dimensional reconstruction of 20 1 µm *xy* CP tissue slices stained with C219 and figure 31B a *xy* control image. Nuclei

stained with PI are shown in blue and C219-stained Pgp in green. Cultured porcine CPEC 14 DIC expressed Pgp.

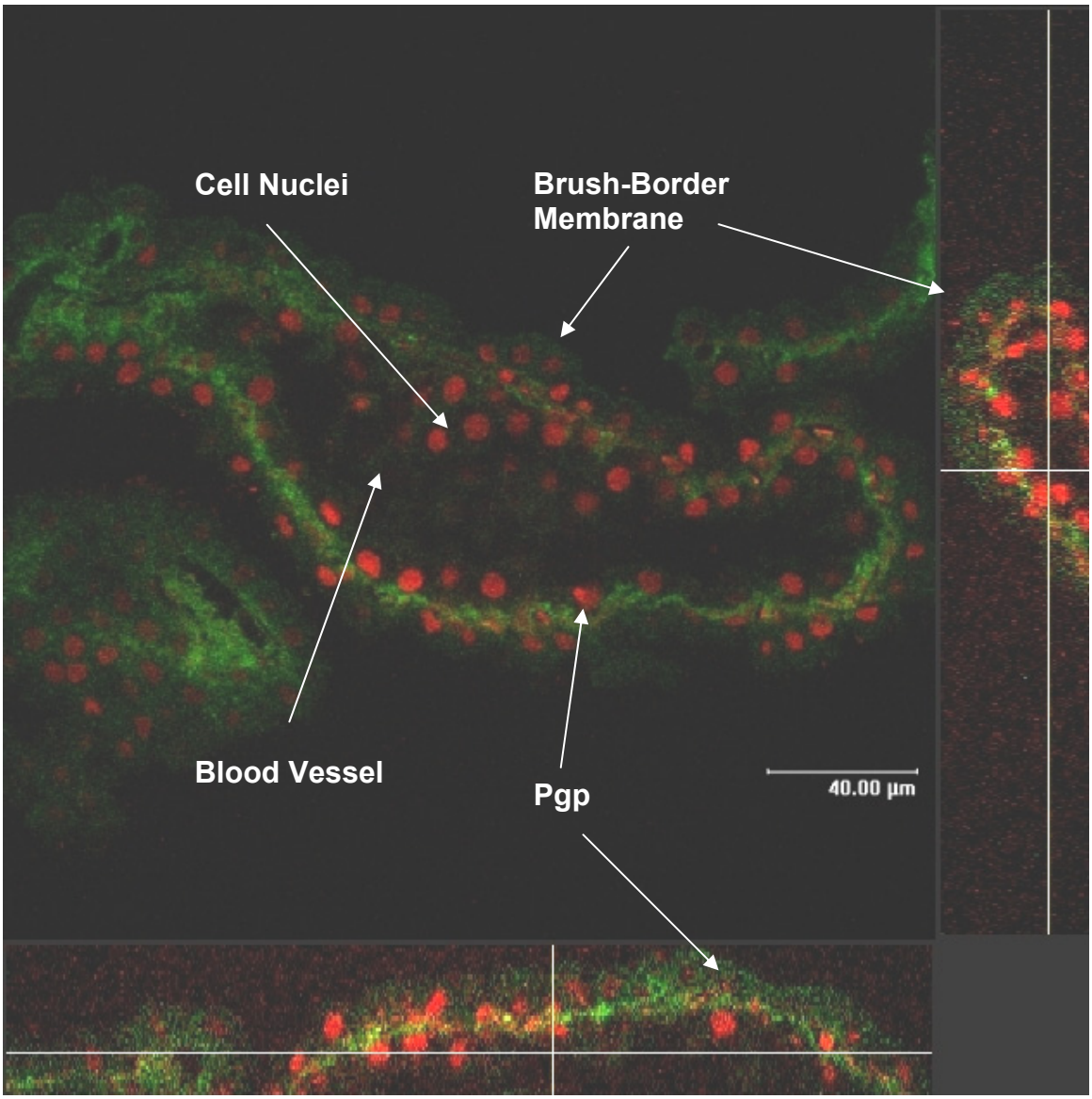

Figure 30: Stack of 40 1µm *XY* Sections of Rat CP Stained with PI and Alexis C219 (Digitally Reconstructed)

Interestingly, CPEC apical or CSF-facing localization is opposite to luminal localization in the BBB capillary endothelium. In BCEC stained with various specific monoclonal antibodies, Pgp localized to the luminal, plasma-facing membrane of endothelial cells *in vivo* and *in vitro* (Sugawara et al., 1990; Biegel et al., 1995; Stewart et al., 1996; Bendayan et al., 2002; Virgintino et al., 2002).

Other studies investigating Pgp expression at the BCSFB of humans, other primates and rodents also suggest apical or sub-apical localization of Pgp in CPEC

(Rao et al, 1999; Warren et al., 2000; de Lange, 2004). Pgp may be contained in vesicles and ready for insertion into membranes. However, insertion of Pgp into the apical membrane does not match the general role of MDR1, which is to protect the brain against chemical insult. Would Pgp incorporate and gain functional activity, its substrates would be moved back into the CSF and possibly contribute to toxicity in the vicinity of CSF. A more likely explanation for sub-apical localization of Pgp is proposed by Begley (2004). Pgp may be responsible for secretion of compounds into vesicles, for subsequent secretion across the basolateral membrane by exocytosis. Removing potentially toxic compounds from the cytoplasm, storing them in vesicles and eventual removal into the blood stream for subsequent elimination in bile and urine seems a more likely explanation in the light of Pgp's physiological protectionist role.

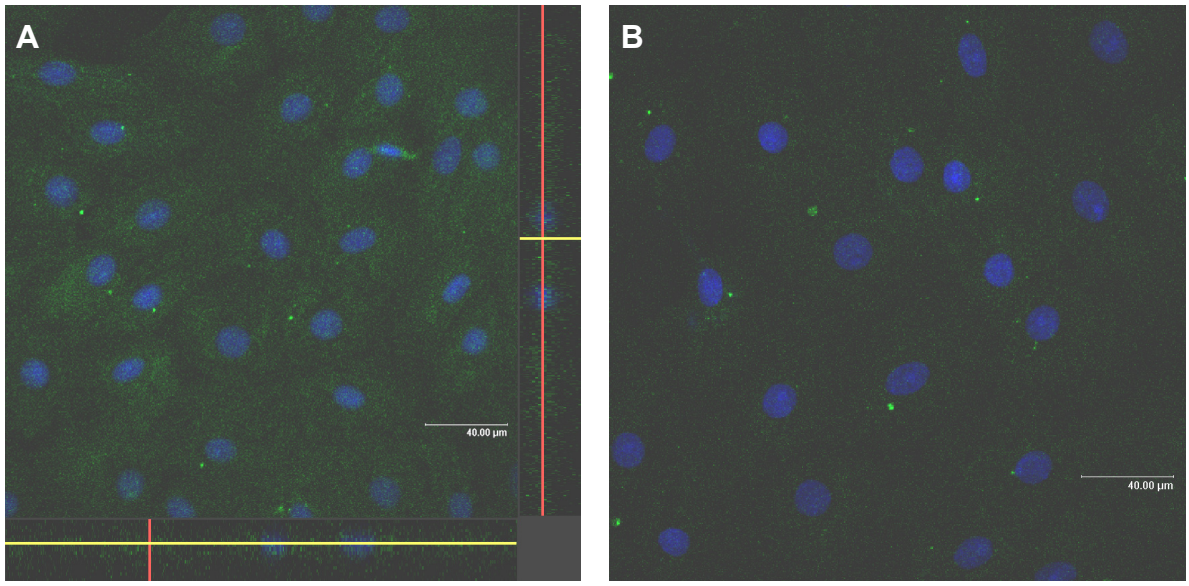

Figure 31: Cultured CPEC 14 DIC Stained with Alexis C219 (A) and with PI Only (B, Control)

3.4.3.3 Characterization of Isolated Choroid Plexus Membrane Fractions

Porcine CP membranes were enriched according to a centrifugation and cation precipitation protocol adapted from a method for kidney cortex membrane preparation (Hilden et al., 1989). Following tissue homogenization, apical and basolateral membrane fractions were prepared from fresh porcine CP tissue.

For apical fractions, the degree of enrichment was assessed with marker enzymes AP and γ-GT. Apical fractions were compared to homogenate, S1 and basolateral membrane fractions. Previous analyses of isolated membrane fractions, cyto-

chemical and immuno-electron microscopy studies demonstrated that both enzymes are located exclusively to the apical, CSF facing side of CPEC in CP of various species, including pig (Sessa et al., 1976; Yoshioka et al., 1988; Bourne et al., 1989; De Bault and Mitro, 1994; Ogawa et al., 1998). Further, both enzymes are well-known markers for BCEC membranes (Schlosshauer, 1993).

Basolateral membrane fraction enrichment was assessed by Western blot expression analyses of Mrp1. Other enzymes commonly employed to characterize basolateral membrane factions, including Na^+/K^+-ATPase, $Na^+/K^+/2Cl^-$-ATPase or ecto-5'-nucleotidase, are not suitable for membrane differentiation in CPEC, as they are also localized to the apical membrane or entirely absent (Masuzawa et al., 1984; Braun et al., 1994; Keep et al., 1994; Marrs et al., 1994). In contrast, the well characterized 190 kDa membrane protein Mrp1 is exclusively localized to the basolateral membranes in CPEC (Rao et al., 1999). Staining was carried out using the monoclonal antibody MRPr1 (Alexis, Grünberg), previously shown to stain entirely specific to its cognate antigen (Scheffer et al., 2000).

Figure 32A and 32B show apical enzyme activity determined for homogenate, S1 and each of the prepared fractions. S1 fractions were not significantly different from homogenate. Basolateral membrane fractions exhibited a slight increase in activity with 3.6 +/- 0.1 -fold and 6.9 +/- 0.6 -fold and apical membrane fractions showed significantly increased activity with values of 27.3 +/- 0.8 -fold and 27.7 +/- 1.0 -fold for AP and γ-GT, respectively.

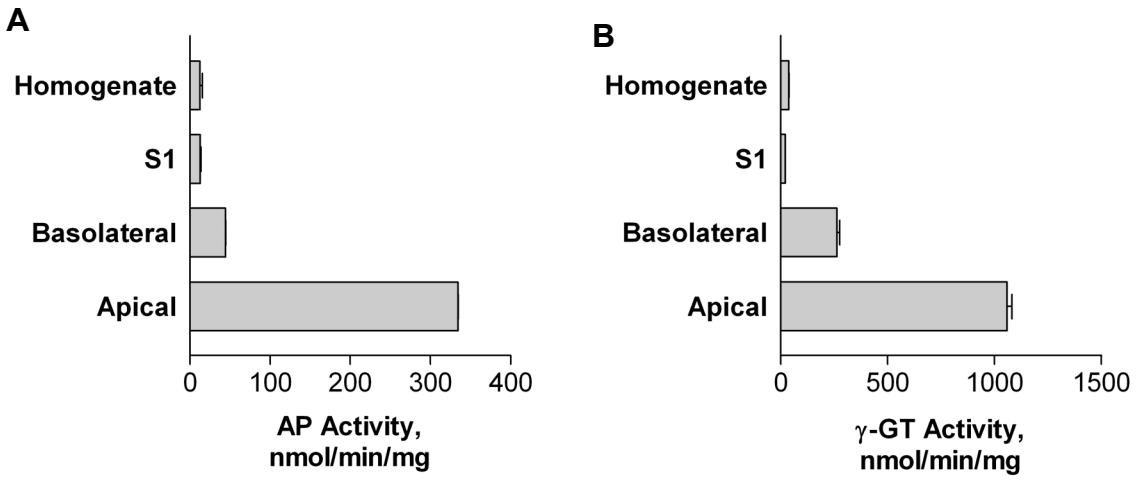

Figure 32: Alkaline Phosphatase (A, AP) and γ-Glutamyl-Transpeptidase (B, γ-GT) Activity in Enriched Membrane Fractions

Porcine kidney, liver and freshly isolated CP tissue protein isolates were separated by SDS-PAGE and stained with anti-Mrp1 MRPr1 antibody (figure 33). The strongest Mrp1 signal was observed in the 25 µg CP samples, followed by kidney and liver preparations. The findings are in accordance with results obtained in quantitative mRNA analyses (Choudhuri et al., 2003).

Figure 34 shows a Western blot of enriched porcine CP apical and basolateral membrane fractions with MRPr1 stained protein bands. Mrp1 expression in CPEC apical fractions was visible at 10 µg and the signal increased when 25 µg of protein were applied. No signal was visible in apical membrane fraction with 10 µg applied and only slight staining was observed with 25 µg of protein. Results obtained are in accordance with other CPEC Mrp1 analyses (Rao et al., 1999).

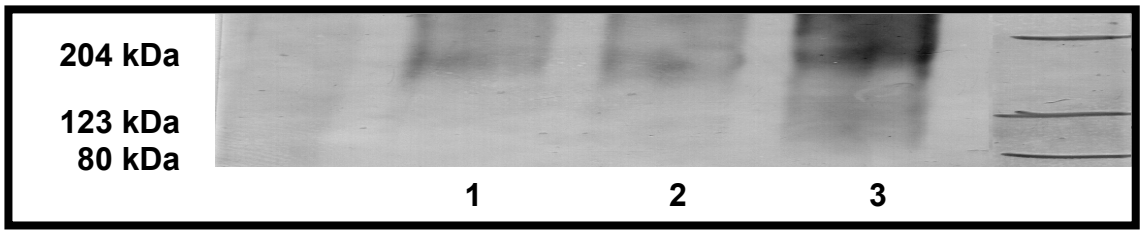

Figure 33: MRPr1 Western Blot of Kidney (Lane 1), Liver (Lane 2) and Freshly Isolated CP (Lane 3)

3.4.3.4 Western Blot Analyses of Pgp in Isolated CP Membrane Fractions

Localization of the 170 kDa ABC-transport protein Pgp (Richert et al., 1988) was studied in more detail. Porcine CP apical and basolateral membrane fractions were enriched and Pgp expression assessed in Western blot analyses (figure 35). CPEC apical fractions showed Pgp expression at 10 µg and 25 µg of protein, with a concentration dependent increase in signal.

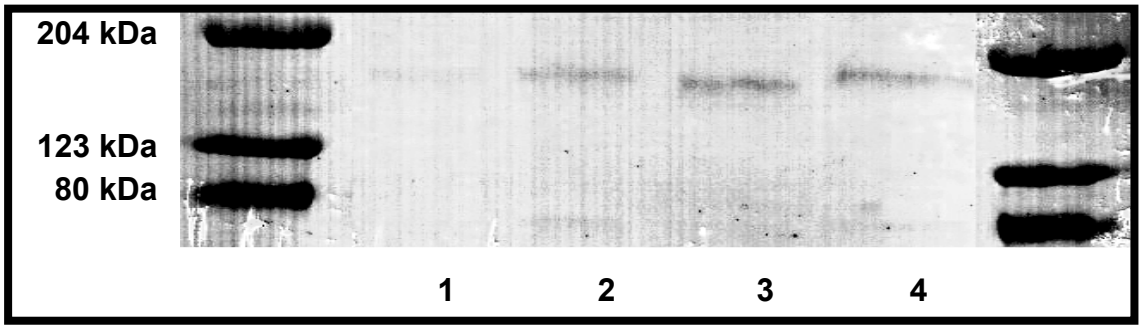

Figure 34: Fresh CP Apical Membrane (Lane 1: 10 µg, Lane 3: 25 µg) and Basolateral Membrane (Lane 2: 10 µg, Lane 4: 25 µg) Fractions

No signal was visible in basolateral preparations, again confirming that Pgp was located towards the apical side of the epithelium, only. Enriched porcine brain capillary endothelial cell membranes were used as control.

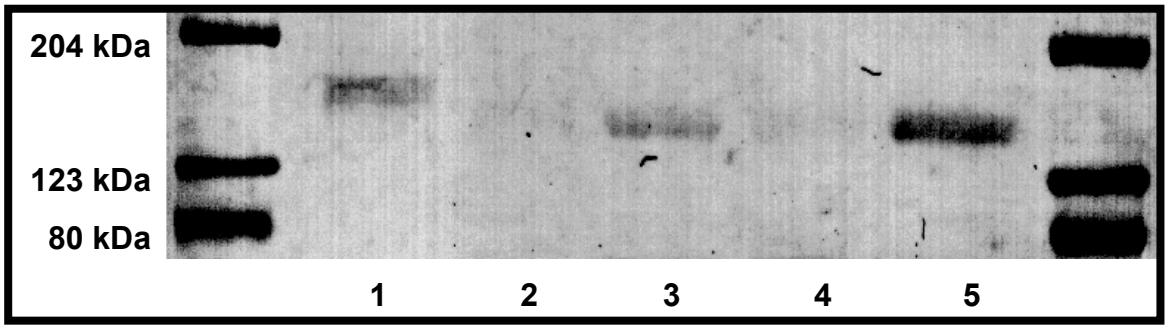

Figure 35: Pgp (C219, Alexis, Grünberg) Western Blot with BCEC (Lane 1: 20 µg), Basolateral CP (Lane 2: 10 µg), Apical CP (Lane 3: 10 µg), Basolateral CP (Lane 4: 25 µg), Apical CP (Lane 5: 25 µg)

3.5 Active Transport of Compounds across Choroid Plexus Epithelial Cells

Active transport is the secretion of ions, nutrients or other molecules against a concentration gradient in an energy-consuming process. Compounds may be actively transported into cells, removed by efflux transport or affected by both, active uptake and efflux. Distribution of certain compounds within the body and partitioning into the brain is greatly affected by a number of different transporters (Lee et al., 2001; Begley, 2004; Graff and Pollack, 2004).

With regard to the BCSFB, partitioning into the brain from the blood stream is limited by efflux proteins located on basolateral membranes. Compounds already in CSF can be actively filtered out across the CP and secreted back into the blood stream. Transport across the BCSFB is further influenced and brain penetration can be limited by drug-drug and drug-excipient interactions. Finally, phenotypic variations in transporter gene expression arising from either pharmacogenetics (inherited, e.g. metabolism) or pharmacogenomics (non-inherited, e.g. point mutations) can alter the distribution of compounds and transport across the BCSFB.

Thus, one of the goals of modern transport physiology is to understand at the molecular level the mechanisms that underlie transcellular movements of ions, water, nutrients and excretory products. This requires four types of information: 1) a list of transport proteins expressed in the tissue, 2) knowledge of their subcellular localization, 3) their functional characterization and 4) a description of the transport characteristics of the tissue.

For the two ABC-transport proteins investigated, RT-PCR, immunostaining and Western blot analyses demonstrated presence of and localized Pgp and Mrp1 in CPEC. However, recent PCR-based studies with rat choroid plexus detected mRNA of even more multidrug-resistance, multidrug-resistance associated transporters and organic anion transporters from the MDR, Mrp, Oat, and Oatp families (Choudhuri et al., 2003). Of these, less than half have been immunolocalized in the tissue and only few have been analyzed on a functional basis and characterized with respect to transport characteristics (figure 6, introduction). None have been assessed with respect to functional characteristics in CPEC cultures. Figure 36 is a schematic diagram for transport proteins identified and localized to date, with functional relevance to organic anion transport.

Assessment of transport function is limited by a number of factors. Most important are scarcity of truly specific substrates and the common overlap of substrate specificity (Borst et al., 1999; Haimeur et al., 2004). For the ABC-transporters investigated, the MDR gene product Pgp preferentially transports large hydrophobic and positively charged molecules, whilst the Mrp family transports both hydrophobic uncharged molecules and water-soluble anions (Bodo et al., 2003). Analyses are further complicated that even if transport proteins have low structural homology and different substrate specificity, such as Pgp and Mrp1, they still transport a similar spectrum of compounds (Renes et al., 2000; Nies et al., 2004)

Strategies to circumvent limitations include analyses of transporters in systems allowing to assess expression and function of a single protein, such as transfected oocytes (Castillo et al., 1990; Morin et al, 1995; Aleu et al., 1997; Tsuruoka et al., 2002), transfection and over-expression in cell systems (Brimer et al., 2000) or conversely knock-out variants of cells or animals (Lorico et al., 1996; Kusuhara et al., 1997; Schinkel et al., 1997; Allen et al., 2000; Wijnholds et al., 2000).

Studies attempting to describe the functional transport characteristics of a tissue are most complicated. For CP analyses, limitations are posed by morphological, size and anatomical constraints, partially overcome using of tissue preparations or *in vitro* models. Quantitative fluorescent microscopy has proved to be a valuable technique for studying transport across CP tissue, allowing visualization of sub-cellular processes (Miller et al., 2000; Breen et al., 2002; Breen et al., 2004). Isolated CPEC can be cultured on either permeable Transwell® systems or on plastic surfaces for

functional analyses (Gath et al., 1997; Hakvoort et al., 1998; Angelow et al., 2003; Angelow et al., 2004). The advantages of *in vitro* cell culture systems are that vectorial transport can be measured in blood to CSF direction and vice versa and that amounts transported can be calculated as concentrations.

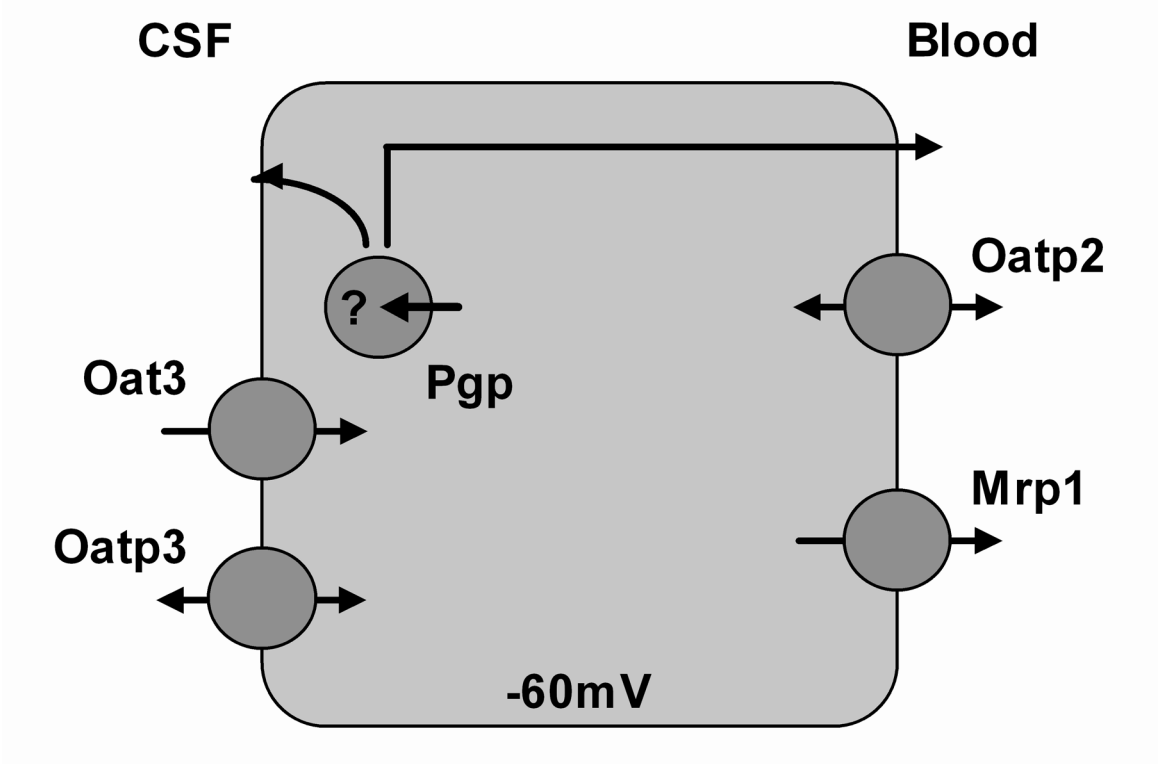

Figure 36: Schematic Representation of CPEC Transport Proteins

3.5.1 Rho123 Uptake into Cultured Choroid Plexus Epithelium

Functional characterization of Pgp was carried out in CPEC 14 DIC using the Pgp-specific substrate Rhodamine-123 (Rho123; Diddens et al., 1987; Hegmann et al., 1992; Nare et al., 1994; Frey et al., 1995; Schinkel et al., 1997). The fluorescent dye is known as multidrug-resistance phenotype substrate and has been used to assess Pgp activity in various models, including cultured BCEC and MDR1-type (MDR1/MDR3 (-/-)) knock-out mice (Schinkel et al., 1997). The molecular structure of Rho123 is shown in figure 37. The compound has a molecular weight of 380.83 g/mol and its excitation and emission spectra maxima are at 460 nm and 520 nm, respectively (Molecular Probes, 2004).

For investigations into transport of Pgp substrate Rho123 in CPEC *in vitro*, cells were grown until fully differentiated as described in the materials and methods

section. Uptake of various concentrations of Rho123 into CPEC 14 DIC cultured in 96-well plates was measured and the effects of transport inhibitors with known affinity for Pgp assessed.

Rhodamine-123
(Rho123)
CAS# : 62669-70-9
$C_{21}H_{17}ClN_2O_3$
MW: 380.83

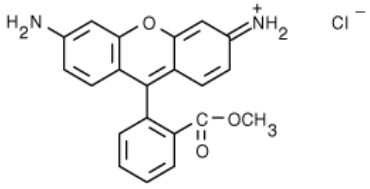

Figure 37: Molecular Structure of Rhodamine-123 (Rho123)

The subapical localization of Pgp leaves room for speculation to if and how compounds are excluded from CPEC. Should Pgp be inserted into the apical membrane of the epithelium, Pgp substrates would be transported back into the medium. Concomitant incubation with inhibitors would reduce efflux and lead to an increase in cellular substrate uptake. If Pgp localized to cytoplasmic vesicles, substrate would be trapped within the cellular vesicles. Exocytosis of substrate filled vesicles would reduce substrate concentrations. Effects of inhibitors on intracellular vesicularized Pgp would only alter cellular concentrations if basolateral exocytosis occurs, leading to an increase in cellular substrate concentrations.

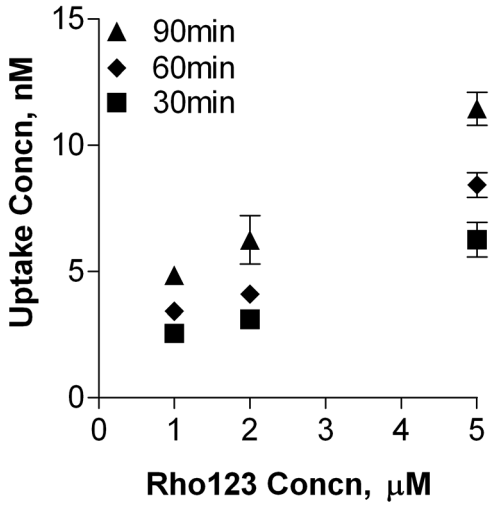

Figure 38: Uptake of Increasing Concentrations of Rho123 at Different Time Intervals

After washing CPEC 14 DIC with KRB, cells were incubated with Rho123 for up to 90 min at 37°C. Excess substrate was removed, cells washed and then lysed in Triton X-100. Fluorescence trapped in the cell was measured at 520 nm. Figure 38 shows concentrations of Rho123 (in nM) transported into the epithelium. Uptake remains linear over the range of 0.5 µM to 5 µM for incubations of 30 min up to 90 min.

Figure 39 shows the time course of 2 µM Rho123 uptake into cultured CPEC14 DIC. Substrate uptake into cells remained linear (R^2 = 0.99) over a 90 min period.

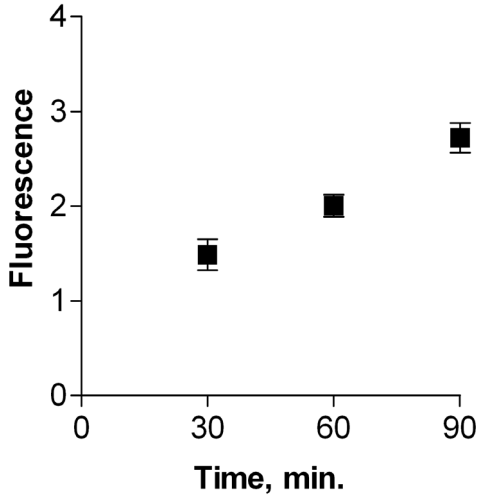

Figure 39: 2 µM Rho123 Time Course

To functionally characterize Pgp activity, cells were incubated with 2 µM of Rho123 for 1 hour with effectors or without (control). Proline was used as a secondary control. Figure 40 shows that in cultured CPEC none of the effectors, including MK571, leukotriene C_4 (LTC_4), Cyclosporine-A (CSA) and its analog PSC883 caused a significant alteration in 2 µM Rho123 uptake over a 1-hour time period.

In many organs, such as liver, kidney, small intestine and brain, Pgp plays a major role in efflux of compounds and transport into the blood stream. For example, at the BBB, Pgp is localized on the luminal side of BCEC and excretes xenobiotics and endogenous compounds into capillaries. Thus, its physiological protectionist role is fulfilled at the brain capillary endothelium (Schinkel et al., 2003).

With Pgp localizing sub-apical at the blood-CSF barrier it was not clear whether Rho123 would efflux into CSF analogous to localization and function at the BBB or whether the compound would be trapped within cytoplasmic vesicles. However, Pgp did not influence CP epithelial Rho123 secretion. Besides Pgp expression

levels being too low to affect CP epithelial drug secretion, both proposed explanations for subapical localization of Pgp may explain the lack of functional activity (Begley, 2004). The protein is either not inserted into membranes of cultured CPEC fast enough or at rates high enough or should Pgp cluster in vesicles, the uptake in the vesicles is not the rate limiting step to Rho123 uptake in CPEC.

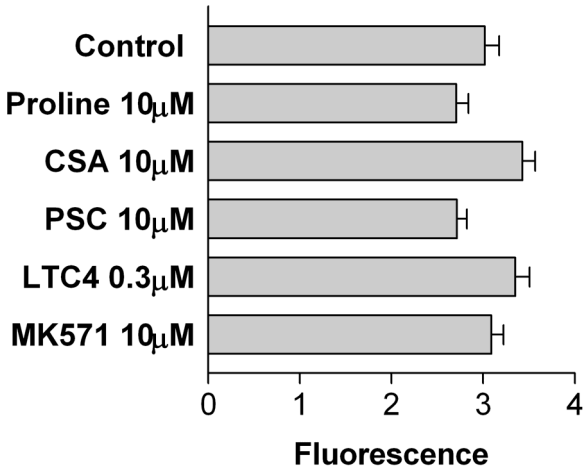

Figure 40: Uptake of 2 µM Rho123 Without (Control) and With Effectors

3.5.2 Organic Anion Secretion across Choroid Plexus *Ex Vivo* and *In Vitro*

To date, available evidence implicates Oat3, Oatp3, Mrp1 and Oatp2 in the transport of organic anions across mouse and rat choroid plexus (figure 36, Angeletti et al., 1997; Gao et al., 1999; Rao et al., 1999; Breen et al., 2002; Nagata et al., 2002; Sweet et al., 2002; Choudhuri et al., 2003; Breen et al., 2004; Nagata et al., 2004). Mouse and rat are the only two species for which information on molecular and functional details is available and for which transporters can be assigned to individual transport steps for specific organic anions, e.g., PAH, benzylpenicillin, FL-MTX and FL, at the CP. However, although transporters responsible for individual steps can be identified, the complete path across the CP taken by any organic anion remains unknown. For example, Oat3 mediates apical entry of both PAH and FL in mouse, but the transporter responsible for basolateral efflux has yet to be identified (Sweet et al, 2002; Sykes et al, 2004).

To further elucidate organic anion secretion across the CP epithelium, transport was studied in two different *ex vivo* models, a mammalian model using male Wistar rats and an elasmobranch model using dogfish shark. Generally, studies on live CP tissue are difficult, due to the tissue's anatomical location, complex morphol-

ogy and small size. The advantages of using dogfish shark as comparative model are that the tissue of this poikilothermic animal is more accessible, less fragile and can be maintained intact *ex vivo* for longer periods of time, besides being similar to rat in morphology and ultrastructure (Villalobos et al., 2002). However, there is little molecular and immunohistological information available and interpretation of results is dependent on mammalian data. Only few members of the Oat, Oatp and Mrp families of transporters have been cloned from fish tissues and partially characterized. For example, an Oat cloned from winter flounder kidney was shown to support Na^+-dependent transport of PAH (Wolff et al., 1997). Subsequent studies suggest that although mammals express five Oat isoforms, fish appear to express only one, with transport properties of both mammalian Oat1 and Oat3 (Dudas and Renfro, 2001; Burckhardt et al., 2003). In little skate, both an Oatp and an Mrp were cloned (Wang et al., 2001; Cai et al., 2003). The Oatp is a two-part transporter, requiring coexpression of two proteins for activity. It transports ES, taurocholate and LTC_4, but not PAH and digoxin. As with other Oatps, transport is not Na^+-dependent. The Mrp resembles mammalian Mrp2; an ATP-driven xenobiotic export pump with wide substrate specificity.

Both mammalian and elasmobranch species were used to functionally analyze organic anion transport. Two different fluorescent organic anions were investigated, fluorescein (FL) and fluorescein-methotrexate (FL-MTX) (figure 41). Uptake from medium across apical membranes into epithelial cells and efflux from cells across basolateral membranes into blood vessels was visualized and quantified in rat and shark CP preparations using confocal laser scanning microscopy. Steady state observations were made and results obtained from both models compared. FL-MTX transport was further investigated using different inhibitors and detailed transport characteristics of uptake and efflux revealed are presented.

Figure 42 compares steady state distributions of FL and FL-MTX within shark CP. Relative to levels in the bath, both compounds accumulated to high levels within the subepithelial/vascular spaces, indicating concentrative transepithelial transport. FL intensity was distributed with lowest intensity in the medium followed by cells and subepithelial/vascular spaces (figure 42C).

Fluorescein
(FL)
CAS# : 2321-07-5
$C_{20}H_{12}O_5$
MW: 332.31

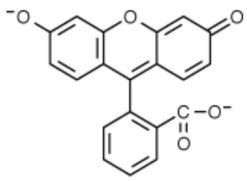

Fluorescein-Methotrexate
(FL-MTX)
CAS# : 71016-04-1
$C_{46}H_{54}N_{14}O_9S$
MW: 979.08

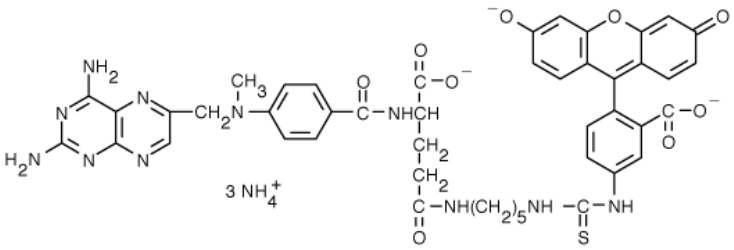

Figure 41: Molecular Structures of Fluorescein and Fluorescein-Methotrexate

In agreement with previous studies in CP tissue from rat, mouse and shark, FL transport across the tissue involved two concentrative steps in series: Na^+-dependent uptake and membrane-potential driven efflux (Breen et al, 2001; Sweet et al, 2002; Villalobos et al, 2002). From studies on an Oat3-null mouse, it was demonstrated that the Na^+-dependent step was mediated by Oat3, with no detectable contribution of Oat1 and the molecular correlate of the efflux step remains to be identified (Sykes et al., 2004).

Although FL-MTX transport from cell to subepithelial/vascular spaces was clearly concentrative, it was not clear from the images whether uptake at the apical membrane was concentrative or even mediated. Indeed, in most experiments cellular fluorescence intensity in control tissue was somewhat lower than that measured for the medium.

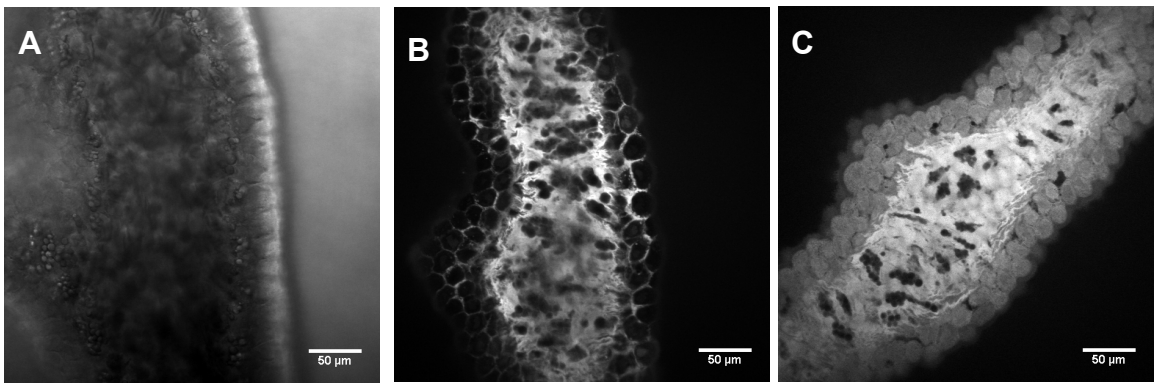

Figure 42: Shark CP Tissue in a Transmitted Light Image (A) and Loaded with 2 µM FL-MTX (B) and 2 µM Fluorescein (C)

In capillary lumens, FL-MTX was concentrated from the subepithelial/vascular spaces to the tight junctions at apical ends of intercellular spaces (figure 43). A similar distribution pattern for FL-MTX was shown for the rat and also reported for mouse (figure 43 A, B; Sweet et al, 2002; Breen et al, 2004).

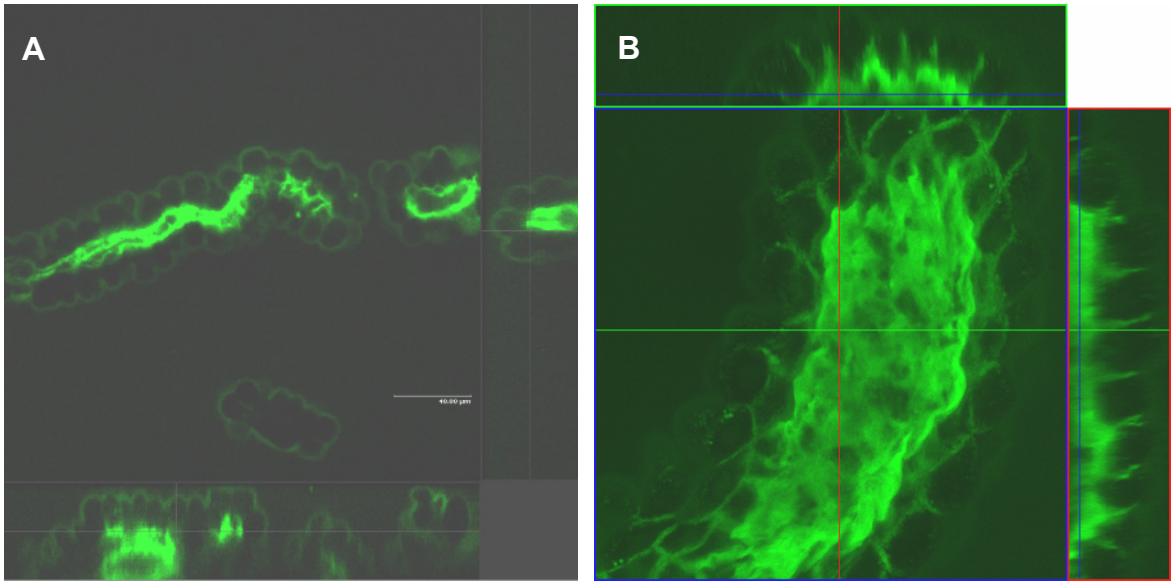

Figure 43: 3D Distribution of 2 µM FL-MTX in Rat (A) and Shark (B)

Figure 44A shows the time course of 2 µM FL-MTX transport across rat and figure 44B secretion across shark CP epithelium into subepithelial/vascular spaces. Transport of FL-MTX across the CP was similar in both species. Fluorescence intensities in subepithelial/vascular spaces increased linearly over the first 30 min and steady state was reached with n 45 min. In these experiments, medium fluorescence averaged about 400 to 600 units, so steady state fluorescence intensity of the subepithelial/vascular spaces was about 5 times that of the medium. Cellular fluorescence increased and reached steady state levels within initial 45 min (figure 44A, B). At steady state, cellular fluorescence intensities averaged about 200 to 400 units, values that were significantly lower than medium fluorescence ($P<0.01$).

Steady state FL-MTX accumulation in cells and subepithelial/vascular spaces of shark saturated at low substrate concentrations (figure 45). At all concentrations studied, subepithelial/vascular fluorescence was substantially higher than cellular fluorescence. These findings suggest that transepithelial transport of FL-MTX did indeed involve two mediated steps, but that efflux at the basolateral membrane could more than keep up with uptake at the apical membrane.

Transepithelial transport of FL-MTX appeared to be dependent on both cellular metabolism and transmembrane Na^+ gradients. Inhibiting metabolism with NaCN decreased fluorescence intensity in cells and vessels by at least 70%, as did incubation in Na^+-free medium (NaCl replacement with *N*-methyl-*D*-glucamine, figure 46 for shark and figure 47 for rat).

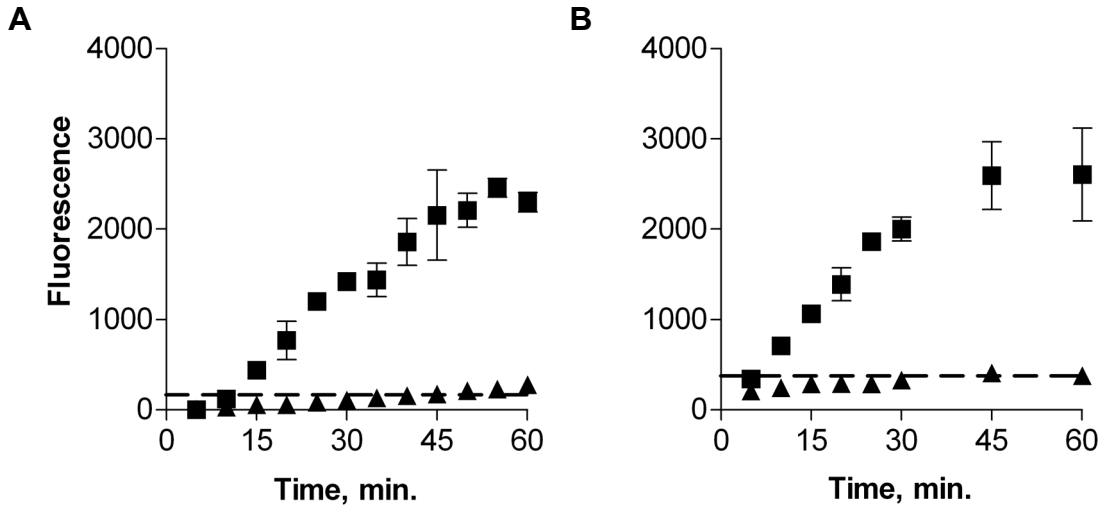

Figure 44: Time Course of 2 µM FL-MTX Secretion across Rat (A) and Shark (B) CP. Triangles represent cellular and squares blood vessel values. The dashed line represents background fluorescence levels.

When tissue was first incubated in Na^+-free medium, before being returned to Na^+-containing ER for steady state FL-MTX uptake measurements, fluorescence intensities in both compartments were not significantly different from control tissue. Thus, effects of Na^+-depletion, although substantial, were fully reversible. Consistent with FL-MTX accumulation being Na^+-dependent, ouabain, a Na^+/K^+-ATPase inhibitor, substantially reduced cellular and subepithelial/vascular fluorescence (figure 46).

Finally, increasing medium K^+ ten-fold (NaCl partially replaced with KCl) was without effect (figure 46). This maneuver depolarized rat choroid plexus cells in culture by 40 mV (Villalobos et al, 1999) and blocked cell-to-vessel transport of FL in intact choroid plexus from rat, mouse and shark (Breen et al, 2001; Villalobos et al, 2002; Sykes et al, 2004). FL-MTX transport was thus driven by cellular metabolism, dependent on Na^+, but not sensitive to electrical potential differences (PD). In addition, the lack of effect of elevated K^+ on FL-MTX transport indicates that depolarization cannot underlie the reduction in transport seen with Na^+ depletion and ouabain.

Further, several organic anions inhibited transport and reduced FL-MTX accumulation in rat CP vessels (figure 47). Organic anions included LTC_4 (0.3 µM), MK571 (5 µM), vinblastine (10 µM), the cyclosporine analog PSC833 (10 µM) and verapamil (10 µM). Concurrent with the model proposed, PSC833 and verapamil had

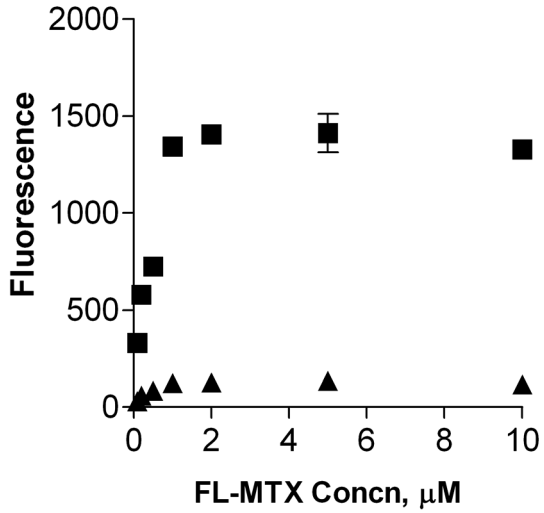

Figure 45: Transport of FL-MTX at Various Concentrations across Shark CP. Triangles represent cellular and squares blood vessel values.

no effect. Both compounds are known Pgp inhibitors and thus do not effect FL-MTX secretion (Fellner et al., 2002; Kemper et al., 2003; Kemper et al., 2004). LTC_4, MK571 and vinblastine are all Mrp1 inhibitors (Regina et al., 1998; Miller et al., 2000; Yan and Taylor, 2002; Gennuso et al., 2004). Results obtained with organic anions and effects measured with addition of NaCN support the proposed basolateral secretion of FL-MTX via Mrp1.

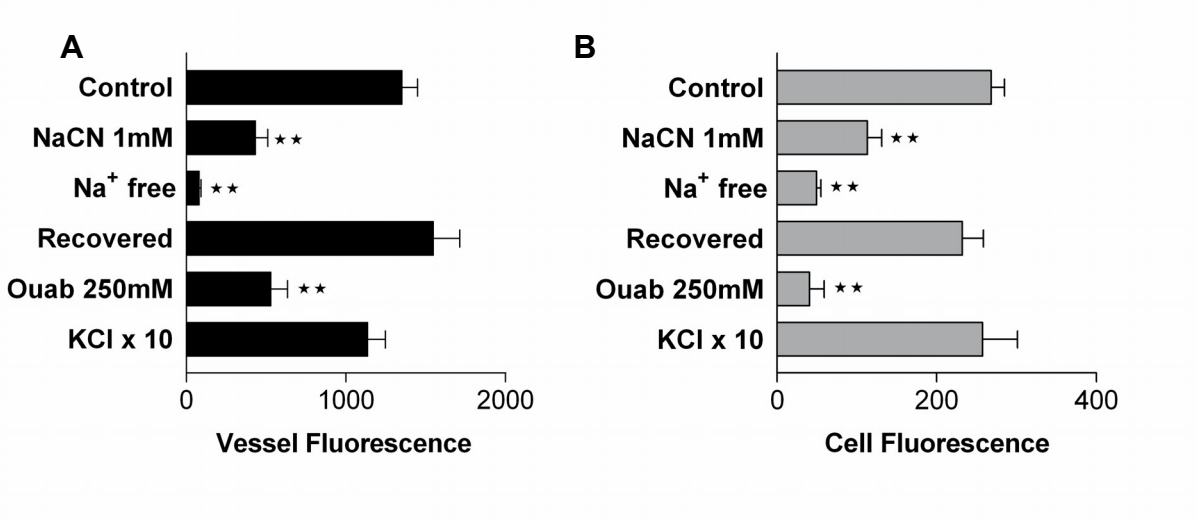

Figure 46: Ion Dependent FL-MTX Secretion in Shark CP.

A more detailed analysis describing effects on the FL-MTX transport in concurrent presence of organic anions was carried out in dogfish shark. Analyses of FL-MTX transported across shark CP in the presence of various organic anions at different concentrations revealed different and distinct inhibition patterns and provided information about transport characteristics at both epithelial membranes.

For probenecid, folate, MTX and taurocholate, increasing the concentration of inhibitor caused roughly parallel decreases in cellular and subepithelial/vessel fluorescence. At the highest concentrations tested, probenecid and folate reduced FL-MTX accumulation in both tissue compartments by at least 90% (figure 48A and figure 48B). Thus, nearly all transepithelial transport of FL-MTX was mediated and, at a minimum, probenecid and folate blocked all mediated uptake at the apical membrane. It is not clear from the data whether one or both of these compounds also affected basolateral efflux. For MTX and taurocholate (TA), cellular and subepithelial/vessel fluorescence decreased in parallel, but inhibition of transport was less than complete (figure 48C and figure 48D): increasing the inhibitor concentration above 100 µM for MTX and 10 µM for taurocholate did not further decrease transport significantly. Since the data for probenecid and folate indicate that essentially all transport was mediated, the partial inhibition found with the highest concentrations of MTX and taurocholate indicates involvement of at least two apical uptake pathways for FL-MTX in CPEC.

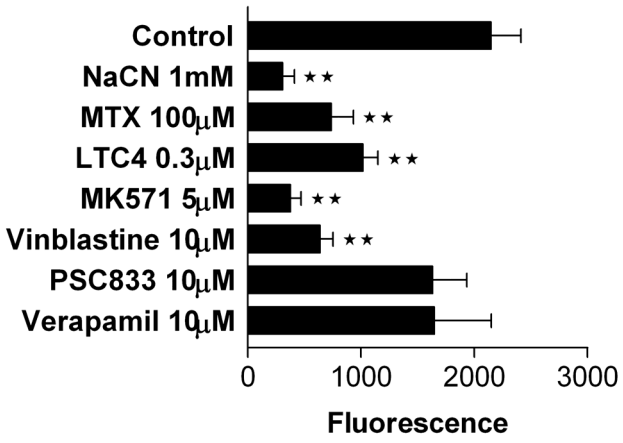

Figure 47: Organic Anion Inhibition of FL-MTX Secretion in Rat CP Blood Vessels

In contrast, dose response curves for estrone sulfate (ES), *p*-aminohippurate (PAH), digoxin, LTC_4 and MK571 did not show parallel decreases in cellular and

subepithelial/vessel fluorescence with increasing the concentrations of inhibitor. Among these inhibitors, two inhibition patterns were evident. First, ES and PAH partially blocked transepithelial transport (reduced subepithelial/vessel fluorescence), but did not affect cellular fluorescence (figure 49). Thus, these compounds appeared to block a component of FL-MTX efflux from the cells without altering cellular accumulation.

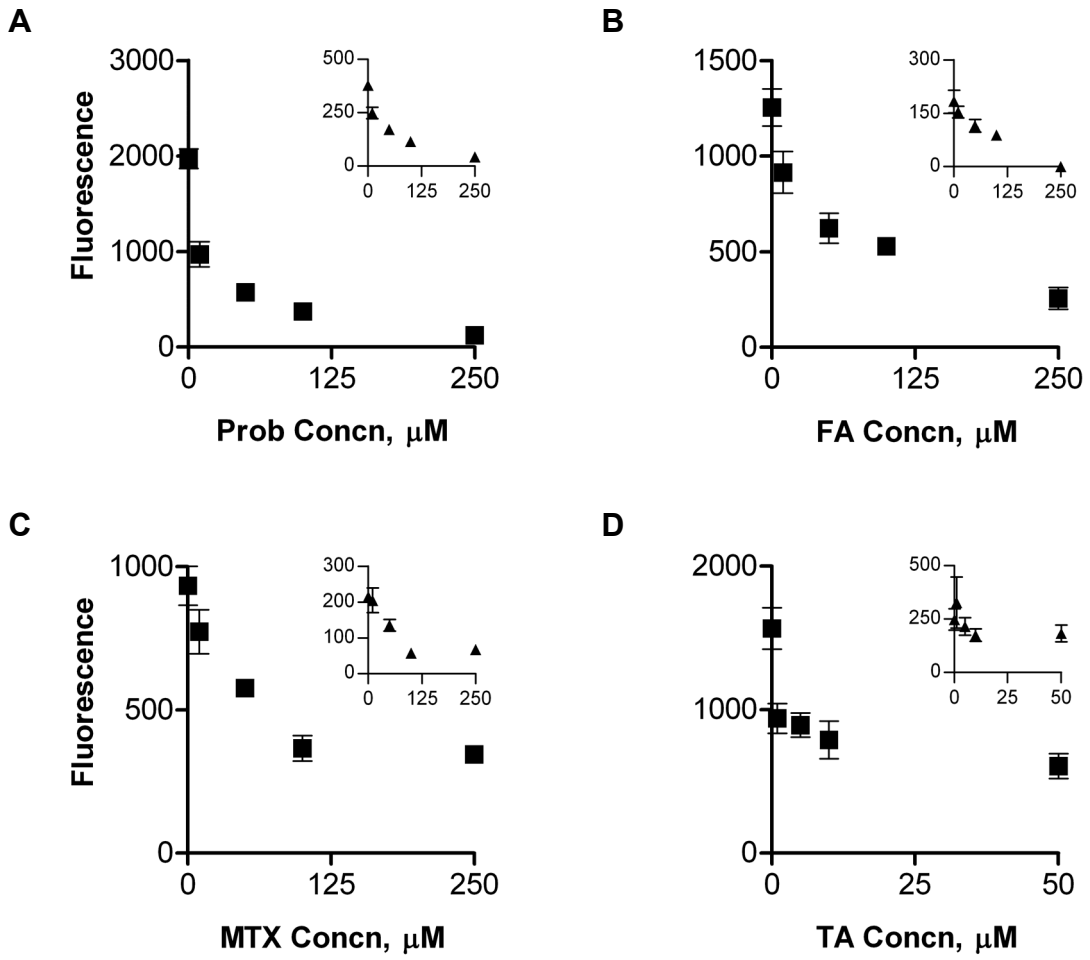

Figure 48: Inhibition of FL-MTX Secretion in Shark CP by Probenecid (A), Folic Acid (B), Methotrexate (C) and Taurocholate (D)

Second, for digoxin, LTC_4 and MK571 subepithelial/vessel fluorescence fell with increasing inhibitor concentration, but at one or more of the inhibitor concentrations used, cellular fluorescence increased significantly (figure 50). For example, with 10-50 μM digoxin and 0.1-0.3 μM LTC_4, subepithelial/vessel fluorescence fell to about 50% of control values, but cellular fluorescence increased to about double control values (figure 50A and figure 50B). With MK571, subepithelial/vessel fluores-

cence fell rapidly with increasing inhibitor concentration and cellular fluorescence increased significantly at 1 µM, but then fell; with 10 to 25 µM MK571, fluorescence in both compartments was nearly abolished (figure 50C). Note that in these experiments medium fluorescence averaged about 250 units; thus, with 10 to 50 µM digoxin, 0.1 to 0.3 µM LTC_4, and 1 µM MK571, cellular accumulation of FL-MTX was about two times higher than medium levels.

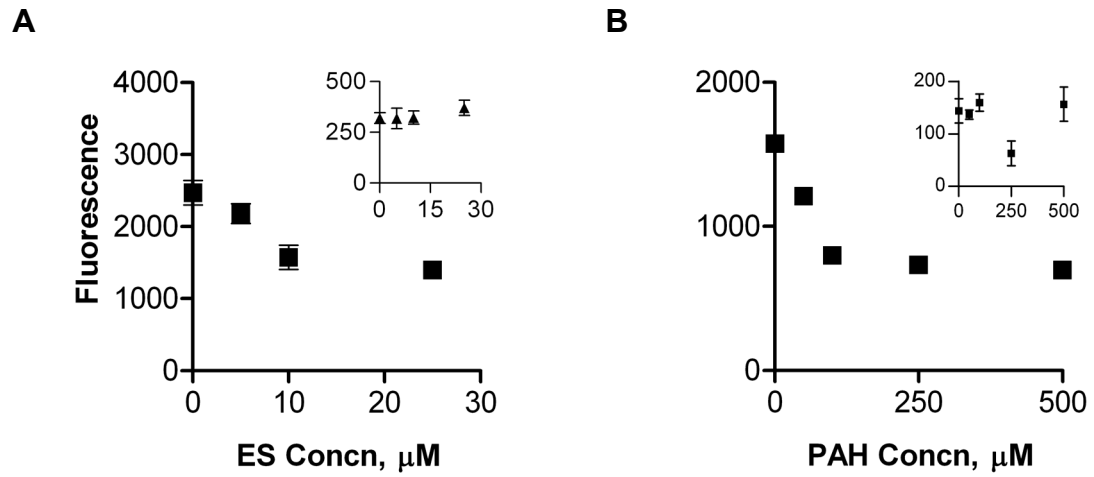

Figure 49: Effects of Estrone Sulfate (ES, A) and *p*-Aminohippurate (PAH, B) on 2 µM FL-MTX Secretion in Shark CP

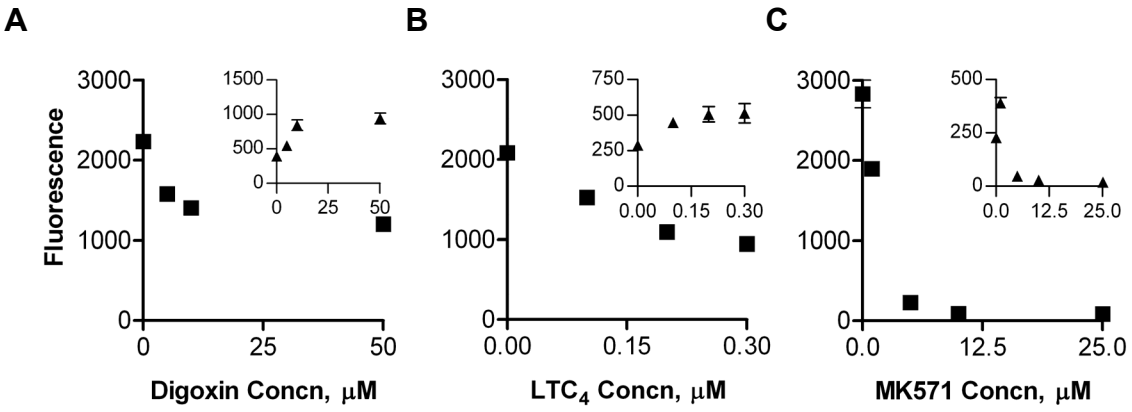

Figure 50: Effects of Digoxin (A), Leukotriene C_4 (LTC_4, B) and MK571 (C) on 2 µM FL-MTX Secretion in Shark CP

To facilitate visualization and further characterize uptake of FL-MTX at the apical membrane of CPEC, digoxin was used enhancing cellular fluorescence accumulation. In the presence of 10 µM digoxin, cellular accumulation of FL-MTX was both Na^+-dependent and ouabain-sensitive (figure 51). In both cases inhibition was incom-

plete. Transport was reduced by probenecid and taurocholate. As in the experiments in which inhibitors were used singly, when used in combination with digoxin, 250 µM probenecid abolished cellular and subepithelial/vessel fluorescence and 10-25 µM taurocholate partially reduced fluorescence in both compartments (figure 52A and B and figure 52C and D). Finally, the effects of 10 µM digoxin plus 5-25 µM ES were not significantly different from the effects of ES alone, suggesting that both compounds blocked the same component of basolateral efflux (figure 52E and 52F).

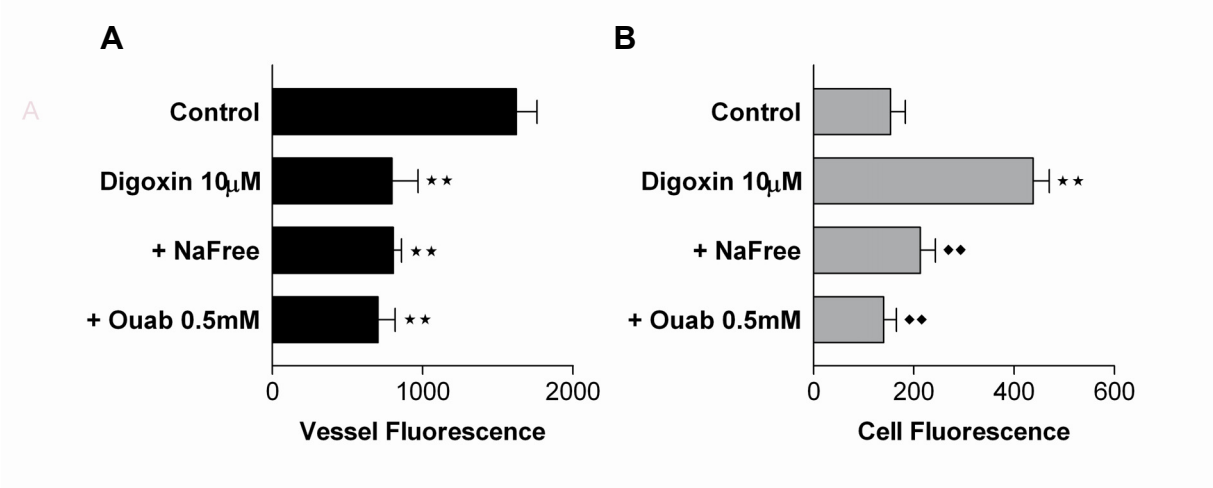

Figure 51: Ionic Environment Effect and Digoxin on 2 µM FL-MTX Secretion in Shark CP
(∗ Significantly different from control; ♦ significantly different from digoxin treatment)

Clearly, in both shark and rat, certain compounds appeared to both preferentially block FL-MTX efflux into the subepithelial/vessel compartment and increase cellular accumulation. In the absence of any molecular-level information about xenobiotic transporters in shark, one can only speculate about the transporters responsible for FL-MTX transport. FL-MTX efflux in shark choroid plexus could be mediated by an Oatp2-like transporter as indicated by digoxin sensitivity and an Mrp as indicated by MK571 sensitivity. Also, the present data for shark CP suggest that at least one of the transporters responsible for FL-MTX uptake is Oat-like, as Oats are the only known family of organic anion transporters able to support Na^+-dependent, concentrative uptake.

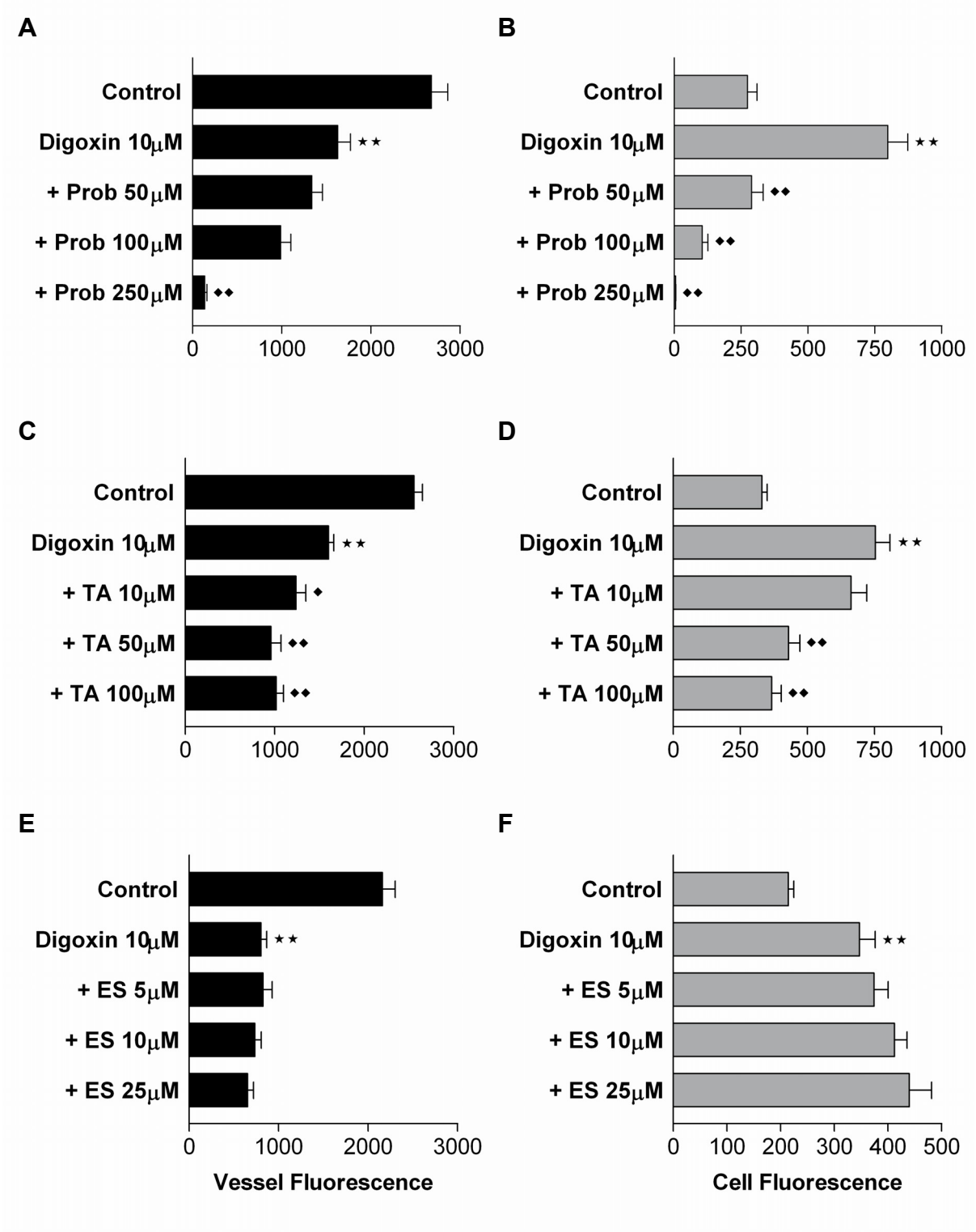

Figure 52: Effects of Digoxin and Organic Anions on 2 µM FL-MTX Secretion in Shark CP
(∗ Significantly different from control; ♦ significantly different from digoxin treatment)

3.5.3 Regulation of Organic Anion Secretion at the Choroid Plexus

The present study identifies for the first time in any species intracellular signals regulating organic anion transport in CP. In renal proximal tubule, organic anion transport is modulated by a variety of signals, including protein kinase C (PKC) activation, which reduces transport on Oats and Mrp2, and mitogen-activated protein (MAP) kinase activation, which increases transport on Oats (Soodvilai et al., 2004). Protein kinase A (PKA) does not appear to modulate renal organic anion transport. Figure (53A) shows that, as in renal proximal tubule, FL-MTX transport across shark choroid plexus was reduced significantly when PKC was activated by 10-100 nM phorbol-12-myristate-13-acetate (PMA). With 100 nM PMA, both cellular and subepithelial/vessel fluorescence were reduced by about 50%. Consistent with specific activation of PKC, the effects of PMA were abolished when tissue was exposed to the PKC-selective inhibitor bisindolylmaleimide (BIM), which by itself did not affect FL-MTX transport (figure 54).

In contrast to PMA, which reduced FL-MTX transport, 10 µM forskolin increased FL-MTX accumulation in both tissue compartments by over 50% (figure 53). Forskolin inhibits phosphodiesterase and increases levels of the 3'-5'-cyclic ester of adenosine monophosphate (cAMP) activating PKA. Forskolin activation of transport was abolished by the PKA selective inhibitor H-89, which by itself did not affect FL-MTX transport (figure 54). Thus, protein-kinase based mechanisms are in place to both increase and decrease transport, presumably in response to hormonal exposure. The identity of the hormones responsible remains to be determined.

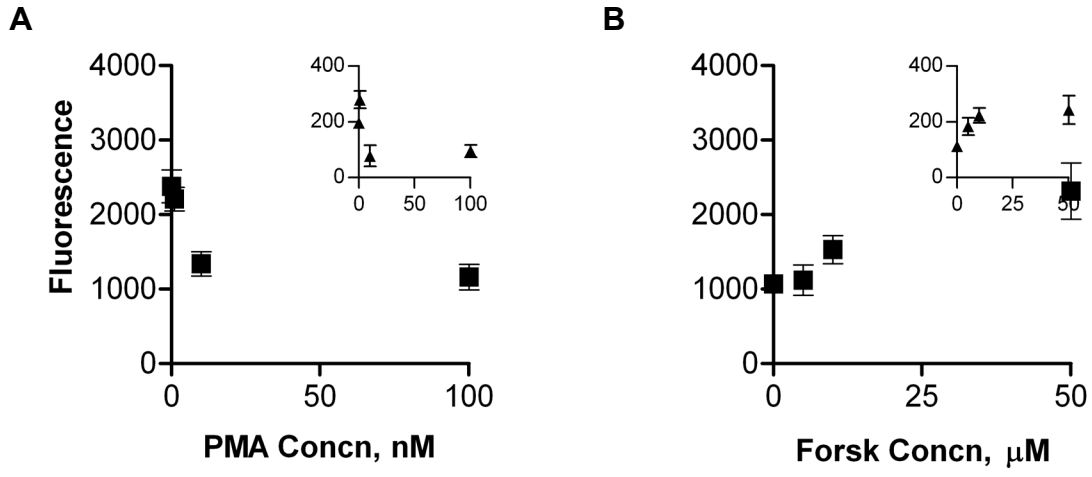

Figure 53: Effects of Phorbol Ester PMA and Forskolin on CP FL-MTX (2 µM) Secretion

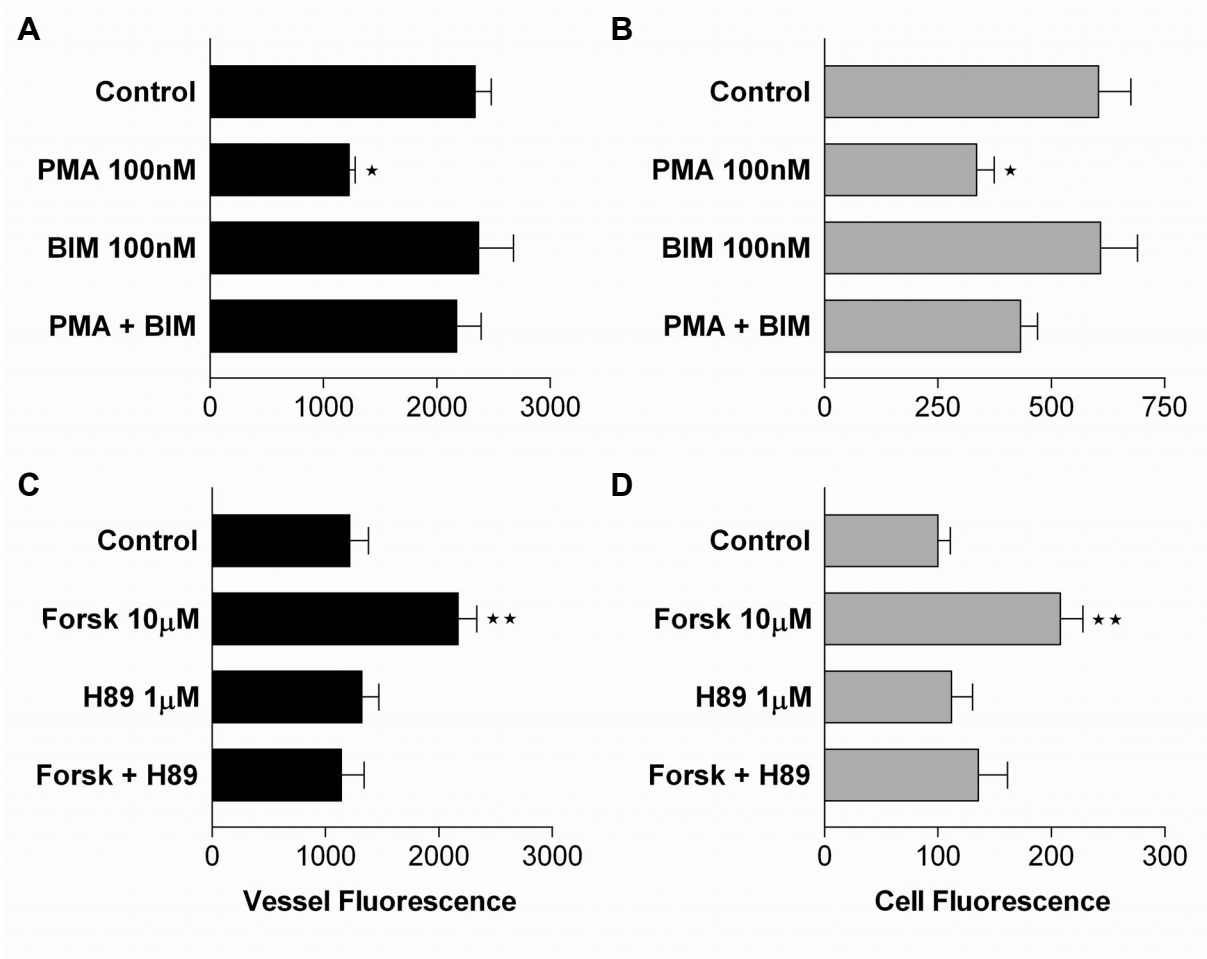

Figure 54: Effects of PMA and Forskolin and Specific Inhibitors on 2 µM FL-MTX Secretion

To determine the time course of forskolin action, shark CP tissue was incubated with 2 µM FL-MTX until fluorescence accumulation reached steady state, before adding 10 µM forskolin and measuring changes in tissue fluorescence. Control experiments (not shown) demonstrated that after the initial 60 min loading period fluorescence in both tissue compartments was constant for at least an additional 90 min of incubation. As shown in figure 55, addition of forskolin to the medium significantly increased cellular fluorescence within 15 min and subepithelial/vessel fluorescence within 30-45 min. Fluorescence in both compartments remained elevated for at least 90 min after addition of forskolin (not shown). Thus, activation of cellular FL-MTX accumulation appeared to be rapid. After a short time lag, subepithelial/vessel accumulation also increased.

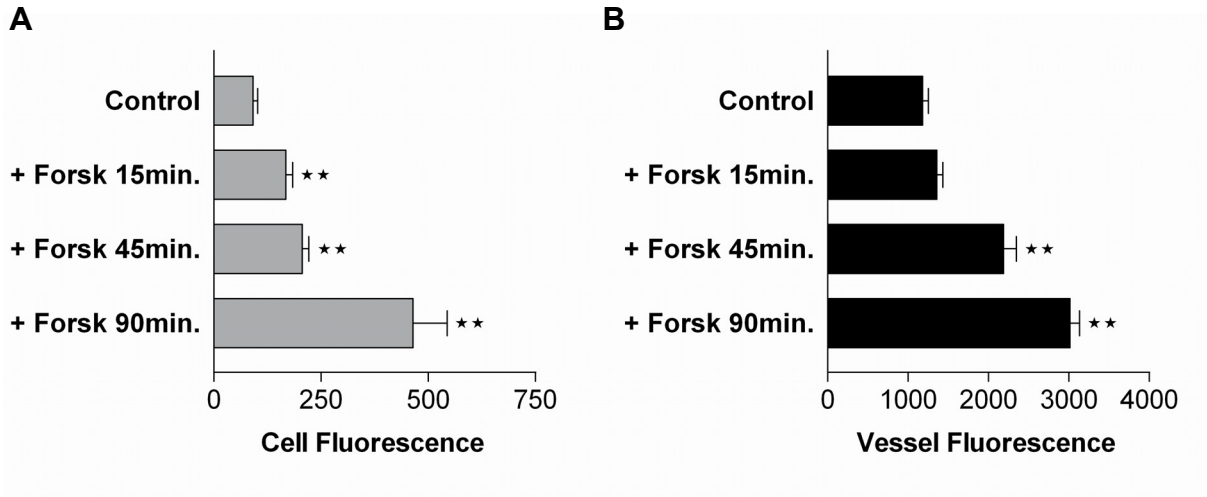

Figure 55: Effect of Forskolin 10 µM on 2 µM FL-MTX Transport into CP Cells (A) and Blood Vessels (B) over Time

3.5.4 FL-MTX Transport across Choroid Plexus Epithelial Cells *In Vitro*

FL-MTX secretion was analyzed in cultured CPEC and fully differentiated at 14 DIC. Uptake of FL-MTX was measured into cells grown in 96-well plates and transport across CPEC grown on Transwell® filter systems was determined. One of the main advantages of using an *in vitro* model is that absolute concentration values can be determined. This is not possible for confocal microscopy determined fluorescence, constrained by the geometrical variability of biological structures. *In vitro* results of FL-MTX uptake and transport were reported as absolute concentrations calculated using an appropriate standard curve. Due to interexperimental variations, pooled results are presented as percent of control.

To elucidate accumulation of FL-MTX in cultured CPEC, cells were incubated with increasing concentrations of FL-MTX, ranging from 1 µM to 50 µM for periods of 30 min, 60 min and 90 min. Figure 56 shows fluorescence values of FL-MTX, applied at various concentrations and transported into CPEC, plotted against time. For all concentrations tested, uptake of FL-MTX remained linear for at least 30 min. After 60 min, the system accumulating FL-MTX in CPEC saturated. The data thus indicates that FL-MTX uptake into cultured cells is transporter-mediated.

Figure 57 shows uptake of 1 µM, 5 µM, 10 µM and 50 µM FL-MTX by cultured CPEC 14 DIC over a time period of up to 90 min, plotted against concentrations of FL-MTX (in nM) accumulated in cultured cells. Over the range of FL-MTX concentrations tested, increased linear uptake was measured at 30 min, 60 min and 90 min (R^2 > 0.99). Conversely to a transport-driven system, differentiated CPEC cultured in 96-

well plates did not show a saturable concentration curve, at least not for concentrations up to 50 µM FL-MTX.

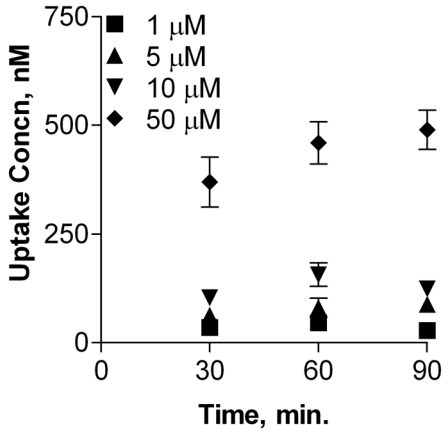

Figure 56: Uptake of FL-MTX at Different Time Intervals

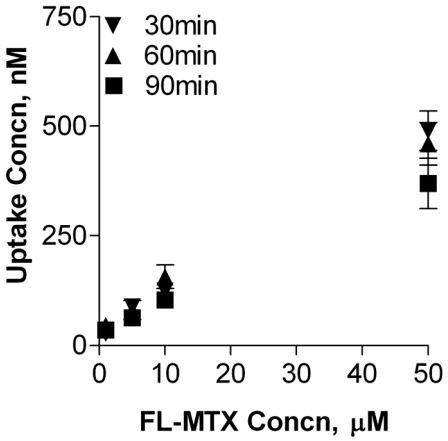

Figure 57: Uptake of Various Concentrations of FL-MTX

As in *ex vivo* analyses, altering ionic buffer environments influenced CPEC FL-MTX transport (figure 58). In cultured CPEC, sodium (Na^+) removal (NaCl replaced with *N*-methyl-*D*-glucamine) increased FL-MTX uptake by approximately 50%. The process was reversible: transport was reestablished upon the addition of sodium containing medium. Notably, the increase in cellular FL-MTX in Na^+-free medium was opposite to effects observed in *ex vivo* analyses. *Ex vivo* Na^+ removal resulted in significantly decreased cellular FL-MTX accumulation. Further, results were also con-

trary to effects observed adding 0.5 mM ouabain. Inhibition of Na^+-K^+-ATPase affects cellular Na^+-gradients, but opposite to Na^+-removal, cellular FL-MTX accumulation was reduced by more than 50%. Increasing KCl 10-fold, altering the cellular membrane potential, did not affect FL-MTX uptake.

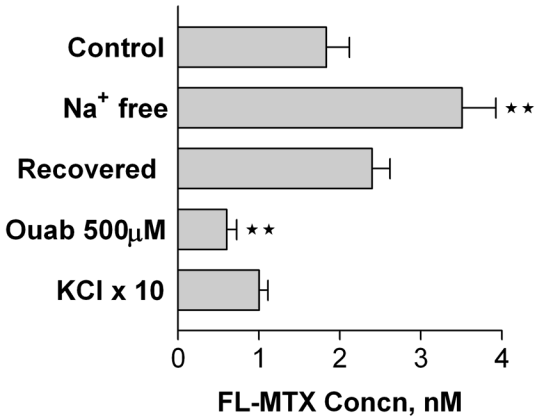

Figure 58: Uptake of FL-MTX in CPEC 14 DIC in Altered Ionic Environment, with Ouabain (Ouab) added and with KCl increased 10-fold

Addition of NaCN, irreversibly inhibiting intracellular oxygen utilization, increased FL-MTX uptake by more than 50% (figure 59). Again, comparable to effects seen removing Na^+, effects on FL-MTX uptake into cultured cells were different to transport observed in *ex vivo* tissue. Only the extent to which FL-MTX transport was affected remained the same. In fact, effects were opposite with FL-MTX concentrations increasing in cultured CPEC compared to a reduced amount of fluorescence measured in rat and shark CP models.

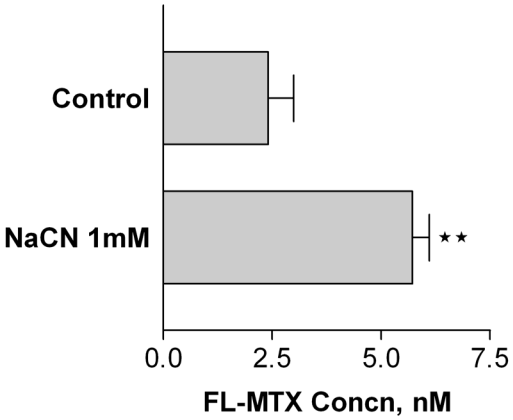

Figure 59: 2 µM FL-MTX Uptake into CPEC 14 DIC with 1 mM NaCN Added

Addition of organic anions reduced uptake of FL-MTX into cultured CPEC in a concentration-dependent manner (figure 60). Concurrent incubation of cells with 2 µM FL-MTX and 250 µM unlabelled methotrexate (MTX), 250 µM probenecid (Prob), 100 µM taurocholate (TA) or 500 µM *p*-aminohippuric acid (PAH) added caused significant reductions in FL-MTX accumulation. Effects were comparable to those observed in *ex vivo* fluorescent confocal microscopy analyses.

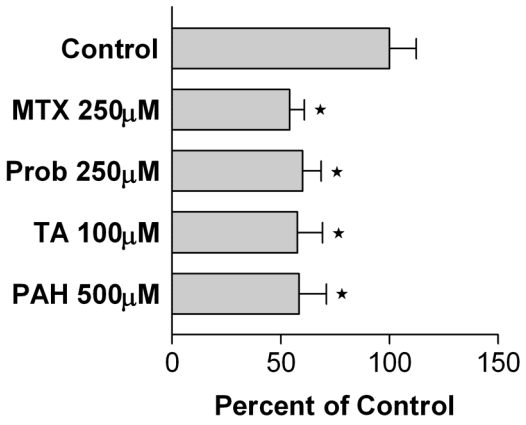

Figure 60: Uptake of 2 µM FL-MTX into Cultured CPEC in Presence of Organic Anions Methotrexate (MTX), Probenecid (Prob), Taurocholate (TA) and *p*-aminohippuric acid (PAH)

Analyses of concentration curves showed that probenecid (Prob) reduced FL-MTX uptake in a linear fashion, with fluorescent values going towards zero at concentrations greater 250 µM (figure 61A). Unlabelled MTX reached a plateau at concentrations above 250 µM (figure 61B). Addition of digoxin caused an increase in FL-MTX accumulation in cultured CPEC: at 100 µM fluorescence accumulation doubled (figure 61C). Thus, for organic anions studied in cultured CPEC uptake studies, inhibition patterns were comparable to those observed *ex vivo*. The main difference was that effects were seen using higher concentrations of inhibitor. Probenecid significantly reduced FL-MTX uptake, but uptake was reduced by less than 50% even at 250 µM. MTX effects, reaching an inhibition plateau, were seen at concentrations of 250 µM in cultured CPEC compared to 100 µM in *ex vivo* analysis of CP tissue. With digoxin, cellular fluorescence doubled at 100 µM in cultured CPEC, compared to 10 µM in live tissue. Whether these concentration effects were species dependent, resulting from differences between the mammalian and elasmobranch species, or due

to culture and experimental conditions altering CPEC function remains to be determined.

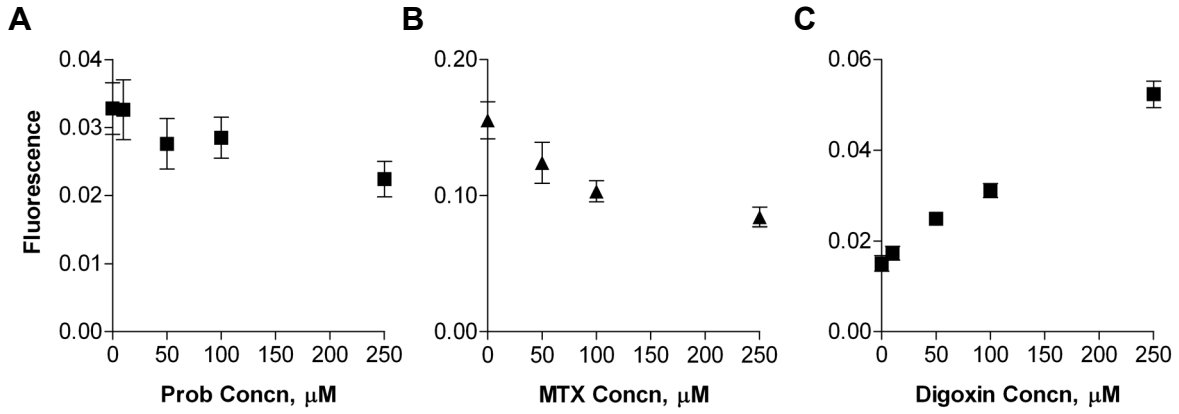

Figure 61: Uptake of 2 µM FL-MTX and Organic Anions Probenecid (Prob, A), Methotrexate (MTX, B) and Digoxin (C) in CPEC 14 DIC

Uptake of FL-MTX into cultured CPEC was further elucidated incubating cultured cells with digoxin alone and incubating with digoxin concurrent with other organic anions (figure 62). As in *ex vivo* investigations, digoxin increased cellular fluorescence accumulation and increased accumulation was reduced, adding various organic anions, including probenecid (Prob), methotrexate (MTX) and *p*-aminohippuric acid (PAH). Again, the only difference was that higher concentrations of inhibitor were needed. Thus, FL-MTX uptake in cultured CPEC and live tissue is comparable, with similar transport mechanisms involved.

Investigations of FL-MTX transport across cultured monolayers were carried out with fully differentiated cells grown on permeable membranes. Using Transwell® filter systems, transport can be determined from apical or CSF-facing to basolateral or blood-facing chambers and vice versa. Permeable membranes are the only experimental system allowing direct access to the blood-facing side of CPEC.

Cells were grown until fully differentiated. After replacing medium with KRB, transport of FL-MTX was determined for substrate (control) or for substrate with concurrent inhibitor incubation. For all inhibitor treatments, cells were pre-incubated with inhibitor alone. For pre-incubation and for transport measurements, inhibitors were added to both apical and basolateral compartments. All transport experiments were carried out with 2 µM FL-MTX applied to one compartment, determining fluorescence

accumulation in corresponding apical or basolateral chambers. Transport at 37°C was followed for a 90 min period.

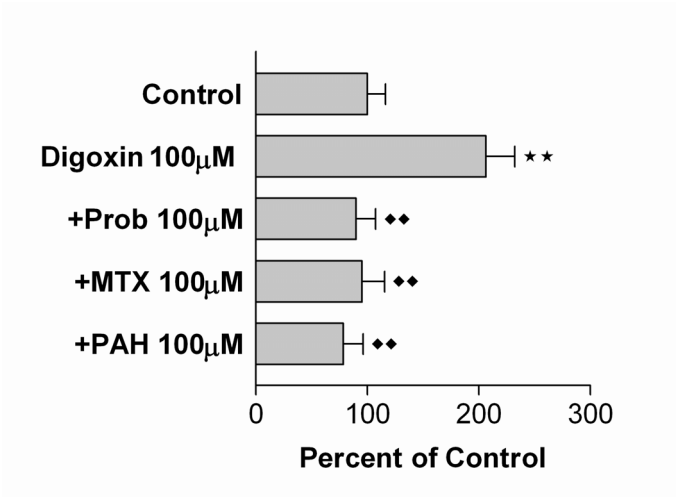

Figure 62: Uptake of 2 µM FL-MTX with Digoxin and Digoxin plus Probenecid (Prob), Methotrexate (MTX) and *p*-aminohippuric acid (PAH)

Figure 63 shows results for transport of 2 µM FL-MTX measured over a 90 min period with FL-MTX applied to the apical and accumulation measured in the basolateral chamber. FL-MTX transport alone served as control. The metabolic inhibitor NaCN reduced transport of FL-MTX by more than 50%, as seen in *ex vivo* tissue. Notably, effects were similar in shark and rat confocal microscopy analyses, cultured porcine CPEC uptake and transport experiments, but in contrast to all other analyses FL-MTX accumulation increased in uptake experiments. Incubation with organic anions leukotriene C_4 (LTC_4), MK571 and vinblastine significantly reduced FL-MTX transport from apical to basolateral compartments, whilst incubation with digoxin increased transport.

Figure 64 shows results of 2 µM FL-MTX transport measured form basolateral to apical chambers. Transport of FL-MTX from basolateral to apical chambers served as control and was not significantly different from apical to basolateral secretion. Incubation with other organic anions, including *p*-aminohippuric acid (PAH), probenecid (Prob) and digoxin did significantly affect transport of FL-MTX.

FL-MTX transport was affected by inhibitors when measured from apical to basolateral chambers and not vice versa. Regarding molecular and immunohistochemical data, inhibitors NaCN, LTC_4 and MK571 are most likely targeting Mrp1, expressed at the basolateral membrane of CPEC. Thus, transport of FL-MTX was reduced due to decreased efflux on Mrp1.

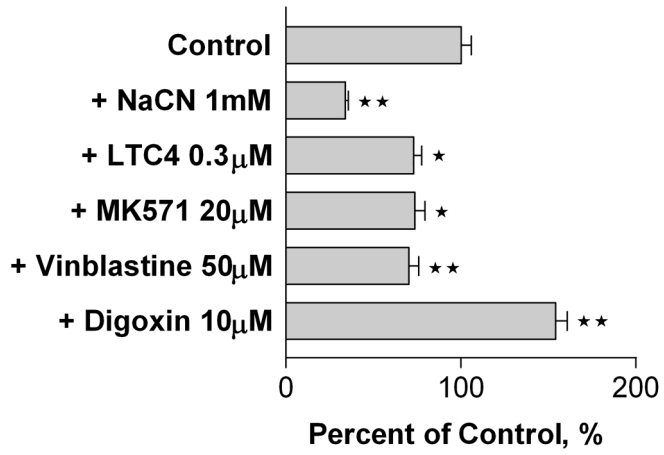

Figure 63: FL-MTX, Digoxin and Organic Anion Transport across Cultured CPEC from Apical to Basolateral Compartments

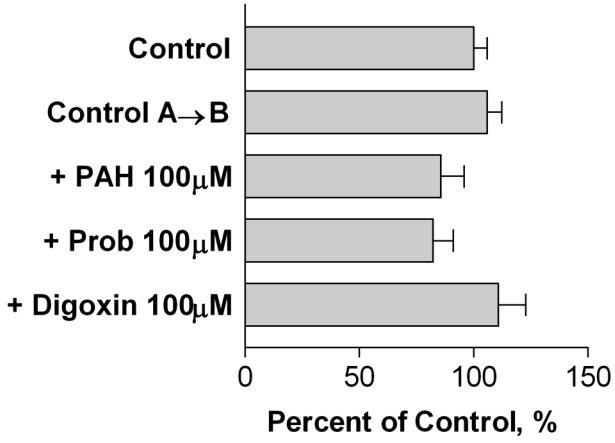

Figure 64: FL-MTX, Digoxin and Organic Anion Transport across Cultured CPEC from Basolateral to Apical Compartments

The increased transport of FL-MTX in presence of digoxin is in contrast to effects seen in uptake studies and *ex vivo* analyses. Interpretation of mammalian molecular and biochemical data suggests that digoxin acts on Oatp2. Oatp2 was previously shown to locate at the basolateral membrane of CPEC (Sun et al., 2001; Graff and Pollack, 2004). In FL-MTX uptake studies the substrate accumulated within CPEC. Quantitative analyses in *ex vivo* studies, revealed increased cellular accumulation of FL-MTX in the presence of digoxin, with transport into blood vessels significantly reduced (>50%). The increased transport of FL-MTX in presence of digoxin across Transwell® filter systems may result from application of digoxin to the basolateral membrane. No other experimental system allowed presenting CPEC with inhibitors from the blood-facing side. Assuming that Oatp2 in CPEC is a bidirectional

transport protein, digoxin may act as a high affinity counter ion, increasing net transport efficiency of FL-MTX.

4 SUMMARY

The choroid plexus forms the blood-liquor barrier and separates blood from CSF. Together with the BBB, the CP helps to maintain a stable environment, supply nutrients and protect the brain from toxic insult. Recent morphological re-analyses of CP surface area revealed that, taking the tissue's apical microvilli and basolateral infoldings into account, the available area for exchange between blood and brain is much greater than previously thought. Since, the CP has gained importance, especially with regard to the pharmacology and distribution of CNS-active compounds into the brain.

Studying xenobiotic transport across mammalian CP is difficult, due to the tissues anatomical location, complex morphology and small size. To help overcome these limitations, a primary porcine CP *in vitro* model was established. Cells were isolated and grown until fully differentiated. The marker protein TTR was used as epithelial marker and demonstrated at the level of gene expression, localized within cultured cells and in Western blots. All cultures were free of contaminating cells, formed intact monolayers and were fully differentiated.

Alkaline phosphatase and γ-glutamyl transferase activity was determined and enzyme activity over the 14-day culture period was at levels comparable to other *in vitro* cultures of barrier forming cells. Quantification of CSF production revealed that the established model secretes volumes at rates previously measured. Permeation across cells grown on permeable surfaces was validated, measuring transepithelial resistance and using markers for transport. Compared to *in vitro* models of other cellular barriers, such as cultured BCEC of the BBB or Caco-2 cells of the intestinal barrier, the BCSFB model was more diffuse or leaky, resembling *in vivo* BCSFB properties.

Two pharmacological important transport proteins, the MDR1 gene product Pgp and the multidrug-resistance associated transport protein Mrp1, were investigated at the level of gene expression, localized within CPEC and stained in Western blots. Semi-quantitative gene expression analyses of Mrp1, in freshly excised porcine CP tissue and fully differentiated CPEC *in vitro*, demonstrated that there is no significant difference in expression levels. Using specific antibodies directed against both transporters, subcellular localization was visualized by confocal laser scanning microscopy. Whereas Pgp localized sub-apical or apical in CPEC and membrane

incorporation was not confirmed, Mrp1 was clearly distributed to and incorporated in the basolateral plasma membrane. Thus, to further elucidate the localization of Pgp, membrane fractions were labeled with anti-Pgp C219 antibody. Clearly the apical membrane fraction stained. However, concluding functional analyses of Pgp activity measured in cultured CPEC using different transport inhibitors showed no significant difference between control and treatment. Thus Pgp was judged functionally inactive in CPEC *in vitro*.

Organic anion transport and active removal of compounds from CSF by the CP has been of interest for several decades, since these transport processes not only reduce CNS circulation time, but may also restrict entry into the brain altogether. Underlying molecular and functional processes governing transport of the FL-MTX, a large organic anion, were revealed. Notably, there was a marked difference in distribution of FL-MTX and fluorescein, a smaller organic anion previously under investigation.

FL-MTX transport is a specific, concentrative and mediated two-step process. Apical uptake of FL-MTX is Na^+-dependent and the powerful basolateral efflux dependent on cellular metabolism. Membrane potential has no influence on FL-MTX epithelial distribution. Based on available mammalian molecular and immunohistochemical data, a model schematically describing transport proteins involved in removing FL-MTX from CSF was put forth.

Active uptake of FL-MTX at the apical membrane is mediated by at least two transporters, most likely by OAT3 and Oatp3. The only type of transport proteins linked to Na^+-dependence is the OAT family. Involvement of Oatp3 is implied, as OAT3 knock-outs showed no difference in FL-MTX distribution, lacking the only Na^+-dependent organic anion exchanger localized to apical CP membranes. Export at the basolateral membrane is also mediated by at least two transport proteins. Inhibition of epithelial efflux with digoxin and increased accumulation within CPEC clearly demonstrated participation of Oatp2. Metabolism dependence and inhibition with LTC_4 and MK571 point towards Mrp1 being involved in the efficient efflux of FL-MTX into blood vessels.

For the first time, regulatory processes of organic anion transport at the CP were revealed. It was demonstrated that both PKA and PKC specifically increase and decrease organic anion transport, respectively. Further, PKA initiated increased

transport at the apical epithelial membrane with a subsequent increased cellular FL-MTX concentration, followed by increased efflux across the basolateral membrane into blood vessels. Time course analyses of this regulatory process showed that the increase in activity could be induced within minutes. Underlying regulatory hormones remain to be identified.

5 OUTLOOK

Detailed analyses demonstrated that CP epithelium can be isolated and cultured, with cells growing into intact monolayers, fully differentiating and with properties resembling the tissue *in vivo*. Comparative experiments using the model compound FL-MTX, which is transported via a complex interplay of at least four different transport proteins, revealed that these complex processes are fully functional in cultured cells. Results obtained *in vitro* mimicked the distribution observed *in vivo*. Thus, the established primary porcine CP model, allowing investigation of complex transport processes, can be used as a reliable tool for analyses of xenobiotic transport across the blood-liquor barrier.

Transport processes underlying the removal of FL-MTX from CSF were visualized by confocal laser microscopy. This relatively recent technology allowed subcellular visualization of transport processes in a detail not seen before. CP physiology can now be accessed in live tissue and in real time.

Compared to previous analyses of fluorescein, a small organic anion, removal of FL-MTX is characterized by different transport properties. Fluorescein and FL-MTX are both actively transported in CP, but both compounds exhibit different patterns of distribution within tissue compartments and removal involves different transport proteins. However, clearance of organic anions from the CNS is even more intricate. A third organic anion under investigation is Texas Red (TR, 625 g/mol), which is of intermediate size when compared to fluorescein and FL-MTX. TR transport across CP tissue was not like fluorescein or FL-MTX, even though tissue distribution resembled more that of fluorescein than FL-MTX (figure 65).

TR fluorescence intensity in epithelial cells, determined by quantitative confocal microscopy, was roughly half the fluorescence intensity measured in perivascu-

lar/subepithelial spaces. In contrast, FL-MTX concentrates in blood vessels with cellular fluorescence remaining low.

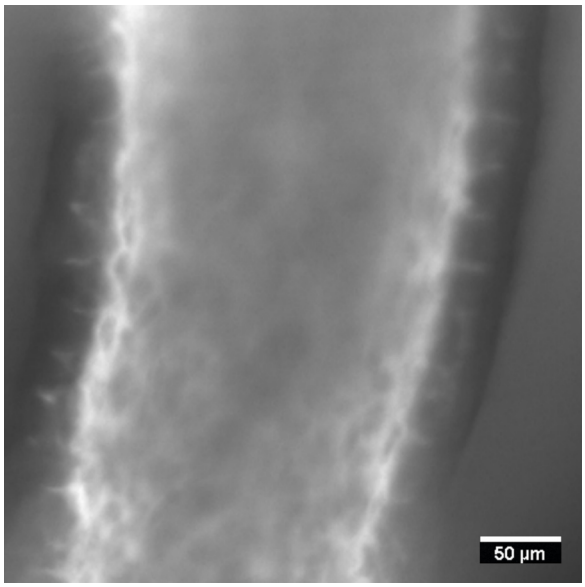

Figure 65: Distribution of Texas Red (TR) within CP Tissue

Transport of both fluorescein and FL-MTX was dependent upon the ionic composition of the incubation medium. Secretion of both fluorescein and FL-MTX was Na^+-dependent. Epithelial efflux of fluorescein was dependent on cellular electrical potential, and blocked when electrical gradients are disrupted with excess potassium. In contrast, TR was handled independently of medium sodium concentrations, and raising potassium ten-fold did not affect secretion.

FL and FL-MTX react differently to the presence of organic anion transport inhibitors. Probenecid, a general effector of organic anion transport, inhibits accumulation of cellular and perivascular/subepithelial FL and FL-MTX fluorescence. TR accumulation in cells and vessels was also inhibited. 2,4-D, an effective inhibitor of FL transport, had no effect on TR transport. Estrone sulfate inhibited accumulation of FL-MTX in the perivascular/subepithelial space, but has no effect on cellular accumulation. TR accumulation in both cells and vessels was inhibited by incubation with estrone sulfate. Digoxin and MK571 both inhibit perivascular/subepithelial accumulation of FL-MTX in CP tissue, but cause an increase in cellular accumulation. While both of these compounds caused significant inhibition of TR accumulation in blood vessels, no increase in cellular fluorescence was found.

The preliminary analyses of TR transport suggest that the intermediate size anion is handled differently from fluorescein and FL-MTX. Influx is uniquely sodium-independent, and efflux is neither potential-dependent, like fluorescein, nor handled by the same transporters as FL-MTX. Thus, even though again active processes are involved in clearance, different organic anions are transported by different underlying molecular mechanisms and different transport proteins seem to be involved. Further analyses are necessary for complete clarification of involved complex functional processes.

6 REFERENCES

A

Abbott NJ. Astrocyte-endothelial interactions and blood-brain barrier permeability. *J Anat*. 2002; 200(6):629-38.

Abou-Donia MB. Neurotoxicology. CRC Press, Inc. Boca Ranton, 1992.

Alebouyeh M, Takeda M, Onozato ML, Tojo A, Noshiro R, Hasannejad H, Inatomi J, Narikawa S, Huang XL, Khamdang S, Anzai N, Endou H. Expression of human organic anion transporters in the choroid plexus and their interactions with neurotransmitter metabolites. *J Pharmacol Sci*. 2003; 93(4):430-6.

Aleu J, Ivorra I, Lejarreta M, Gonzalez-Ros JM, Morales A, Ferragut JA. Functional incorporation of P-glycoprotein into Xenopus oocyte plasma membrane fails to elicit a swelling-evoked conductance. *Biochem Biophys Res Commun*. 1997; 237(2):407-12.

Allen JD, Brinkhuis RF, van Deemter L, Wijnholds J, Schinkel AH. Extensive contribution of the multidrug transporters P-glycoprotein and Mrp1 to basal drug resistance. *Cancer Res*. 2000; 60(20):5761-6.

Altschul SF, Gish W, Miller W, Myers, EW, Lipman DJ. Basic local alignment search tool. *J Mol Biol*. 1990; 215:403-410.

Ancillotti R, Goto-Silva L, Montesano G, Oliveira S, Redondo PA, Barbosa LA, De Souza W, Morgado-Diaz JA. Assembly and functional analysis of tight junction in a colon adenocarcinoma cell line: effect of glucose depletion. *Cell Mol Biol (Noisy-le-grand)*. 2003; 49(1):113-22.

Anderson JM, Van Itallie CM. Tight junctions and the molecular basis for regulation of paracellular permeability. *Am J Physiol*. 1995; 269(4 Pt 1):G467-75.

Angeletti RH, Novikoff PM, Juvvadi SR, Fritschy JM, Meier PJ, Wolkoff AW. The choroid plexus epithelium is the site of the organic anion transport protein in the brain. *Proc Natl Acad Sci USA*. 1997; 94(1):283-6.

Angelow S, Haselbach M, Galla HJ. Functional characterisation of the active ascorbic acid transport into cerebrospinal fluid using primary cultured choroid plexus cells. *Brain Res*. 2003; 988(1-2):105-13.

Angelow S, Zeni P, Galla HJ. Usefulness and limitation of primary cultured porcine choroid plexus epithelial cells as an in vitro model to study drug transport at the blood-CSF barrier. *Adv Drug Deliv Rev*. 2004; 56(12):1859-73.

Apiwattanakul N, Sekine T, Chairoungdua A, Kanai Y, Nakajima N, Sophasan S, Endou H. Transport properties of nonsteroidal anti-inflammatory drugs by organic anion transporter 1 expressed in Xenopus laevis oocytes. *Mol Pharmacol*. 1999; 55(5):847-54.

Archibald AL, Couperwhite S, Jiang ZH. The porcine TTR locus maps to chromosome 6q. *Unpublished*. 1995.

Arndt-Jovin DJ, Jovin TM. Fluorescence labeling and microscopy of DNA. *Methods Cell Biol*. 1989; 30:417-48.

Asaba H, Hosoya K, Takanaga H, Ohtsuki S, Tamura E, Takizawa T, Terasaki T. Blood-brain barrier is involved in the efflux transport of a neuroactive steroid, dehydroepiandrosterone sulfate, via organic anion transporting polypeptide 2. *J Neurochem*. 2000; 75(5):1907-16.

Aschner A and Kerper LE. Transport of metals in the central nervous system. In Zalpus, RK and Koropatnick J. Molecular Biology and Toxicology of Metals. CRC Press; 1st edition, 2000.

Artursson P, Karlsson J. Correlation between oral drug absorption in humans and apparent drug permeability coefficients in human intestinal epithelial (Caco-2) cells. *Biochem Biophys Res Commun*. 1991; 175(3):880-5.

B

Bacallao R. The role of the cytoskeleton in renal development. *Semin Nephrol*. 1995; 15(4):285-90.

Baskin DG, Brewitt B, Davidson DA, Corp E, Paquette T, Figlewicz DP, Lewellen TK, Graham MK, Woods SG, Dorsa DM. Quantitative autoradiographic evidence for insulin receptors in the choroid plexus of the rat brain. *Diabetes*. 1986; 35(2):246-9.

Bauer B, Hartz AM, Fricker G, Miller DS. Pregnane X receptor up-regulation of P-glycoprotein expression and transport function at the blood-brain barrier. *Mol Pharmacol*. 2004; 66(3):413-9.

Behrens I, Kissel T. Do cell culture conditions influence the carrier-mediated transport of peptides in Caco-2 cell monolayers? *Eur J Pharm Sci*. 2003; 19(5):433-42.

Bendayan R, Lee G, Bendayan M. Functional expression and localization of P-glycoprotein at the blood-brain barrier. *Microsc Res Tech*. 2002; 57(5):365-80.

Berezowski V, Landry C, Dehouck MP, Cecchelli R, Fenart L. Contribution of glial cells and pericytes to the mRNA profiles of P- glycoprotein and multidrug resistance-associated proteins in an in vitro model of the blood-brain barrier. *Brain Res*. 2004; 1018(1):1-9.

Bessey OA, Lowry OH, Brock MJ. A method for the rapid determination of alkaline phosphatase with five cubic centimetres of serum. *J Bio Chem*. 1946; 164(321):.

Beuckmann C, Hellwig S, Galla HJ. Induction of the blood/brain-barrier-associated enzyme alkaline phosphatase in endothelial cells from cerebral capillaries is mediated via cAMP. *Eur J Biochem*. 1995; 229(3):641-4.

Biegel D, Spencer DD, Pachter JS. Isolation and culture of human brain microvessel endothelial cells for the study of blood-brain barrier properties in vitro. *Brain Res*. 1995; 692(1-2):183-9.

Borst P, Evers R, Kool M, Wijnholds J. The multidrug resistance protein family. *Biochim Biophys Acta*. 1999; 1461(2):347-57.

Borst, P and Elferink, RO. Mammalian ABC transporters in health and disease. *Annu Rev Biochem*. 2002; 71: 537-92.

Boudry G, Peron V, Le Huerou-Luron I, Lalles JP, Seve B. Weaning induces both transient and long-lasting modifications of absorptive, secretory, and barrier properties of piglet intestine. *J Nutr*. 2004; 134(9):2256-62.

Bouffard, G. Injection des eouleurs de benzidine aux animaux normaux. *Ann de l'Inst Pasteur*. 1906; xx:539.

Bourne A, Barnes K, Taylor BA, Turner AJ, Kenny AJ. Membrane peptidases in the pig choroid plexus and on other cell surfaces in contact with the cerebrospinal fluid. *Biochem J*. 1989; 259(1):69-80.

Bradford, MA. Rapid and Sensitive Method for the Quantitation of Microgram Quantities of Protein Utilizing the Principle of Protein-Dye Binding. *Anal Biochem*. 1976; 72:248-254.

Breen CM, Sykes DB, Fricker G, Miller DS. Confocal imaging of organic anion transport in intact rat choroid plexus. *Am J Physiol Renal Physiol*. 2002; 282(5):F877-85.

Brimer C, Dalton JT, Zhu Z, Schuetz J, Yasuda K, Vanin E, Relling MV, Lu Y, Schuetz EG. Creation of polarized cells coexpressing CYP3A4, NADPH cytochrome P450 reductase and MDR1/P-glycoprotein. *Pharm Res*. 2000; 17(7):803-10.

Broman T. The possibilities of the passage of substances from the blood to the central nervous system. *Acta Psychiatr Neurol Scand*. 1941;16:38011.

Burckhardt G, Wolff NA. Structure of renal organic anion and cation transporters. *Am J Physiol Renal Physiol*. 2000 Jun; 278(6):F853-66.

Burckhardt BC, Brai S, Wallis S, Krick W, Wolff NA, Burckhardt G. Transport of cimetidine by flounder and human renal organic anion transporter 1. *Am J Physiol Renal Physiol*. 2003; 284(3):F503-9.

Busch AE, Karbach U, Miska D, Gorboulev V, Akhoundova A, Volk C, Arndt P, Ulzheimer JC, Sonders MS, Baumann C, Waldegger S, Lang F, Koepsell H. Human neurons express the polyspecific cation transporter hOCT2, which translocates monoamine neurotransmitters, amantadine, and memantine. *Mol Pharmacol*. 1998; 54(2):342-52.

Bustin SA. Absolute quantification of mRNA using real-time reverse transcription polymerase chain reaction assays. *J Mol Endocrinol*. 2000; 25(2):169-93.

C

Cai SY, Soroka CJ, Ballatori N, Boyer JL. Molecular characterization of a multidrug resistance-associated protein, Mrp2, from the little skate. *Am J Physiol Regul Integr Comp Physiol*. 2003; 284(1):R125-30.

Caspers ML, Diglio CA. Expression of gamma-glutamyltranspeptidase in a transformed rat cerebral endothelial cell line. *Biochim Biophys Acta*. 1984; 803(1-2):1-6.

Castillo G, Vera JC, Yang CP, Horwitz SB, Rosen OM. Functional expression of murine multidrug resistance in Xenopus laevis oocytes. *Proc Natl Acad Sci USA*. 1990; 87(12):4737-41.

Chang CW, Yilinag W and Caldwell RB. Serum opens tight junctions and reduces ZO1 protein in retinal epithelial cells. *J Neurochem*. 1997; 69(2): 859-864.

Chen EY, Emerich DF, Bartus RT, Kordower JH. B2 bradykinin receptor immunoreactivity in rat brain. *J Comp Neurol*. 2000; 427(1):1-20.

Chen L, Segal DM, Mash DC. Semi-quantitative reverse-transcriptase polymerase chain reaction: an approach for the measurement of target gene expression in human brain. *Brain Res Brain Res Protoc*. 1999; 4(2):132-9.

Chen XZ, Zhu T, Smith DE, Hediger MA. Stoichiometry and kinetics of the high-affinity H+-coupled peptide transporter PepT2. *J Biol Chem*. 1999; 274(5):2773-9.

Cho MJ, Thompson DP, Cramer CT, Vidmar TJ, Scieszka JF. The Madin Darby canine kidney (MDCK) epithelial cell monolayer as a model cellular transport barrier. *Pharm Res*. 1989; 6(1):71-7.

Chodobski A, Szmydynger-Chodobska J, Segal MB, McPherson IA. The role of angiotensin II in regulation of cerebrospinal fluid formation in rabbits. *Brain Res*. 1992; 594(1):40-6.

Chodobski A, Szmydynger-Chodobska J. Choroid plexus: target for polypeptides and site of their synthesis. *Microsc Res Tech*. 2001; 52(1):65-82.

Choudhuri S, Cherrington NJ, Li N, Klaassen CD. Constitutive expression of various xenobiotic and endobiotic transporter mRNAs in the choroid plexus of rats. *Drug Metab Dispos*. 2003; 31(11):1337-45.

Crook RB, Kasagami H, Prusiner SB. Culture and characterization of epithelial cells from bovine choroid plexus. *J Neurochem*. 1981; 37(4):845-54.

Croop JM, Gros P, Housman DE. Genetics of multidrug resistance. *J Clin Invest*. 1988; 81(5):1303-9.

Cserr HF. Physiology of the choroid plexus. *Phys Rev*. 1971; 51(2):273.

D

Dagenais C, Rousselle C, Pollack GM, Scherrmann JM. Development of an in situ mouse brain perfusion model and its application to mdr1a P-glycoprotein-deficient mice. J *Cereb Blood Flow Metab*. 2000; 20(2):381-6.

Dahl SG, Sylte I, Ravna AW. Structures and models of transporter proteins. *J Pharmacol Exp Ther*. 2004; 309(3):853-60.

Daniel H. Molecular and integrative physiology of intestinal peptide transport. *Annu Rev Physiol*. 2004;66:361-84.

Daniel H, Rubio-Aliaga I. An update on renal peptide transporters. *Am J Physiol Renal Physiol*. 2003; 284(5):F885-92.

Daniel H, Kottra G. The proton oligopeptide cotransporter family SLC15 in physiology and pharmacology. *Pflugers Arch*. 2004; 447(5):610-8.

D'Aquila RT, Bechtel LJ, Videler JA, Eron JJ, Gorczycy P, Kaplan JC. Maximizing sensitivity and specificity of PCR by preamplification heating. *Nucleic Acids Res*. 1991; 19:3749.

Davson HA. Comparative study of the aqueous humour and cerebrospinal fluid in the rabbit. *J Physiol*. 1955; 129:111-133.

Davson H, Segal MB. Physiology of the CSF and blood-brain barriers, CRC Press, Boca Ranton, FL, 1996.

De Bault LE, Mitro A. Species differences in the distribution of gamma-glutamyl transpeptidase in choroid plexus of lateral ventricle and microvessels of adjacent brain. *Histochem J*. 1994; 26(5):447-52.

De Lange EC. Potential role of ABC transporters as a detoxification system at the blood-CSF barrier. *Adv Drug Deliv Rev*. 2004; 56(12):1793-809.

Dean M, Rzhetsky A, Allikmets R. The human ATP-binding cassette (ABC) transporter superfamily. *Genome Res*. 2001; 11(7):1156-66.

Decleves X, Regina A, Laplanche JL, Roux F, Boval B, Launay JM, Scherrmann JM. Functional expression of P-glycoprotein and multidrug resistance-associated protein (Mrp1) in primary cultures of rat astrocytes. *J Neurosci Res*. 2000; 60(5):594-601.

Deguchi Y, Naito Y, Ohtsuki S, Miyakawa Y, Morimoto K, Hosoya K, Sakurada S, Terasaki T. Blood-brain barrier permeability of novel [D-arg2]dermorphin (1-4) analogs: transport property is related to the slow onset of antinociceptive activity in the central nervous system. *J Pharmacol Exp Ther*. 2004; 310(1):177-84.

Deguchi Y, Naito Y, Ohtsuki S, Miyakawa Y, Morimoto K, Hosoya K, Sakurada S, Terasaki T. Blood-brain barrier permeability of novel [D-arg2]dermorphin (1-4) analogs: transport property is related to the slow onset of antinociceptive activity in the central nervous system. *J Pharmacol Exp Ther*. 2004; 310(1):177-84.

Dehouck MP, Jolliet-Riant P, Bree F, Fruchart JC, Cecchelli R, Tillement JP. Drug transfer across the blood-brain barrier: correlation between in vitro and in vivo models. *J Neurochem*. 1992; 58(5):1790-7.

de Lange EC. Potential role of ABC transporters as a detoxification system at the blood-CSF barrier. *Adv Drug Deliv Rev*. 2004; 56(12):1793-809.

Denk GU, Soroka CJ, Mennone A, Koepsell H, Beuers U, Boyer JL. Down-regulation of the organic cation transporter 1 of rat liver in obstructive cholestasis. *Hepatology*. 2004; 39(5):1382-9.

Dickson PW, Aldred AR, Marley PD, Tu GF, Howlett GJ, Schreiber G. High prealbumin and transferrin mRNA levels in the choroid plexus of rat brain. *Biochem Biophys Res Commun*. 1985; 127(3):890-5.

Diddens H, Gekeler V, Neumann M, Niethammer D. Characterization of actinomycin-D-resistant CHO cell lines exhibiting a multidrug-resistance phenotype and amplified DNA sequences. *Int J Cancer*. 1987; 40(5):635-42.

Docherty K, Shennan KI, Marsden RF, Ramsden DB. Subunit assembly and secretion of transthyretin: studies in a cell-free translation system and in microinjected Xenopus oocytes. *J Mol Endocrinol*. 1989; 3(3):191-7.

Doring F, Walter J, Will J, Focking M, Boll M, Amasheh S, Clauss W, and Daniel H. Delta-aminolevulinic acid transport by intestinal and renal peptide transporters and its physiological and clinical implications. *J Clin Invest*. 1998; 101:2761-2767.

Douglas A, Atchinson B. Degradation of DNA during denaturation step of PCR. *PCR-Methods and Applications*. 1993; 3(2):133-134.

Duan Z, Brakora KA, Seiden MV. Inhibition of ABCB1 (MDR1) and ABCB4 (MDR3) expression by small interfering RNA and reversal of paclitaxel resistance in human ovarian cancer cells. *Mol Cancer Ther*. 2004; 3(7):833-8.

Dudas PL, Renfro JL. Assessment of tissue-level kidney functions with primary cultures. *Comp Biochem Physiol A Mol Integr Physiol*. 2001; 128(2):199-206.

E

Ehrlich P. Das Sauerstoff-Bedürfnis des Organismus. Eine farbenanalytische Studie. Verlag August Hirschwald, 1885.

Ecker GF, Noe CR. In silico prediction models for blood-brain barrier permeation. *Curr Med Chem*. 2004 Jun;11(12):1617-28.

el-Bacha RS, Minn A. Drug metabolizing enzymes in cerebrovascular endothelial cells afford a metabolic protection to the brain. *Cell Mol Biol (Noisy-le-grand)*. 1999; 45(1):15-23.

Eckert K A, Kunkel TA. The fidelity of DNA polymerases used in the polymerase chain reactions. PCR A practical approach; Eds.: M.J. Mcpherson, P. Quirke & G.R. Taylor, IRL Press, 1991.

F

Fagqmiag MG, Palade GE. Junctional complexes in various epithelia. *Cell Bio*. 1963; 17:375.

Faulstich H, Zobeley S, Heintz D, Drewes G. Probing the phalloidin binding site of actin. *FEBS Lett*. 1993; 318(3):218-22.

Fellner S, Bauer B, Miller DS, Schaffrik M, Fankhanel M, Spruss T, Bernhardt G, Graeff C, Farber L, Gschaidmeier H, Buschauer A, Fricker G. Transport of paclitaxel (Taxol) across the blood-brain barrier in vitro and in vivo. *J Clin Invest*. 2002; 110(9):1309-18.

Fischer W, Muller E. Alkaline phosphatase in the choroid plexus and the leptomeninx of man. *Acta Biol Med Ger*. 1970; 25(5):905-13.

Fishman RA. 2000. Cerebrospinal Fluid in Diseases of the Nervous System. Ed. Saunders W B. Philadelphia, 1980.

Fletcher M, Kelly SP, Part P, O'Donnell MJ, Wood CM. Transport properties of cultured branchial epithelia from freshwater rainbow trout: a novel preparation with mitochondria-rich cells. *J Exp Biol*. 2000; 203 Pt 10:1523-37.

Food and Drug Administration (FDA). Biopharmaceutical Classification System: Guidance for Industry, 2000. URL: http://www.fda.gov/cder/guidance/3618fnl.pdf.

Frey T, Yue S, Haugland RP. Dyes providing increased sensitivity in flow-cytometric dye-efflux assays for multidrug resistance. *Cytometry*. 1995; 20(3):218-27.

Fujimaki S, Funato T, Harigae H, Fujiwara J, Kameoka J, Meguro K, Kaku M, Sasaki T. Quantitative analysis of a MDR1 transcript for prediction of drug resistance in acute leukemia. *Clin Chem*. 2002; 48(6 Pt 1):811-7.

Fujita T, Kishida T, Wada M, Okada N, Yamamoto A, Leibach FH, Ganapathy V. Functional characterization of brain peptide transporter in rat cerebral cortex: identification of the high-affinity type H+/peptide transporter PEPT2. *Brain Res*. 2004; 997(1):52-61.

Fukushima H, Fujimoto M, Ide M. Quantitative detection of blood-brain barrier-associated enzymes in cultured endothelial cells of porcine brain microvessels. *In Vitro Cell Dev Biol*. 1990; 26(6):612-20.

G

Gaillard PJ, de Boer AG. Relationship between permeability status of the blood-brain barrier and in vitro permeability coefficient of a drug. *Eur J Pharm Sci*. 2000; 12(2):95-102.

Ganapathy ME, Brandsch M, Prasad PD, Ganapathy V, and Leibach FH. Differential recognition of beta -lactam antibiotics by intestinal and renal peptide transporters, PEPT 1 and PEPT 2. *J Biol Chem*.1995; 270:25672-25677.

Ganapathy ME, Prasad PD, Mackenzie B, Ganapathy V, and Leibach FH. Interaction of anionic cephalosporins with the intestinal and renal peptide transporters PEPT 1 and PEPT 2. *Biochim Biophys Acta*. 1997; 1324: 296-308.

Ganapathy ME, Huang W, Wang H, Ganapathy V, and Leibach FH. Valacyclovir: a substrate for the intestinal and renal peptide transporters PEPT1 and PEPT2. *Biochem Biophys Res Commun*.1998; 246: 470-475.

Gao B, Meier PJ. Organic anion transport across the choroid plexus. *Microsc Res Tech*. 2001; 52(1):60-4.

Gao B, Stieger B, Noe B, Fritschy JM, Meier PJ. Localization of the organic anion transporting polypeptide 2 (Oatp2) in capillary endothelium and choroid plexus epithelium of rat brain. *J Histochem Cytochem*. 1999; 47(10):1255-64.

Gao B, Hagenbuch B, Kullak-Ublick GA, Benke D, Aguzzi A, Meier PJ. Organic anion-transporting polypeptides mediate transport of opioid peptides across blood-brain barrier. *J Pharmacol Exp Ther*. 2000; 294(1):73-9.

Garberg, P. In vitro models of the blood-brain barrier. *ATLA*. 1996; 26:821-847.

Gath U, Hakvoort A, Wegener J, Decker S, Galla HJ. Porcine choroid plexus cells in culture: expression of polarized phenotype, maintenance of barrier properties and apical secretion of CSF-components. *Eur J Cell Biol*. 1997; 74(1):68-78.

Gennuso F, Fernetti C, Tirolo C, Testa N, L'Episcopo F, Caniglia S, Morale MC, Ostrow JD, Pascolo L, Tiribelli C, Marchetti B. Bilirubin protects astrocytes from its own toxicity by inducing up-regulation and translocation of multidrug resistance-associated protein 1 (Mrp1). *Proc Natl Acad Sci USA*. 2004; 101(8):2470-5.

Ghersi-Egea JF, Leninger-Muller B, Suleman G, Siest G, Minn A. Localization of drug-metabolizing enzyme activities to blood-brain interfaces and circumventricular organs. *J Neurochem*. 1994; 62(3):1089-96.

Ghersi-Egea Jf, Strazielle N. Brain Drug Delivery, Drug Metabolism, and Multidrug Resistance at the Choroid Plexus. *Micro Res Tech*. 2001; 52:83–88 .

Golden PL, Pollack GM. Blood-brain barrier efflux transport. *J Pharm Sci*. 2003; 92(9):1739-53.

Goldmann, EE. Die äußere und innere Sekretion des gesunden und kranken Organismus im Lichte der vitalen Färbung. *Beitr. Klin. Chir*. 1909; 64**:**192-265.

Goodson HV, Hawse WF. Molecular evolution of the actin family. *J Cell Sci*. 2002; 115(Pt 13):2619-22.

Gorboulev V, Ulzheimer JC, Akhoundova A, Ulzheimer-Teuber I, Karbach U, Quester S, Baumann C, Lang F, Busch AE, Koepsell H. Cloning and characterization of two human polyspecific organic cation transporters. *DNA Cell Biol*. 1997; 16(7):871-81.

Graff CL, Pollack GM. Drug transport at the blood-brain barrier and the choroid plexus. *Curr Drug Metab*. 2004; 5(1):95-108.

Grebenkamper K, Galla HJ. Translational diffusion measurements of a fluorescent phospholipid between MDCK-I cells support the lipid model of the tight junctions. *Chem Phys Lipids*. 1994; 71(2):133-43.

Gumbleton M, Audus KL. Progress and limitations in the use of in vitro cell cultures to serve as a permeability screen for the blood-brain barrier. *J Pharm Sci*. 2001; 90(11):1681-98.

Gygi SP, Rochon Y, Franza BR, Aebersold R. Correlation between protein and mRNA abundance in yeast. *Mol Cell Biol*. 1999; 19(3):1720-30.

H

Haimeur A, Conseil G, Deeley RG, Cole SP. The MRP-related and BCRP/ABCG2 multidrug resistance proteins: biology, substrate specificity and regulation. *Curr Drug Metab*. 2004; 5(1):21-53.

Hakvoort A, Haselbach M, Galla HJ. Active transport properties of porcine choroid plexus cells in culture. *Brain Res*. 1998; 795:247-256.

Hakvoort A, Haselbach M, Wegener J, Hoheisel D, Galla HJ. The polarity of choroid plexus epithelial cells in vitro is improved in serum free medium. *J Neurochem*. 1998; 71(3):1141-1150.

Hansen DK, Scott DO, Otis KW, Lunte SM.Comparison of in vitro BBMEC permeability and in vivo CNS uptake by microdialysis sampling. *J Pharm Biomed Anal*. 2002; 27(6):945-58.

Harris MJ, Kuwano M, Webb M, Board PG. Identification of the apical membrane-targeting signal of the multidrug resistance-associated protein 2 (MRP2/MOAT). *J Biol Chem*. 2001; 276(24):20876-81.

Haselbach M, Wegener J, Decker S, Engelbertz C, Galla HJ. Porcine Choroid plexus epithelial cells in culture: regulation of barrier properties and transport processes. *Microsc Res Tech*. 2001; 52(1):137-52.

Hediger MA, Romero MF, Peng JB, Rolfs A, Takanaga H, Bruford EA. The ABCs of solute carriers: physiological, pathological and therapeutic implications of human membrane transport proteins. *Pflugers Arch*. 2004; 447(5):465-8.

Hegmann EJ, Bauer HC, Kerbel RS. Expression and functional activity of P-glycoprotein in cultured cerebral capillary endothelial cells. *Cancer Res*. 1992; 52(24):6969-75.

Hayashi K. Manipulation of DNA by PCR. PCR - the Polymerase chain reaction, 3-14. Eds. K.B. Mullis, F. Ferre & R.A. Gibbs, Birkhäuser, 1994.

Herbert J, Wilcox JN, Pham KT, Fremeau RT Jr, Zeviani M, Dwork A, Soprano DR, Makover A, Goodman DS, Zimmerman EA. Transthyretin: a choroid plexus-specific transport protein in human brain. *Neurology*. 1986; 36(7):900-11.

Higgins, C. ABC transporters from microorganisms to man. *Ann Rev Cell Biol*. 1992; 8:67-113.

Higuchi R, Fockler C, Dollinger G, Watson R. Kinetic PCR analysis: real-time monitoring of DNA amplification reactions. *Biotech*. 1993; 11:1026-1030.

Hilden SA, Johns CA, Guggino WB, Madias NE. Techniques for isolation of brush-border and basolateral membrane vesicles from dog kidney cortex. *Biochim Biophys Acta*. 1989; 983(1):77-81.

Hosoya K, Hori S, Ohtsuki S, Terasaki T. A new in vitro model for blood-cerebrospinal fluid barrier transport studies: an immortalized choroid plexus epithelial cell line derived from the tsA58 SV40 large T-antigen gene transgenic rat. *Adv Drug Deliv Rev*. 2004; 56(12):1875-85.

Hosoyamada M, Sekine T, Kanai Y Endou H. Molecular cloning and functional expression of a multispecific organic anion transporter from human kidney. *Am J Physiol Renal Physiol*. 1999; 276:F122-F128.

Hosta F. Enhancement of specifity and yield of PCR. *United States Biochemical Corp. Editorial comments*. 1993; 18(3):1-5.

Huber JD, Egleton RD, Davis, TP. Molecular physiology and pathophysiology of tight junctions in the blood-brain barrier. *Trends in Neuroscience*. 2001; 24(12):719-725.

I

Inada K. Localization of prealbumin in human eye. *Jpn J Ophthalmol*. 1988; 32(4):438-43.

Innis MA, Gelfand DH. Optimization of PCRs. PCR Protocols: A guide to methods and applications, 3-11, Academic press, 1991.

Inui KI, Masuda S, Saito H. Cellular and molecular aspects of drug transport in the kidney. *Kidney Int*. 2000; 58(3):944-58.

J

Janshoff A, Wegener J, Steinem C, Sieber M, Galla HJ. Applications of impedance spectroscopy in biochemistry and biophysics. *Acta Biochim Pol*. 1996; 43(2):339-48.

Jariyawat S, Sekine T, Takeda M, Apiwattanakul N, Kanai Y, Sophasan S, Endou H. The interaction and transport of beta-lactam antibiotics with the cloned rat renal organic anion transporter 1. *J Pharmacol Exp Ther*. 1999; 290(2):672-7.

Jegou B. The Sertoli cell in vivo and in vitro. *Cell Biol Toxicol*. 1992; 8(3):49-54.

Johanson CE. Neuroscience in Medicine. Ventrikels and Cerebrospinal Fluid. Ed, Conn M. Philadelphia, J.B: Lipincott Company, 1995.

Johanson CE. Arachnoid membrane, subarachnoid CSF and pia-glia. From: WM Pardrige. Introduction to the Blood-Brain Barrier. Methodology, biology and pathology. Cambridge University Press, 1998.

Johanson CE, Preston JE, Chodobski A, Stopa EG, Szmydynger-Chodobska J, McMillan PN. AVP V1 receptor-mediated decrease in Cl. *Am J Physiol* . 1999; 276(1 Pt 1):C82-90.

Johnson JA, el Barbary A, Kornguth SE, Brugge JF, Siegel FL. Glutathione S-transferase isoenzymes in rat brain neurons and glia. *J Neurosci*. 1993; 13(5):2013-23.

Johnson MD, Anderson BD. In vitro models of the blood-brain barrier to polar permeants: comparison of transmonolayer flux measurements and cell uptake kinetics using cultured cerebral capillary endothelial cells. *J Pharm Sci*. 1999; 88(6):620-5.

Johnson WW. P-glycoprotein-mediated efflux as a major factor in the variance of absorption and distribution of drugs: modulation of chemotherapy resistance. *Methods Find Exp Clin Pharmacol*. 2002; 24(8):501-14.

K

Keep RF, Jones HC. A morphometric study on the development of the lateral ventricle choroid plexus, choroid plexus capillaries and ventricular ependyma in the rat. *Brain Res Dev Brain Res*. 1990; 56(1):47-53.

Keep RF, Xiang J, Betz AL. Potassium cotransport at the rat choroid plexus. *Am J Physiol*. 1994; 267(6 Pt 1):C1616-22.

Kemper EM, van Zandbergen AE, Cleypool C, Mos HA, Boogerd W, Beijnen JH, van Tellingen O. Increased penetration of paclitaxel into the brain by inhibition of P-Glycoprotein. *Clin Cancer Res*. 2003; 9(7):2849-55.

Kemper EM, Verheij M, Boogerd W, Beijnen JH, van Tellingen O. Improved penetration of docetaxel into the brain by co-administration of inhibitors of P-glycoprotein. *Eur J Cancer*. 2004; 40(8):1269-74.

Kim DH, Iijima H, Goto K, Sakai J, Ishii H, Kim HJ, Suzuki H, Kondo H, Saeki S, Yamamoto T. Human apolipoprotein E receptor 2. A novel lipoprotein receptor of the low density lipoprotein receptor family predominantly expressed in brain. *J Biol Chem*. 1996; 271(14):8373-80.

Kimura Y, Matsuo M, Takahashi K, Saeki T, Kioka N, Amachi T, Ueda K. ATP hydrolysis-dependent multidrug efflux transporter: MDR1/P-glycoprotein. *Curr Drug Metab*. 2004; 5(1):1-10.

Kniesel U, Reichenbach A, Risau W, Wolburg H. Quantification of tight junction complexity by means of fractal analysis. *Tissue Cell*. 1994; 26(6):901-12.

Kobayashi H, Minami S, Itoh S, Shiraishi S, Yokoo H, Yanagita T, Uezono Y, Mohri M, Wada A. Aquaporin subtypes in rat cerebral microvessels. *Neurosci Lett*. 2001; 297:163–166.

Kobayashi Y, Ohshiro N, Tsuchiya A, Kohyama N, Ohbayashi M, Yamamoto T. Renal transport of organic compounds mediated by mouse organic anion transporter 3 (mOat3): further substrate specificity of mOat3. *Drug Metab Dispos*. 2004; 32(5):479-83.

Konig J, Cui Y, Nies AT, Keppler D. A novel human organic anion transporting polypeptide localized to the basolateral hepatocyte membrane. *Am J Physiol Gastrointest Liver Physiol*. 2000; 278(1):G156-64.

Koepsell H. Organic cation transporters in intestine, kidney, liver and brain. *Annu Rev Physiol*. 1998; 60:243-66.

Koepsell H, Schmitt BM, Gorboulev V. Organic cation transporters. *Rev Physiol Biochem Pharmacol*. 2003; 150:36-90.

Koepsell H, Endou H. The SLC22 drug transporter family. *Pflugers Arch*. 2004; 447(5):666-76.

Koh AS, Simmons-Willis TA, Pritchard JB, Grassl SM, Ballatori N. Identification of a mechanism by which the methylmercury antidotes N-acetylcysteine and dimercaptopropanesulfonate enhance urinary metal excretion: transport by the renal organic anion transporter-1. *Mol Pharmacol*. 2002; 62(4):921-6.

Kohzuki M, Chai SY, Paxinos G, Karavas A, Casley DJ, Johnston CI, Mendelsohn FA. Localization and characterization of endothelin receptor binding sites in the rat brain visualized by in vitro autoradiography. *Neuroscience*. 1991; 42(1):245-60.

Konno T, Ebihara T, Hisaeda K, Uchiumi T, Nakamura T, Shirakusa T, Kuwano M, Wada M. Identification of domains participating in the substrate specificity and subcellular localization of the multidrug resistance proteins MRP1 and MRP2. *J Biol Chem*. 2003; 278(25):22908-17.

Kreuzer KA, Lass U, Landt O, Nitsche A, Laser J, Ellerbrok H, Pauli G, Huhn D, Schmidt CA. Highly sensitive and specific fluorescence reverse transcription-PCR assay for the pseudogene-free detection of beta-actin transcripts as quantitative reference. *Clin Chem*. 1999; 45:297-300.

Kruh GD, Belinsky MG. The MRP family of drug efflux pumps. *Oncogene*. 2003; 22(47):7537-52.

Kusuhara H, Suzuki H, Terasaki T, Kakee A, Lemaire M, Sugiyama Y. P-Glycoprotein mediates the efflux of quinidine across the blood-brain barrier. *J Pharmacol Exp Ther*. 1997; 283(2):574-80.

Kusuhara H, Han YH, Shimoda M, Kokue E, Suzuki H, and Sugiyama Y. Reduced folate derivatives are endogenous substrates for cMOAT in rats. *Am J Physiol Gastrointest Liver Physiol*. 1998; 275:G789-G796.

Kusuhara H, Suzuki H, Sugiyama Y. The role of P-glycoprotein and canalicular multispecific organic anion transporter in the hepatobiliary excretion of drugs. *J Pharm Sci*. 1998; 87(9):1025-40.

Kusuhara H, Sekine T, Utsunomiya-Tate N, Tsuda M, Kojima R, Cha SH, Sugiyama Y, Kanai Y, Endou H. Molecular cloning and characterization of a new multispecific organic anion transporter from rat brain. *J Biol Chem*. 1999; 274(19):13675-80.

Kusuhara H, Sugiyama Y. Efflux transport systems for drugs at the blood-brain barrier and blood-cerebrospinal fluid barrier (Part 2). *Drug Discov Today*. 2001; 6(4):206-212.

L

Lauer R, Bauer R, Linz B, Pittner F, Peschek GA, Ecker G, Friedl P, Noe CR. Development of an in vitro blood-brain barrier model based on immortalized porcine brain microvascular endothelial cells. *Farmaco*. 2004; 59(2):133-7.

Lee G, Dallas S, Hong M, Bendayan R. Drug transporters in the central nervous system: brain barriers and brain parenchyma considerations. *Pharmacol Rev*. 2001; 53(4):569-96.

Lee MD, King LS, Agre P. The aquaporin family of water channel proteins in clinical medicine. *Medicine (Baltimore)*. 1997; 76(3):141-56.

Leggas M, Adachi M, Scheffer GL, Sun D, Wielinga P, Du G, Mercer KE, Zhuang Y, Panetta JC, Johnston B, Scheper RJ, Stewart CF, Schuetz JD. Mrp4 confers resistance to topotecan and protects the brain from chemotherapy. *Mol Cell Biol*. 2004; 24(17):7612-21.

Leininger-Muller B, Ghersi-Egea JF, Siest G, Minn A. Induction and immunological characterization of the uridine diphosphate-glucuronosyltransferase conjugating 1-naphthol in the rat choroid plexus. *Neurosci Lett*. 1994; 175(1-2):37-40.

Levin, VA. Relationship of octanol/water partition coefficient and molecular weight to rat brain capillary permeability. *J. Med. Chem.* 1980, 23: 682–684.

Lewandowsky, M. Zur Lehre von der Cerebrospinalflüssigkeit. *Z Klein Med*. 1900; 40:480-94.

Lin TH, Lin JH. Effects of protein binding and experimental disease states on brain uptake of benzodiazepines in rats. *J Pharmacol Exp Ther*. 1990; 253(1):45-50.

Lippoldt A, Jansson A, Kniesel U, Andbjer B, Andersson A, Wolburg H, Fuxe K, Haller H. Phorbol ester induced changes in tight and adherens junctions in the choroid plexus epithelium and in the ependyma. *Brain Res*. 2000; 854(1-2):197-206.

Lippoldt A, Liebner S, Andbjer B, Kalbacher H, Wolburg H, Haller H, Fuxe K. Organization of choroid plexus epithelial and endothelial cell tight junctions and regulation of claudin-1, -2 and -5 expression by protein kinase C. *Neuroreport*. 2000; 11(7):1427-31.

Ljubojevic M, Herak-Kramberger CM, Hagos Y, Bahn A, Endou H, Burckhardt G, Sabolic I. Rat renal cortical OAT1 and OAT3 exhibit gender differences determined by both androgen stimulation and estrogen inhibition. *Am J Physiol Renal Physiol*. 2004; 287(1):F124-38.

Loew I, Wieland T. The interaction of phalloidin, some of its derivatives, and other cyclic peptides with muscle actin as studied by viscometry. *FEBS letters*. 1974; 44:340-343.

Lohmann C, Huwel S, Galla HJ. Predicting blood-brain barrier permeability of drugs: evaluation of different in vitro assays. *J Drug Target*. 2002; 10(4):263-76.

Lorico A, Rappa G, Flavell RA, Sartorelli AC. Double knockout of the MRP gene leads to increased drug sensitivity in vitro. *Cancer Res*. 1996; 56(23):5351-5.

Louvard D. Polarity of epithelial cells. Role of the actin microfilament system Nephrologie. *Nephrologie*. 1996; 17(7):351-7.

Low SH, Miura M, Roche PA, Valdez AC, Mostov KE, Weimbs T. Intracellular redirection of plasma membrane trafficking after loss of epithelial cell polarity. *Mol Biol Cell*. 2000; 11(9):3045-60.

Lowndes HE, Beiswanger CM, Philbert MA, Reuhl KR. Substrates for neural metabolism of xenobiotics in adult and developing brain. *Neurotoxicology*. 1994; 15(1):61-73.

Lu R, Chan BS, and Schuster VL. Cloning of the human kidney PAH transporter: narrow substrate specificity and regulation by protein kinase C. *Am J Physiol Renal Physiol*. 1999; 276:F295-F303.

Lundquist S, Renftel M, Brillault J, Fenart L, Cecchelli R, Dehouck MP. Prediction of drug transport through the blood-brain barrier in vivo: a comparison between two in vitro cell models. *Pharm Res*. 2002; 19(7):976-81.

M

Mahmood B, Daood MJ, Hart C, Hansen TW, Watchko JF. Ontogeny of P-glycoprotein in mouse intestine, liver, and kidney. *J Investig Med*. 2001; 49(3):250-7.

Maness LM, Kastin AJ, Farrell CL, Banks WA. Fate of leptin after intracerebroventricular injection into the mouse brain. *Endocrinology*. 1998; 139(11):4556-62.

Marrs JA, Napolitano EW, Murphy-Erdosh C, Mays RW, Reichardt LF, Nelson WJ. Distinguishing roles of the membrane-cytoskeleton and cadherin mediated cell-cell adhesion in generating different Na+,K(+)-ATPase distributions in polarized epithelia. *J Cell Biol*. 1993; 123(1):149-64.

Martinasevic MK, King CD, Rios GR, Tephly TR. Immunohistochemical localization of UDP-glucuronosyltransferases in rat brain during early development. *Drug Metab Dispos*. 1998; 26(10):1039-41.

Marzolini C, Paus E, Buclin T, Kim RB. Polymorphisms in human MDR1 (P-glycoprotein): recent advances and clinical relevance. *Clin Pharmacol Ther*. 2004; 75(1):13-33.

Masseguin C, Corcoran M, Carcenac C, Daunton NG, Guell A, Verkman AS, Gabrion J. Altered gravity downregulates aquaporin-1 protein expression in choroid plexus. *J Appl Physiol*. 2000; 88:843–850.

Masungi C, Borremans C, Willems B, Mensch J, Dijck AV, Augustijns P, Brewster ME, Noppe M. Usefulness of a novel Caco-2 cell perfusion system in in vitro prediction of the absorption potential of passively diffused compounds. *J Pharm Sci*. 2004; 93(10):2507-21.

Masuzawa T, Ohta T, Kawamura M, Nakahara N, Sato F. Immunohistochemical localization of Na+, K+-ATPase in the choroid plexus. *Brain Res*. 1984; 302(2):357-62.

Mauchamp J, Chambard M, Verrier B, Gabrion J, Chabaud O, Gerard C, Penel C, Pialat B, Anfosso F. Epithelial cell polarization in culture: orientation of cell polarity and expression of specific functions, studied with cultured thyroid cells. *J Cell Sci Suppl*. 1987; 8:345-58.

Mealey KL. Therapeutic implications of the MDR-1 gene. *J Vet Pharmacol Ther*. 2004; 27(5):257-64.

Meier PJ, Eckhardt U, Schroeder A, Hagenbuch B, Stieger B. Substrate specificity of sinusoidal bile acid and organic anion uptake systems in rat and human liver. *Hepatology*. 1997;26(6):1667-77.

Meyer J, Mischeck U, Veyhl M, Henzel K, Galla HJ. Blood-brain barrier characteristic enzymatic properties in cultured brain capillary endothelial cells. *Brain Res*. 1990; 514(2):305-9.

Meyer J, Rauh J, Galla HJ. The susceptibility of cerebral endothelial cells to astroglial induction of blood-brain barrier enzymes depends on their proliferative state. *J Neurochem*. 1991; 57(6):1971-7.

Miller DS, Nobmann SN, Gutmann H, Toeroek M, Drewe J, Fricker G. Xenobiotic transport across isolated brain microvessels studied by confocal microscopy. *Mol Pharmacol*. 2000; 58(6):1357-67.

Miller D, Lowes S and Pritchard ,JB. The molecular basis of xenobiotic transport and metabolism in choroid plexus. In: The Blood-Cerebrospinal Fluid Barrier. Eds., Zhang W, Chodobski A. In press.

Mitic LL, Van Itallie CM, Anderson JM. Molecular physiology and pathophysiology of tight junctions I. Tight junction structure and function: lessons from mutant animals and proteins. *Am J Physiol Gastrointest Liver Physiol*. 2000; 279(2):G250-4.

Mobasheri A, Marples D. Expression of the AQP-1 water channel in normal human tissues: a semiquantitative study using tissue microarray technology.*Am J Physiol Cell Physiol*. 2004; 286(3):C529-37.

Molecular Probes. URL: http://www.probes.com. 2004.

Moller W, Kummer W. The blood-brain barrier of the chick glycogen body (corpus gelatinosum) and its functional implications. *Cell Tissue Res*. 2003; 313(1):71-80.

Mollgard K, Rostgaard J . Morphological aspects of some sodium transporting epithelia suggesting a transcellular pathway via elements of endoplasmic reticulum. *J Membr Biol*. 1978; 40:71-89.

Monro OR, Mackic JB, Yamada S, Segal MB, Ghiso J, Maurer C, Calero M, Frangione B, Zlokovic BV. Substitution at codon 22 reduces clearance of Alzheimer's amyloid-beta peptide from the cerebrospinal fluid and prevents its transport from the central nervous system into blood. *Neurobiol Aging*. 2002; 23(3):405-12.

Morin XK, Bond TD, Loo TW, Clarke DM, Bear CE. Failure of P-glycoprotein (MDR1) expressed in Xenopus oocytes to produce swelling-activated chloride channel activity. *J Physiol*. 1995; 486 (Pt 3):707-14.

Morse DC, Stein AP, Thomas PE, Lowndes HE. Distribution and induction of cytochrome P450 1A1 and 1A2 in rat brain. *Toxicol Appl Pharmacol*. 1998; 152(1):232-9.

Mostov K, Su T, ter Beest M. Polarized epithelial membrane traffic: conservation and plasticity. *Nat Cell Biol*. 2003; 5(4):287-93.

Motohashi H, Sakurai Y, Saito H, Masuda S, Urakami Y, Goto M, Fukatsu A, Ogawa O, Inui K. Gene expression levels and immunolocalization of organic ion transporters in the human kidney. *J Am Soc Nephrol*. 2002; 13(4):866-74.

Mukherjee T, Squillantea E, Gillespieb M, Shao J. Transepithelial electrical resistance is not a reliable measurement of the Caco-2 monolayer integrity in Transwell. *Drug Deliv*. 2004; 11(1):11-8.

Muller M, Jansen PL. Molecular aspects of hepatobiliary transport. *Am J Physiol*. 1997; 272(6 Pt 1):G1285-303.

Murata M, Tamai I, Kato H, Nagata O, Tsuji A. Efflux transport of a new quinolone antibacterial agent, HSR-903, across the blood-brain barrier. *J Pharmacol Exp Ther*. 1999; 290(1):51-7.

Muruganandam A, Herx LM, Monette R, Durkin JP, Stanimirovic DB. Development of immortalized human cerebromicrovascular endothelial cell line as an in vitro model of the human blood-brain barrier. *FASEB J*. 1997; 11(13):1187-97.

N

Nag S. Effect of atrial natriuretic factor on permeability of the blood-cerebrospinal fluid barrier. *Acta Neuropathol*. 1991; 82(4):274-9.

Nagata Y, Kusuhara H, Endou H, Sugiyama Y. Expression and functional characterization of rat organic anion transporter 3 (rOat3) in the choroid plexus. *Mol Pharmacol*. 2002; 61(5):982-8.

Nagata Y, Kusuhara H, Imaoka T, Endou H, Sugiyama Y. Involvement of rat organic anion transporter 3 in the uptake of an organic herbicide, 2,4-dichlorophenoxyacetate, by the isolated rat choroid plexus. *J Pharm Sci*. 2004; 93(11):2724-2732.

Nare B, Prichard RK, Georges E. Characterization of rhodamine 123 binding to P-glycoprotein in human multidrug-resistant cells. *Mol Pharmacol*. 1994; 45(6):1145-52.

Narisawa S, Hasegawa H, Watanabe K, Millan JL. Stage-specific expression of alkaline phosphatase during neural development in the mouse. *Dev Dyn*. 1994; 201(3):227-35.

National Institute of Health. URL: http://www.nhgri.nih.gov. NIH News Release. 2004.

Neumann J, Bruch M, Gebauer S, Brandsch M. Transport of the phosphonodipeptide alafosfalin by the H+/peptide cotransporters PEPT1 and PEPT2 in intestinal and renal epithelial cells. *Eur J Biochem*. 2004; 271(10):2012-7.

Nielsen S, Smith BL, Christensen EI, Agre P. Distribution of the aquaporin CHIP in secretory and resorptive epithelia and capillary endothelia. *Proc Natl Acad Sci USA*. 1993; 90(15):7275-9.

Nies AT, Jedlitschky G, Konig J, Herold-Mende C, Steiner HH, Schmitt HP, Keppler D. Expression and immunolocalization of the multidrug resistance proteins, MRP1-MRP6 (ABCC1-ABCC6), in human brain. *Neuroscience*. 2004; 129(2):349-60.

Nies AT, Konig J, Cui Y, Brom M, Spring H, Keppler D. Structural requirements for the apical sorting of human multidrug resistance protein 2 (ABCC2). *Eur J Biochem*. 2002; 269(7):1866-76.

Nilsson C, Lindvall-Alexsson M, Owman C. Neuroendocrine regulatory mechanisms in the choroid plexus-cerebrospinal fluid system. *Brain Res Rev*. 1992; 17:109-38.

Nishino J, Suzuki H, Sugiyama D, Kitazawa T, Ito K, Hanano M, Sugiyama Y. Transepithelial transport of organic anions across the choroid plexus: possible involvement of organic anion transporter and multidrug resistance-associated protein. *J Pharmacol Exp Ther*. 1999; 290(1):289-94.

Nitz T, Eisenblatter T, Psathaki K, Galla HJ. Serum-derived factors weaken the barrier properties of cultured porcine brain capillary endothelial cells in vitro. *Brain Res*. 2003; 981(1-2):30-40.

Ng WF, Sarangi F, Zastawny RL, Veinot-Drebot L, Ling V. Identification of members of the P-glycoprotein multigene family. *Mol Cell Biol*. 1989; 9(3):1224-32.

Nooter K, Stoter G. Molecular mechanisms of multidrug resistance in cancer chemotherapy. *Pathol Res Pract*. 1996; 192(7):768-80.

O

Ocheltree SM, Shen H, Hu Y, Xiang J, Keep RF, Smith DE. Mechanisms of cefadroxil uptake in the choroid plexus: studies in wild-type and PEPT2 knockout mice. *J Pharmacol Exp Ther*. 2004; 308(2):462-7.

Ocheltree SM, Shen H, Hu Y, Xiang J, Keep RF, Smith DE. Role of PEPT2 in the choroid plexus uptake of glycylsarcosine and 5-aminolevulinic acid: studies in wild-type and null mice. *Pharm Res*. 2004; 21(9):1680-5.

Ogawa M, Shiozawa M, Hiraoka Y, Takeuchi Y, Aiso S. Immunohistochemical study of localization of gamma-glutamyl transpeptidase in the rat brain. *Tissue Cell*. 1998; 30(6):597-601.

Ogawa M, Shiozawa M, Hiraoka Y, Takeuchi Y, Aiso S. Immunohistochemical study of localization of gamma-glutamyl transpeptidase in the rat brain. *Tissue Cell*. 1998; 30(6):597-601.

Ohtsuki S, Takizawa T, Takanaga H, Terasaki N, Kitazawa T, Sasaki M, Abe T, Hosoya K, Terasaki T. In vitro study of the functional expression of organic anion transporting polypeptide 3 at rat choroid plexus epithelial cells and its involvement in the cerebrospinal fluid-to-blood transport of estrone-3-sulfate. *Mol Pharmacol*. 2003; 63(3):532-7.

Ohtsuki S, Takizawa T, Takanaga H, Hori S, Hosoya K, Terasaki T. Localization of organic anion transporting polypeptide 3 (oatp3) in mouse brain parenchymal and capillary endothelial cells. *J Neurochem*. 2004; 90(3):743-9.

Ohtsuki S. New aspects of the blood-brain barrier transporters; its physiological roles in the central nervous system. *Biol Pharm Bull*. 2004; 27(10):1489-96.

Omidi Y, Campbell L, Barar J, Connell D, Akhtar S, Gumbleton M. Evaluation of the immortalised mouse brain capillary endothelial cell line, bEnd3, as an in vitro blood-brain barrier model for drug uptake and transport studies. *Brain Res*. 2003; 990(1-2):95-112.

Oshio K, Song Y, Verkman AS, Manley GT. Aquaporin-1 deletion reduces osmotic water permeability and cerebrospinal fluid production. *Acta Neurochir Suppl*. 2003; 86:525-8.

Otieno MA, Baggs RB, Hayes JD, Anders MW. Immunolocalization of microsomal glutathione S-transferase in rat tissues. *Drug Metab Dispos*. 1997; 25(1):12-20.

Oude Elferink RP, Meijer DK, Kuipers F, Jansen PL, Groen AK, Groothuis GM. Hepatobiliary secretion of organic compounds; molecular mechanisms of membrane transport. *Biochim Biophys Acta*. 1995; 1241(2):215-68.

P

Pade V, Stavchansky S. Link between drug absorption solubility and permeability measurements in Caco-2 cells. *J Pharm Sci*. 1998; 87(12):1604-7.

Pansky B, Hatfield JS. Cerebral localization of insulin by immunofluorescence. *Am J Anat*. 1978; 153(3):459-67.

Pappenheimer JR, Heisey SR, Jordan EF. Active transport of Diodrast and phenolsulfonphthalein from cerebrospinal fluid to blood. *Am J Physiol*. 1961 Jan;200:1-10.

Pardridge WM, Frank HJL, Cornford EM, Braun LD, Crane PD and Oldendorf WH. Neuropeptides and the blood-brain barrier. Eds.: Martin JB, Reichlin S and Bick KL. Neurosecretion and brain peptides. Raven Press, New York, 1981.

Pardridge WM, Triguero D, Yang J, Cancilla PA. Comparison of in vitro and in vivo models of drug transcytosis through the blood-brain barrier. *J Pharmacol Exp Ther*. 1990; 253(2):884-91.

Pardridge WM, Triguero D, Yang J, Cancilla PA. Comparison of in vitro and in vivo models of drug transcytosis through the blood-brain barrier. *J Pharmacol Exp Ther*. 1990; 253(2):884-91.

Pardridge WM. Blood-Brain Barrier: Cellular and Molecular Biology. Lippincott Williams & Wilkins, 1993.

Pardridge WM. Blood-brain barrier biology and methodology. *J Neurovirol*. 1999; 5(6):556-69.

Persing DH. Target selection and optimization of amplification reaction. Diagnostic molecular microbiology, 88-102. Eds.: Persing DH, Smith TF, Tenover FC, White TJ, ASM, 1993.

Pleban K, Kopp S, Csaszar E, Peer M, Hrebicek T, Rizzi A, Ecker GF, Chiba P. P-glycoprotein substrate binding domains are located at the transmembrane domain : transmembrane domain interfaces - A combined photoaffinity labeling - protein homology modeling approach. *Mol Pharmacol*. 2004; Epub ahead of print.

Pritchard JB and Miller DS. Mechanisms mediating renal secretion of organic anions and cations. *Physiol Rev*. 1993; 73(4):765-96.

Pritchard JB, Sweet DH, Miller DS, Walden R. Mechanism of organic anion transport across the apical membrane of choroid plexus. *J Biol Chem*. 1999; 274(47):33382-7.

Pulaski L, Jedlitschky G, Leier I, Buchholz U, and Keppler D. Identification of the multidrug-resistance protein (MRP) as the glutathione-*S*-conjugate export pump of erythrocytes. *Eur J Biochem*. 1996; 241: 644-648.

R

Rabito CA, Kreisberg JI, Wight D. Alkaline phosphatase and gamma-glutamyl transpeptidase as polarization markers during the organization of LLC-PK1 cells into an epithelial membrane .*J Biol Chem* . 1984; 259(1):574-582.

Ramsohoye PV, Fritz IB. Preliminary characterization of glial-secreted factors responsible for the induction of high electrical resistances across endothelial monolayers in a blood-brain barrier model. *Neurochem Res*. 1998; 23(12):1545-51.

Rao VV, Dahlheimer JL, Bardgett ME, Snyder AZ, Finch RA, Sartorelli AC, Piwnica-Worms D. Choroid plexus epithelial expression of MDR1 P glycoprotein and multidrug resistance-associated protein contribute to the blood-cerebrospinal-fluid drug-permeability barrier. *Proc Natl Acad Sci USA*. 1999; 96(7):3900-5.

Regina A, Koman A, Piciotti M, El Hafny B, Center MS, Bergmann R, Couraud PO, Roux F. Mrp1 multidrug resistance-associated protein and P-glycoprotein expression in rat brain microvessel endothelial cells. *J Neurochem*. 1998; 71(2):705-15.

Reinhardt RR, Bondy CA. Insulin-like growth factors cross the blood-brain barrier. *Endocrinology*. 1994; 135(5):1753-61.

Renes J, de Vries EG, Jansen PL, Muller M. The (patho)physiological functions of the MRP family. *Drug Resist Updat*. 2000; 3(5):289-302.

Richert ND, Aldwin L, Nitecki D, Gottesman MM, Pastan I. Stability and covalent modification of P-glycoprotein in multidrug-resistant KB cells. *Biochemistry*. 1988; 27(20):7607-13.

Risau W, Esser S, Engelhardt B. Differentiation of blood-brain barrier endothelial cells. *Pathol Biol (Paris)*. 1998; 46(3):171-5.

Robbins J. Transthyretin from discovery to now. *Clin Chem Lab Med*. 2002; 40(12):1183-90.

Rodriguez OC, Schaefer AW, Mandato CA, Forscher P, Bement WM, Waterman-Storer CM.Conserved microtubule-actin interactions in cell movement and morphogenesis. *Nat Cell Biol*. 2003; 5(7):599-609.

Rodriguez-Boulan E, Nelson WJ. Morphogenesis of the polarized epithelial cell phenotype. *Science*. 1989; 245(4919):718-25.

Rolfs A, Schuller I, Finckh U, Weber-Rolfs I. Physical features of thermocyclers and their influence on the efficiency of PCR amplification, 259-262. PCR: Clinical diagnostics and research, Springer, 1992.

S

Saiki RK, Scharf SJ, Faloona F, Mullis KB, Horn GT, Erlich HA, Arnheim, N. Enzymatic amplification of ß-globin genomic sequences and restriction site analysis for diagnosis of sickle cell anemia. *Proc Natl Acad Sci USA*. 1985; 230:1350-1354.

Saito T, Zhang ZJ, Tokuriki M, Ohtsubo T, Noda I, Shibamori Y, Yamamoto T, Saito H. Expression of multidrug resistance protein 1 (MRP1) in the rat cochlea with special reference to the blood-inner ear barrier. *Brain Res*. 2001; 895(1-2):253-7.

Saito Y, Wright EM. Bicarbonate transport across the frog choroid plexus and its control by cyclic nucleotides. *J Physiol*. 1983; 336:635-48.

Sambrook J, Fritsch EF and Maniatis T. Molecular cloning. A laboratory manual. 2nd Edition, Cold Spring Harbor Laboratory Press, 1989.

Saunders NR, Habgood MD, Dziegielewska KM. Barrier mechanisms in the brain. Adult brain. *Clin Pharm Phys*. 1999; 26:9-11.

Sawada K, Terada T, Saito H, Hashimoto Y, Inui K.Effects of glibenclamide on glycylsarcosine transport by the rat peptide transporters PEPT1 and PEPT2. *Br J Pharmacol*. 1999;128(6):1159-64.

Schielke GP, Betz AL. Electrolyte transport. M. W. B. Bradbury (ed.), Physiology and Pharmacology of the Blood-Brain Barrier. Heidelberg: Springer-Verlag, 1992.

Scheffer GL, Kool M, Heijn M, de Haas M, Pijnenborg AC, Wijnholds J, van Helvoort A, de Jong MC, Hooijberg JH, Mol CA, van der Linden M, de Vree JM, van der Valk P, Elferink RP, Borst P, Scheper RJ. Specific detection of multidrug resistance proteins MRP1, MRP2, MRP3, MRP5, and MDR3 P-glycoprotein with a panel of monoclonal antibodies. *Cancer Res*. 2000; 60(18):5269-77.

Schinkel AH, Roelofs EM, Borst P. Characterization of the human MDR3 P-glycoprotein and its recognition by P-glycoprotein-specific monoclonal antibodies. *Cancer Res*. 1991; 51(10):2628-35.

Schinkel AH, Mayer U, Wagenaar E, Mol CA, van Deemter L, Smit JJ, van der Valk MA, Voordouw AC, Spits H, van Tellingen O, Zijlmans JM, Fibbe WE, Borst P. Nor-

mal viability and altered pharmacokinetics in mice lacking mdr1-type (drug-transporting) P-glycoproteins. *Proc Natl Acad Sci USA*. 1997; 94(8):4028-33.

Schinkel AH. P-Glycoprotein, a gatekeeper in the blood-brain barrier. *Adv Drug Deliv Rev*. 1999; 36(2-3):179-194.

Schinkel AH, Jonker JW. Mammalian drug efflux transporters of the ATP binding cassette (ABC) family: an overview. *Adv Drug Deliv Rev*. 2003; 55(1):3-29.

Schlosshauer B. The blood-brain barrier: morphology, molecules, and neurothelin. *Bioessays*. 1993; 15(5):341-6.

Schonenberger M, Schultze He, Schwick G. A prealbumin of human serum. *Biochem Z*. 1956; 328(4):267-84.

Schreiber G, Aldred AR, Jaworowski A, Nilsson C, Achen MG, Segal MB. Thyroxine transport from blood to brain via transthyretin synthesis in choroid plexus. *Am J Physiol*. 1990; 258(2 Pt 2):R338-45.

Segal MB. The choroid plexuses and the barriers between the blood and the cerebrospinal fluid. *Cell Mol Neuro*. 2000; 20(2):183-96.

Segal MB, Burgess AM. A combined physiological and morphological study of the secretory process in the rabbit choroid plexus. *J Cell Sci*. 1974; 14(2):339-50.

Sekine T, Watanabe N, Hosoyamada M, Kanai Y, Endou H. Expression cloning and characterization of a novel multispecific organic anion transporter. *J Biol Chem*. 1997; 272(30):18526-9.

Sekine T, Cha SH, Endou H. The multispecific organic anion transporter (OAT) family. *Pflugers Arch*. 2000; 440(3):337-50.

Sessa G, Orlowski M, Green JP. Isolation from bovine brain of a fraction containing capillaries and a fraction containing membrane fragments of the choroid plexus. *J Neurobiol*. 1976; 7(1):51-61.

Shen H, Smith DE, Keep RF, Xiang J, Brosius FC 3rd. Targeted disruption of the PEPT2 gene markedly reduces dipeptide uptake in choroid plexus. *J Biol Chem*. 2003; 278(7):4786-91.

Shine HD, Haber B. Immunocytochemical localization of gamma-glutamyl transpeptidase in the rat CNS. *Brain Res*. 1981; 217(2):339-49.

Shu C, Shen H, Teuscher NS, Lorenzi PJ, Keep RF, Smith DE. Role of PEPT2 in peptide/mimetic trafficking at the blood-cerebrospinal fluid barrier: studies in rat choroid plexus epithelial cells in primary culture. *J Pharmacol Exp Ther*. 2002; 301(3):820-9.

Smit JJ, Schinkel AH, Oude Elferink RP, Groen AK, Wagenaar E, van Deemter L, Mol CA, Ottenhoff R, van der Lugt NM, van Roon MA, et al. Homozygous disruption of the murine mdr2 P-glycoprotein gene leads to a complete absence of phospholipid from bile and to liver disease. *Cell*. 1993; 75(3):451-62.

Smit JW, Schinkel AH, Weert B, Meijer DK. Hepatobiliary and intestinal clearance of amphiphilic cationic drugs in mice in which both mdr1a and mdr1b genes have been disrupted. *Br J Pharmacol*. 1998; 124(2):416-24.

Smith DE, Johanson CE, Keep RF. Peptide and peptide analog transport systems at the blood-CSF barrier. *Adv Drug Deliv Rev*. 2004; 56(12):1765-91.

Smith QR, Rapoport SI. Cerebrovascular permeability coefficients to sodium, potassium, and chloride. *J Neurochem*. 1986; 46(6):1732-42.

Soodvilai S, Chatsudthipong V, Evans KK, Wright SH, Dantzler WH. Acute regulation of OAT3-mediated estrone sulfate transport in isolated rabbit renal proximal tubules. *Am J Physiol Renal Physiol*. 2004; 287(5):F1021-9.

Southwell BR, Duan W, Alcorn D, Brack C, Richardson SJ, Kohrle J, Schreiber G. Thyroxine transport to the brain: role of protein synthesis by the choroid plexus. *Endocrinology*. 1993; 133(5):2116-26.

Speake T, Freeman LJ, Brown PD. Expression of aquaporin 1 and aquaporin 4 water channels in rat choroid plexus. *Biochim Biophys Acta*. 2003; 1609(1):80-6.

Speake T, Whitwell C, Kajita H, Majid A, Brown PD. Mechanisms of CSF Secretion by the Choroid Plexus. *Microsc Res Tech*. 2001; 52:49–59.

Stauder AJ, Dickson PW, Aldred AR, Schreiber G, Mendelsohn FA, Hudson P. Synthesis of transthyretin (pre-albumin) mRNA in choroid plexus epithelial cells, localized by in situ hybridization in rat brain. *J Histochem Cytochem*. 1986; 34(7):949-52.

Stern L, Gautier R. Rapports entre le liquide céphalorachidien et la circulation sanguine. *Arch Int Physiol*. 1921; 17:138–192.

Stern L, Gautier R. Les rapports entre le liquide céphalorachidien et les éléments nerveux de l'axe cérébrospinal. *Arch Int Physiol*. 1922; 17:391–448.

Stewart PA, Beliveau R, Rogers KA. Cellular localization of P-glycoprotein in brain versus gonadal capillaries. *Histochem Cytochem*. 1996; 44(7):679-85.

Strazielle N, Ghersi-Egea JF. Demonstration of a coupled metabolism-efflux process at the choroid plexus as a mechanism of brain protection toward xenobiotics. *J Neurosci*. 1999; 19(15):6275-89.

Strazielle N, Khuth ST, Ghersi-Egea JF. Detoxification systems, passive and specific transport for drugs at the blood-CSF barrier in normal and pathological situations. *Adv Drug Deliv Rev*. 2004; 56(12):1717-40.

Stride, BD, Grant CE, Loe DW, Hipfner DR, Cole SPC, and Deeley RG. Pharmacological characterization of the murine and human orthologs of multidrug-resistance protein in transfected human embryonic kidney cells. *Mol Pharmacol*.1997; 52:344-353.

Sugawara I, Hamada H, Tsuruo T, Mori S. Specialized localization of P-glycoprotein recognized by MRK 16 monoclonal antibody in endothelial cells of the brain and the spinal cord. *Jpn J Cancer Res*. 1990; 81(8):727-30.

Sugiyama Y, Kusuhara H, Suzuki H. Kinetic and biochemical analysis of carrier-mediated efflux of drugs through the blood-brain and blood-cerebrospinal fluid barriers: importance in the drug delivery to the brain. *J Control Release*. 1999; 62(1-2):179-86.

Sun H, Dai H, Shaik N, Elmquist WF. Drug efflux transporters in the CNS. *Adv Drug Deliv Rev*. 2003; 55(1):83-105.

Suzuki H, Terasaki T, Sugiyama Y. Role of efflux transport across the blood-brain barrier and blood-cerebrospinal fluid barrier on the disposition of xenobiotics in the central nervous system. *Adv Drug Deliv Rev*. 1997; 25(1,2):129-307.

Sweet DH, Wolff NA, Pritchard JB. Expression cloning and characterization of ROAT1. The basolateral organic anion transporter in rat kidney. *J Biol Chem*. 1997; 272(48):30088-95.

Sweet DH, Pritchard JB. rOCT2 is a basolateral potential-driven carrier, not an organic cation/proton exchanger. *Am J Physiol*. 1999; 277(6 Pt 2):F890-8.

Sweet DH, Miller DS, Pritchard JB. Localization of an organic anion transporter-GFP fusion construct (rROAT1-GFP) in intact proximal tubules. *Am J Physiol*. 1999; 276(6 Pt 2):F864-73.

Sweet DH, Miller DS, Pritchard JB. Ventricular choline transport: a role for organic cation transporter 2 expressed in choroid plexus. *J Biol Chem*. 2001; 276(45):41611-9.

Sweet DH, Chan LM, Walden R, Yang XP, Miller DS, Pritchard JB. Organic anion transporter 3 (Slc22a8) is a dicarboxylate exchanger indirectly coupled to the Na+ gradient. *Am J Physiol Renal Physiol*. 2003; 284(4):F763-9.

Sykes D, Sweet DH, Lowes S, Nigam SK, Pritchard JB, Miller DS. Organic anion transport in choroid plexus from wild-type and organic anion transporter 3 (Slc22a8)-null mice. *Am J Physiol Renal Physiol*. 2004; 286(5):F972-8.

T

Takakura Y, Audus KL, Borchardt RT. Blood-brain barrier: transport studies in isolated brain capillaries and in cultured brain endothelial cells. *Adv Pharmacol*. 1991; 22:137-65.

Takano M, Horie M, Yayama K, Okamoto H. Lipopolysaccharide injection into the cerebral ventricle evokes kininogen induction in the rat brain. *Brain Res*. 2003; 978(1-2):72-82.

Tao-Cheng JH, Brightman MW. Development of membrane interactions between brain endothelial cells and astrocytes in vitro. *Int J Dev Neurosci*. 1988; 6(1):25-37.

Tayarani I, Cloez I, Clement M, Bourre JM. Antioxidant enzymes and related trace elements in aging brain capillaries and choroid plexus. *J Neurochem*. 1989; 53(3):817-24.

Terada T, Sawada K, Saito H, Hashimoto Y, Inui K. Inhibitory effect of novel oral hypoglycemic agent nateglinide (AY4166) on peptide transporters PEPT1 and PEPT2. *Eur J Pharmacol*. 2000; 392(1-2):11-7.

Terada T, Inui K. Peptide transporters: structure, function, regulation and application for drug delivery. *Curr Drug Metab*. 2004;5(1):85-94.

Terasaki T, Hosoya K. Conditionally immortalized cell lines as a new in vitro model for the study of barrier functions. *Biol Pharm Bull*. 2001; 24(2):111-8.

Terasaki T, Ohtsuki S, Hori S, Takanaga H, Nakashima E, Hosoya K. New approaches to in vitro models of blood-brain barrier drug transport. *Drug Discov Today*. 2003; 8(20):944-54.

Teuscher NS, Shen H, Shu C, Xiang J, Keep RF, Smith DE. Carnosine uptake in rat choroid plexus primary cell cultures and choroid plexus whole tissue from PEPT2 null mice. *J Neurochem*. 2004; 89(2):375-82.

Thomas SA, Preston JE, Wilson MR, Farrell CL, Segal MB. Leptin transport at the blood--cerebrospinal fluid barrier using the perfused sheep choroid plexus model. *Brain Res*. 2001; 895(1-2):283-90.

Thomas SA, Segal MB. The transport of the anti-HIV drug, 2',3'-didehydro-3'-deoxythymidine (D4T), across the blood-brain and blood-cerebrospinal fluid barriers. *Brit J Pharm*. 1998; 125:49-54.

Torok M, Huwyler J, Gutmann H, Fricker G, Drewe J. Modulation of transendothelial permeability and expression of ATP-binding cassette transporters in cultured brain capillary endothelial cells by astrocytic factors and cell-culture conditions. *Exp Brain Res*. 2003; 153(3):356-65.

Tsuda M, Sekine T, Takeda M, Cha SH, Kanai Y, Kimura M, Endou H. Transport of ochratoxin A by renal multispecific organic anion transporter 1. *J Pharmacol Exp Ther*. 1999; 289(3):1301-5.

Tsuruoka S, Ishibashi K, Yamamoto H, Wakaumi M, Suzuki M, Schwartz GJ, Imai M, Fujimura A. Functional analysis of ABCA8, a new drug transporter. *Biochem Biophys Res Commun*. 2002; 298(1):41-5.

U

Uwai Y, Okuda M, Takami K, Hashimoto Y, Inui K. Functional characterization of the rat multispecific organic anion transporter OAT1 mediating basolateral uptake of anionic drugs in the kidney. *FEBS Lett*. 1998; 438(3):321-4.

V

Van Itallie CM, Anderson JM. The molecular physiology of tight junction pores. *Physiology (Bethesda)*. 2004;19:331-8.

van Montfoort JE, Hagenbuch B, Groothuis GM, Koepsell H, Meier PJ, Meijer DK. Drug uptake systems in liver and kidney. *Curr Drug Metab*. 2003; 4(3):185-211.

Vega-Salas DE, Salas PJ, Gundersen D, Rodriguez-Boulan E. Formation of the apical pole of epithelial (Madin-Darby canine kidney) cells: polarity of an apical protein is independent of tight junctions while segregation of a basolateral marker requires cell-cell interactions. *J Cell Biol*. 1987; 104(4):905-16.

Venero JL, Vizuete ML, Machado A, Cano J. Aquaporins in the central nervous system.*Prog Neurobiol*. 2001; 63(3):321-36.

Villalobos AR, Miller DS, Renfro JL. Transepithelial organic anion transport by shark choroid plexus. *Am J Physiol Regul Integr Comp Physiol*. 2002; 282(5):R1308-16.

Villalobos AR, Parmelee JT, Pritchard JB. Functional characterization of choroid plexus epithelial cells in primary culture. *J Pharmacol Exp Ther*. 1997; 282(2):1109-16.

Villalobos AR, Parmelee JT, Renfro JL. Choline uptake across the ventricular membrane of neonate rat choroid plexus. *Am J Physiol*. 1999; 276(6 Pt 1):C1288-96.

Violante GD, Zerrouk N, Richard I, Frendo JL, Zhiri A, Li-Khuan R, Tricottet V, Provot G, Chaumeil JC, Arnaud P.Short Term Caco-2/TC7 Cell Culture: Comparison between of Conventional 21-d and a Commercially Available 3-d System. *Biol Pharm Bull*. 2004; 27(12):1986-92.

Virgintino D, Robertson D, Errede M, Benagiano V, Girolamo F, Maiorano E, Roncali L, Bertossi M. Expression of P-glycoprotein in human cerebral cortex microvessels. *J Histochem Cytochem*. 2002; 50(12):1671-6.

W

Wada S, Tsuda M, Sekine T, Cha SH, Kimura M, Kanai Y, Endou H.Rat multispecific organic anion transporter 1 (rOAT1) transports zidovudine, acyclovir, and other antiviral nucleoside analogs. *J Pharmacol Exp Ther*. 2000; 294(3):844-9.

Wang W, Seward DJ, Li L, Boyer JL, Ballatori N. Expression cloning of two genes that together mediate organic solute and steroid transport in the liver of a marine vertebrate. *Proc Natl Acad Sci USA*. 2001; 98(16):9431-6.

Waring MJ. Complex formation between ethidium bromide and nucleic acids. *J Mol Biol*. 1965; 13(1):269-82.

Warren KE, Patel MC, McCully CM, Montuenga LM, Balis FM. Effect of P-glycoprotein modulation with cyclosporin A on cerebrospinal fluid penetration of doxorubicin in non-human primates. *Cancer Chemother Pharmacol*. 2000; 45(3):207-12.

Watson PM, Anderson JM, Vanltallie CM, Doctrow SR. The tight-junction-specific protein ZO-1 is a component of the human and rat blood-brain barriers. *Neurosci Lett*. 1991; 129(1):6-10.

Wegener J, Sieber M, Galla HJ. Impedance analysis of epithelial and endothelial cell monolayers cultured on gold surfaces. *J Biochem Biophys Methods*. 1996; 32(3):151-70.

Whittico MT, Hui AC, Giacomini KM. Preparation of brush border membrane vesicles from bovine choroid plexus. *J Pharmacol Meth*. 1991; 25(3):215-27.

Wijnholds J, deLange EC, Scheffer GL, van den Berg DJ, Mol CA, van der Valk M, Schinkel AH, Scheper RJ, Breimer DD, Borst P. Multidrug resistance protein 1 protects the choroid plexus epithelium and contributes to the blood-cerebrospinal fluid barrier. *J Clin Invest*. 2000; 105(3):279-85.

Wijnholds J, deLange EC, Scheffer GL, van den Berg DJ, Mol CA, van der Valk M, Schinkel AH, Scheper RJ, Breimer DD, Borst P. Multidrug resistance protein 1 protects the choroid plexus epithelium and contributes to the blood-cerebrospinal fluid barrier. *J Clin Invest*. 2000; 105(3):279-85.

Wijnholds J. Drug resistance caused by multidrug resistance-associated proteins. *Novartis Found Symp*. 2002; 243:69-79; discussion 80-2, 180-5.

Wolburg H, Neuhaus J, Kniesel U, Krauss B, Schmid EM, Ocalan M, Farrell C, Risau W. Modulation of tight junction structure in blood-brain barrier endothelial cells. Effects of tissue culture, second messengers and cocultured astrocytes. *J Cell Sci*. 1994; 107 (Pt 5):1347-57.

Wolburg H, Wolburg-Buchholz K, Liebner S, Engelhardt B. Claudin-1, claudin-2 and claudin-11 are present in tight junctions of choroid plexus epithelium of the mouse. *Neurosci Lett*. 2001; 307(2):77-80.

Wolff NA, Werner A, Burkhardt S, Burckhardt G. Expression cloning and characterization of a renal organic anion transporter from winter flounder. *FEBS Lett*. 1997; 417(3):287-91.

Wright SH, Dantzler WH. Molecular and cellular physiology of renal organic cation and anion transport. *Physiol Rev*. 2004; 84(3):987-1049.

Y

Yan R, Taylor EM. Neotrofin is transported out of brain by a saturable mechanism: possible involvement of multidrug resistance and monocarboxylic acid transporters. *Drug Metab Dispos*. 2002; 30(5):513-8.

Yee S. In vitro permeability across Caco-2 cells (colonic) can predict in vivo (small intestinal) absorption in man-fact or myth. *Pharm Res*. 1997; 14(6):763-6.

Yoo JW, Kim YS, Lee SH, Lee MK, Roh HJ, Jhun BH, Lee CH, Kim DD. Serially passaged human nasal epithelial cell monolayer for in vitro drug transport studies. *Pharm Res*. 2003; 20(10):1690-6.

Yoshioka T, Tanaka O, Otani H, Shinohara H, Inomata K. Alkaline phosphatase activity of the IVth ventricular choroidal epithelium of rats during embryonic and neonatal development. *Histol Histopathol*. 1988; 3(2):173-80.

Youdim KA, Avdeef A, Abbott NJ. In vitro trans-monolayer permeability calculations: often forgotten assumptions. *Drug Discov Today*. 2003; 8(21):997-1003.

Young LC, Campling BG, Cole SP, Deeley RG, Gerlach JH. Multidrug resistance proteins MRP3, MRP1, and MRP2 in lung cancer: correlation of protein levels with drug response and messenger RNA levels. *Clin Cancer Res*. 2001; 7(6):1798-804.

Z

Zenker D, Begley D, Bratzke H, Rubsamen-Waigmann H, von Briesen H. Human blood-derived macrophages enhance barrier function of cultured primary bovine and human brain capillary endothelial cells. *J Physiol*. 2003; 551(Pt 3):1023-32.

Zeuthen T, Wright EM. Epithelial potassium transport: tracer and electrophysiological studies in choroid plexus. *J Membrane Biol*. 1981; 60:105-128.

Zhang W, Ling V. Cell-cycle-dependent turnover of P-glycoprotein in multidrug-resistant cells. *J Cell Physiol*. 2000; 184(1):17-26.

Zhang Y, Schuetz JD, Elmquist WF, Miller DW. Plasma Membrane Localization of Multidrug Resistance-Associated Protein (MRP) Homologues in Brain Capillary Endothelial Cells. *J Pharmacol Exp Ther*. 2004; 311(2):449-55.

Zheng W, Zhao Q, Graziano JH. Primary culture of choroidal epithelial cells: characterization of an in vitro model of blood-CSF barrier. *In Vitro Cell Dev Biol Anim*. 1998 Jan; 34(1):40-5.

Zheng W, Zhao Q. Establishment and characterization of an immortalized Z310 choroidal epithelial cell line from murine choroid plexus. *Brain Res*. 2002; 958(2):371-80.

Zheng W, Zhao Q. The blood-CSF barrier in culture. Development of a primary culture and transepithelial transport model from choroidal epithelial cells. *Methods Mol Biol*. 2002; 188:99-114.

Zlokovic BV, Segal MB, Begley DJ, Davson H, Rakic L. Permeability of the blood-cerebrospinal fluid and blood-brain barriers to thyrotropin-releasing hormone. *Brain Res*. 1985; 358(1-2):191-9.